Delft University of Technology

Master Thesis

Carbon Glass Hybrid Materials for Wind Turbine Rotor Blades

Pietro Bortolotti

May 16, 2012

Master of Science in Sustainable Energy Technology
Wind Energy track

Supervisors:
Ir. T. Westphal
Dr.ir. W.A.A.M. Bierbooms

Delft University of Technology
Department of Wind Energy

The undersigned hereby certify that they have read and recommend to the Faculty of Applied Sciences for acceptance a thesis entitled **"Carbon glass hybrid materials for wind turbine rotor blades"** by **P. Bortolotti B.Sc.** in partial fulfillment of the requirements for the degree of **Master of Science**.

Dated: May 16, 2012

Head of department:

Prof.dr. G.J.W. van Bussel

Supervisor:

Dr.ir. W.A.A.M. Bierbooms

Supervisor:

Ir. T. Westphal

Reader:

Dr.ir. O.K. Bergsma

. . . il termine -libertà- ha notoriamente molti sensi,
ma forse il tipo di libertà più accessibile,
più goduto soggettivamente,
e più utile al consorzio umano,
coincide con l'essere competenti nel proprio lavoro,
e quindi nel provare piacere a svolgerlo.

. . . the word -freedom- has notoriously many meanings,
but maybe the most accessible,
the most subjectively enjoyed,
and the most useful to the human society kind of freedom,
coincides with the being competent in our own job,
and so with enjoying it.

Primo Levi
La chiave a stella

Abstract

Wind turbine rotor blades have seen a strong growth in length and industry is facing new structural problems. New lighter and stiffer materials would be useful to improve the blade design. This research analyses the potential of carbon glass hybrid composites.
Three laminates typical of the laminates used in the spar caps and in the trailing edge reinforcement are manufactured and tested: a reference GFRP, a hybrid laminate and a carbon dominated laminate. For the hybrid material, the results show a positive behavior under static tensile and fatigue loads, while relatively low UCS; a positive hybrid effect is denoted. As for the carbon laminate, the high carbon fraction leads to the best performance under all loads but to a poor infusibility during the VARTM process.
The experimental research is followed by a computational study using the wind turbine design software package Focus 6 to evaluate the design of hybrid blades. Thanks to the higher stiffness and the better fatigue resistance of carbon fibers, the simulations return very good expectations with the new blade models considerably lighter and slightly cheaper than the baseline model with pure GFRP spar caps.
Based on this study, hybrid laminates seem to be an interesting alternative to glass or carbon laminates. Further study on the optimal structure of hybrid laminates is recommended.

Acknowledgments

This work fell within the Wind Energy specialization of the Master of Science "Sustainable Energy Technology" from the Technical University of Delft and was conducted thanks to a collaboration with the Knowledge Centre Wind Turbine Materials and Constructions WMC. I am thankful to all the people I met on the path of this research and a particular acknowledgment goes to my WMC supervisors Tim Westphal and Rogier Nijssen. Their guidance and helpfulness were crucial for the success of this research. I also would like to offer my thanks to Wim Bierbooms, assistant professor of the Wind Energy group of TU Delft.

My last two years of university have been full of challenges, fun and new people. I am glad to now have so many new friends and in particular the Portuguese ones: I won't forget our dinners.
A special thank you also goes to my Italian friends: Deba, Gioppy, Pisto e Teo. Your friendship helped me a lot and it is now time to organize a new trip together somewhere in the world!

Now that I am at this milestone, my deepest thoughts go out to my grandfathers: they have been showing me a bright example of probity and integrity. This thesis is dedicated to them. My gratitude also goes to my large family: everyone has a part in my life, from my father to Bas.
Finally, my last thanks go to Cecilia: we do deserve some time together after all this.

Contents

List of Figures

List of Tables

Notation

ASTM	American Society for Testing and Materials
b	Intercept of the S–N log–log line
Biax	Short for Bi-axial; fabric with fibers at $\pm 45^\circ$
BSDS	Blade System Design Studies, SNL research project
C	Carbon
CFRP	Carbon Fiber Reinforced Plastics
CLD	Constant Life Diagram
E_x	Young's modulus in x-direction
ECN	Energy Centre of the Netherlands
EU	European Union
F	Force, load
FSF	Fatigue Stress Factor
G	Glass
G_{xy}	Shear stiffness xy
GFRP	Glass Fiber Reinforced Plastics
GL	Germanischer Lloyd SE
I03	Geometry for compression tests, standard ASTM D6641
I13	Geometry for shear tests, standard ASTM D7078
IEC	International Electrotechnical Commission
m	Slope of the S–N log–log line
MD	Multi-Directional
MSU	Montana State University
N	Number of cycles
OptiDAT	Database from OPTIMAT
OPTIMAT	EU funded research program on wind turbine blade materials
Prepreg	Pre-impregnated fabrics
QQ1	$[45_G/0_{2G}]_S$ MSU plate
R	Ratio of minimum to maximum load
ROM	Rule of mixture
R09	General geometry of the coupons
R^2	R squared value of the linear regression
s	Standard deviation based on a sample
S	Stress

SNL	Sandia National Laboratories, New Mexico
UD	Uni-Directional
Upwind	EU funded research program on wind energy
USS	Ultimate Shear Strength
USϵ	Ultimate Shear Strain
UT(C)S	Ultimate Tensile (Compressive) Strength
UT(C)ϵ	Ultimate Tensile (Compressive) Strain
Triax	Short for Tri-Axial fabric; fabric with roving at 0° and ±45°
VARTM	Vacuum Assisted Resin Transfer Molding
WMC	Knowledge Centre Wind turbine Materials and Constructions

γ	Safety factor
ϵ	Strain
θ	Coefficient of variation
ν	Poisson's ratio
ξ	Fiber fraction
ρ	Material density
σ	Axial stress
τ	Shear stress
ψ	Fiber volume fraction
ω	Rotational speed

$\overline{x}$	Average of x
#	Number of test results

Chapter 1

Introduction

This introductory chapter is split in four sections. The thesis background is presented in Section 1.1. Then, the objective of this work is shown in Section 1.2, followed in Section 1.3 by the approach that was adopted to achieve it. Finally, the thesis outline can be consulted in Section 1.4.

1.1 Background

In the last two decades, the increasing global demand of energy and the environmental threats associated with fossil fuel consumption have led to an exponential growth of energy production from renewable sources. Up to now, this development has been possible mainly thanks to wind power [1].
This positive trend of wind energy is likely to continue. However, while for 20 years most of the wind power installations have been on land, the current trend is to go offshore. This change poses new challenges. In particular, an offshore wind turbine needs to achieve higher energy production to be economically justified; this primarily means a larger rotor.
In this scenario, industry is hence developing new longer wind turbine rotor blades and manufacturers are now approaching the impressive length of 100 meters. As examples, the latest Vestas 7 MW turbine [2] has a rotor diameter equal to 164 m, while turbine prototypes up to 20 MW are under design [3].

To achieve the successful construction of these huge structures, research is called to overcome some limiting factors related to materials and structural design.

[1] Renewables 2011, Global Status Report, www.ren21.net, accessed 02/04/2012
[2] www.vestas.com, accessed 02/04/2012
[3] Wind in our Sails, EWEA report, www.ewea.org, accessed 05/03/2012

Wind turbine blades have historically been constructed with materials used in the marine industry and with the same concepts as sailplane wings (Kensche, 2004). The selection has been driven by precise guidelines: cost considerations, ease in handling during fabrication, lightness and finally stiffness.
To follow these indications, composites have usually been the primary choice. The optimal composite for wind turbine blades has high strength and high stiffness to weight ratios, but it is also cheap.
Up to now, the class of materials that has best met these requirements has been glass fiber reinforced plastics (GFRP). GFRP composites are generally characterized by good static and fatigue mechanical properties combined with low cost components and fabrication processes.

Nevertheless, in the last few years research has highlighted some important issues in long wind turbine rotor blades made of GFRP.
First, the design of blades longer than 40-50 meters presents bending stiffness as crucial parameter (Griffin, 2001); very thick structural elements are nowadays necessary to maintain sufficient tower clearance under strong wind conditions. Moreover, wind turbine blades can approximately be considered as cantilever beams and while the rated output power of a turbine scales with the square of blade length, the mass of an ideal cantilever beam scales with the cube of the length and gravity loads at the root scale with exponent four (Griffith and Ashwill, 2011). Finally, fatigue resistance is also a problematic issue as wind turbine blades experience an enormous number of cycles during their lifetime (van Delft, 1994); in particular, the trailing edge materials need to withstand very high strains, which are expected to grow with blade length (Peeringa et al., 2011).

Due to these considerations, stiffer, lighter and more fatigue resistant materials would therefore be useful to improve the design of innovative wind turbine rotor blades. Carbon fiber reinforced plastics (CFRP) have been studied (Joosse et al., 2001b) and employed (Ashwill, 2009) thanks to their considerably higher stiffness to weight ratio. However, up to now the use of CFRP has been strongly limited by manufacturing problems, high material costs and sensitivity to production quality (Tong, 2010).

In this scenario, it is interesting to study the combination of glass and carbon fibers to obtain a hybrid composite trying to combine the good properties of the two components. Glass may reduce the laminate cost and facilitate the manufacturing process, with carbon being a strong and stiff reinforcement.
A significant industrial interest is present on these hybrid materials and scientific literature is limited. Therefore, research is needed on the potential of the combination of hybrid carbon glass fiber reinforced plastics for wind turbine rotor blades.

1.2 Objective

The objective of this project is to evaluate the potential of glass carbon hybrid composites for wind turbine rotor blade structures. Ultimately, the goal is to quantify the potential weight saving and the cost impact of the application of these laminates in a blade design.

1.3 Approach

This study consists of two main parts: the experimental characterization of the mechanical properties of hybrid and reference laminates and the computational development of several blade designs to evaluate the materials.

This project focuses on unidirectional laminates representative of the materials used in the spar caps, namely the two flanges of the long beam structure that give the main flatwise stiffness to a wind turbine blade.
Three materials are characterized: a baseline material made of glass, a hybrid material and a carbon dominated material.
The experiments aim at characterizing these three laminates under longitudinal and transverse tension and compression static loads, static shear loads and tension – tension, tension – compression and compression – compression longitudinal fatigue loads. Static tests are run following the international standards of ASTM, while fatigue tests follow the internal guidelines of WMC.

The experimental phase provides the input for a computational study focused on the comparison of the materials. This study uses the wind turbine design software package Focus 6. A baseline blade model developed during the European project Upwind is analyzed and modified to evaluate the materials on a blade scale. The blade is modified only in the thickness and in the width of the spar caps and of the trailing edge reinforcement, and the design limiting factors are assumed to be flapwise stiffness and fatigue and buckling resistance. The design process respects the guidelines of Germanischer Lloyd for wind turbine certification.

1.4 Structure of the report

This thesis report is divided into three main parts. After the introduction, the first part shows the current background on wind turbine blade materials and on blade design, focusing on the spar caps and on the use of carbon fiber reinforced plastics. After this, Part II shows the experimental phase of

this project: Chapter 4 describes the preparation of the samples, Chapter 5 the testing procedure and equipment, Chapter 6 the experimental results and finally Chapter 7 reports the analyses and the comments about these results. After these sections, the blade design phase is faced in Part III, which includes Chapter 8 with the analysis of the reference model developed during Upwind, Chapter 9 with the blade design procedure, and finally Chapter 10 with the four blade models that are developed. The report is closed by the conclusions and recommendations, which are listed in Chapter 11.

Part I

Background

Chapter 2

Materials

This chapter starts with a short overview of composite materials; then, it presents a literature study on wind turbine rotor blades dedicated materials and deals with glass fiber reinforced plastics (GFRP), carbon fiber reinforced plastics (CFRP) and hybrids.

2.1 General overview of composites

Wind turbine blades require stiff and light materials and composites have for long been the primary choice of industry. Composites are characterized by high stiffness to weight ratio and good fatigue and corrosion resistance. Composite materials are made of fibers embedded in a matrix. The fibers are designed to withstand the loads while the matrix works as a binder that permits load transfer from fiber to fiber, protects fibers from damage and supports them in compression.
One of the major advantages of composite materials is their high versatility. A laminate is composed by several laminae; each lamina influences the behavior of the complete laminate. Many different parameters can be varied in a composite and the final properties strongly depend on the adopted layup. Generally, the loads on a structure are the main design drivers.
First, the lay-up of the fibers is crucial for the mechanical properties. Fibers come in fabrics; these fabrics can be either woven or stitched. Woven fabrics are generally considered as "aerospace" fabrics and are often used where good impact resistance is needed. Wind turbine blades are instead generally made of stitched fabrics, which often show better static and fatigue performance than woven fabrics.
In a laminate, fibers can be oriented at any angle; however, three classes of fabrics are usually identified:

- Unidirectional (UD): the majority of the fibers is parallel in one direction, while few rovings may be 90 ° oriented to give stability to the tow and make the handling easier. The UD layers are responsible for the main longitudinal strength and stiffness of a laminate and are particularly important to withstand loads aligned in the fiber direction. UD fibers are hence mostly used in structural elements loaded uni-directionally.

- Biaxial (biax): two fiber layers are perpendicularly stitched together; these layers are generally 45 ° rotated compared to the UD layers so that 50 % of the fibers result to be at +45 ° while the other 50 % is oriented at −45 °. The biaxial fabrics are important to improve shear resistance and might act as crack arresters; hence, they are also often used in structural elements. However, being weak in the longitudinal direction, the percentage of 45 layers needs to be carefully balanced in respect to UD fibers.

- Triaxial (triax), quadraxial and other multi-axial fabrics: often this kind of fabric is a combination of UD and biax fabrics, with 0° and ±45° oriented fibers stitched together; other orientations are also used and the fabrics can be very different one from the other, but they are generally used for components loaded multi-directionally.

Considering the loads, the fiber orientation and the number of layers are decided.
In addition to this, the fiber volume fraction ψ also needs to be determined. It has been demonstrated that high values of ψ lead to better static performance, but too high values can have a detrimental effect on fatigue resistance (Mandell et al., 2002). Moreover, structures characterized by very high ψ values cannot be realized because of manufacturing problems during infusion processes: fibers obstruct resin flow and infusion processes can become very hard; this issue is particularly problematic for carbon where its thin threads are hardly permeable by resin.
However, a trade-off is often necessary because structures usually need high stiffness to weight ratio thus implying high fiber volume fractions. Moreover, structural elements are often characterized by nonlinear geometries, flaws and defects and while for high ψ the presence of ply drops and structure irregularities is not significant, for low ψ a considerable drop in fatigue resistance might occur (Mandell et al., 2002).

2.2 Wind turbine rotor blade composites

Wind turbine blades are long structures that require light, stiff and cheap materials; hence, the choice of materials has usually been strictly limited to composites.
Compared to other aerospace applications, wind turbine blade dedicated composites have always been made of cheaper fibers and resins characterized by worse performance. Historically, glass has been the most often used material for fibers while polyester has been the most often used resin.
Nowadays, blades are still mainly made of glass with carbon slowly becoming a feasible opportunity; among resins, epoxy is now preferred thanks to its better strength, chemical resistance, adhesion to the fibers, lower thermal shrinkage and easier workability compared to the other low cost resins (Kensche, 2004). Vinylesters are also used by industry (Tong, 2010).

Composite materials can be manufactured with different methods, but wind turbine blade composites are generally made via a hand lay-up process, an infusion process or using pre-impregnated (prepreg) fabrics (Brøndsted et al., 2005).
The hand lay-up fabrication process is labor intensive and is slowly being abandoned.
The vacuum assisted resin transferred molding (VARTM) is now the most common infusion method, thanks to the good trade-off between costs and finished laminate properties: vacuum infused composites have uniform thickness, low porosity, excellent fiber wet-out and negligible fiber wash. In VARTM, fibers are placed in a half-mold with the right layup and orientation and then, thanks to a vacuum pump and a vacuum bag, resin is forced to flow through the fibers. When the flow is completed, a curing cycle begins at atmospheric pressure. The most important issue for the process is to ensure that all fibers are thoroughly wetted by resin; this does not always happen, as voids or air bubbles might emerge.
The alternative fabrication method uses prepregs. The fibers are pre-wetted with resin and kept at low temperature to limit the spontaneous curing reaction. Once fibers are in position, a vacuum bag is placed to compress the lamina and the laminate is put in an autoclave where pressure and temperature are raised. This method is used only by few blade manufacturers because although it ensures really high laminate qualities, it also has much higher production costs (Brøndsted et al., 2005).

During the last twenty years, research on wind turbine rotor blade dedicated materials has made impressive steps forward thanks to different large research programs. In Europe, the projects OPTIMAT and Upwind were financed by the European Commission and led to the creation of the public database OptiDAT. The Knowledge Centre for Wind turbine Materials and Construc-

tions (WMC), Delft University of Technology and the Energy Centre of the Netherlands (ECN) were deeply involved.
In the U.S., intensive research has been financed by the Department of Energy (DOE) through Sandia National Laboratories (SNL); Montana State University (MSU) created an important research group that has conducted most of the studies. MSU first report was published in 1992 (Mandell et al., 1992); since then, every year new reports or scientific papers have been published updating the results for many materials suitable for wind turbine blade construction (Mandell et al., 2010); in addition to this, the complete database comprising all the results of the tests has been made available to the public and updated yearly (Mandell and Samborsky, 2010).
All these research programs mainly focused on VARTM processed GFRP; however, prepreg fabrics, CFRP and hybrids have also been studied by MSU researchers. During the European projects, limited research was conducted on carbon or prepreg fabrics.

2.3 Glass fiber reinforced plastics

Glass fiber reinforced plastics are a class of relatively cheap materials with good static and fatigue properties. Almost all the wind turbine rotor blade manufacturers use GFRP to build the structural elements of the blades and a good characterization of representative materials is publicly available. Indicative standard values for UD GFRP at 50 % of ψ can be assumed as:

Young's modulus (GPa)	39
Ultimate tensile strength (MPa)	+810
Ultimate compressive strength (MPa)	−510
Ultimate tensile strain (%)	+2.2
Ultimate compressive strain (%)	−1.6

Table 2.1: UD glass (50 % ψ, VARTM processed) indicative properties from OptiDAT

Recently, studies to build longer and slenderer blades found these values design limiting. Particularly, the low Young's modulus of UD GFRP resulted to be a considerable drawback and caused the need for very thick spar caps. The design of 60 or more meters long blades showed very high tip deflections in addition to high stresses at the blade root caused by gravity loads, and suggested the use of stiffer and lighter materials (Griffin, 2001).
Hence, in the last decade research focused on new structural designs and new materials to build innovative blades. Different structural solutions have been identified and among them the glass full or partial replacement by carbon ap-

peared to be promising to meet the new requirements (Joosse et al., 2001b), (Griffin, 2002), (Griffin and Ashwill, 2009).

2.4 Carbon fiber reinforced plastics

CFRP has similar properties to GFRP but is lighter and has higher Young's modulus, higher ultimate tensile strength and better fatigue resistance. A double mechanism advices the use of carbon: first, for the same blade geometry and the same bending stiffness, equal to $E \cdot I$, the laminate thickness can be smaller reducing I to the extent E increases; secondly, the thinner and less dense laminate allows blade weight reduction. Alternatively, the higher stiffness and strength can allow the use of thinner and more aerodynamically efficient profiles.
Historically, carbon has been limited to aerospace applications; in fact, carbon has always been characterized by very good mechanical properties, but also by high manufacturing costs and sensitivity to production quality. Traditionally, woven fabrics have been used.

At the end of the 1990s a breakthrough innovation appeared: low cost large tows of stitched carbon. Carbon fibers are produced using a polyacrylonitrile (PAN) textile precursor, which is stabilized and carbonized. While aerospace fabrics are generally characterized by strands made of 6 thousands (6K) or 12K filaments, wind turbine dedicated carbon fabrics have 24K, 48K or more strands. These thicker filaments generally result in lower production costs but also lower performance.
Dedicated experiments on these new carbon fabrics were performed at TU Delft (Joosse et al., 2001a) and (Joosse et al., 2002); the results that were obtained were quite contradictory, with large scatter always present; moreover, tests were often invalid due to gripping problems, tab failures or thermal effects due to too high frequency. Results were generally unsatisfying when compared to data present in literature on aerospace fabrics, with lower strains and higher fatigue sensitivity than expected; this poorer behavior was particularly marked in compression. However, promising values were obtained for tensile tests or for very high numbers of cycles, namely N above 10 million, using epoxy as resin. Moreover, despite the non-excellent results, blade design simulations returned positive economic parameters with long CFRP blades up to 10 % cheaper than the equivalent ones made of pure glass (Joosse et al., 2001b).

The MSU/SNL report from 2002 (Mandell et al., 2002) also coped with the emerging fabrics; the results obtained were positive but some considerable negative indications were highlighted. While tensile experiments were in the expected high range for both static and fatigue tests, carbon weakness to

compression and its extreme sensitivity to fiber misalignment, fiber waviness, small defects and ply drops were detected. The consequence was that GFRP and CFRP had comparable compressive properties for low cost manufacturing processes, while CFRP being significantly more expensive. Moreover, carbon fabrics suffered from very poor infusibility, posing problems for the manufacturing of full scale blades.

Youngs modulus (GPa)	100
Ultimate tensile strength (MPa)	+1600
Ultimate compressive strength (MPa)	–500 / –700
Ultimate tensile strain (%)	+1.6
Ultimate compressive strain (%)	–0.6 / –1.1

Table 2.2: UD carbon (50 % ψ, VARTM processed) indicative properties from MSU/SNL database

The effect of waviness was subject of specific research (Mandell et al., 2003), (Avery et al., 2004). MSU experiments showed a decrease of ultimate strain from $-1/-1.2$ % for straight-fiber carbon down to $-0.6/-0.8$ % for small misalignments. These values were claimed to be too small for wind turbine designs. Waviness was assumed to reduce compressive strength due to buckling of fibers or layers and due to matrix dominated failures for plies normally dominated by fiber properties.
The results of the researches also indicated that straight-fiber stitched and prepreg fabrics had a better behavior compared to woven fabrics, which suffered the most from waviness; moreover, epoxies and vinylesters were found to be the best matrices, with epoxies slightly prevailing. Finally, structural defects had to be minimized particularly with carbon. Only if all these conditions were achieved, then carbon use would be advisable.
In practice, MSU essentially focused on prepreg fabrics and left behind the development of infused pure carbon.

Compression weakness of carbon was matter of research also recently and a study was conducted on aerospace fabrics by Reis et al. (Reis et al., 2009) to investigate it. Two main failure mechanisms were individuated: micro-buckling and kinking. The researchers detected that in tensile conditions carbon fibers behaved linearly, while in compression plastic behavior took place due to carbon specific micro-structure. The final rupture of carbon was controlled by strain and was caused by longitudinal fractures in tension and $\pm 45\,^{\circ}$ ones in compression.

In conclusion, carbon is still attractive but has not been widely used by the wind energy industry; wind turbine blades are generally infused elements and carbon results to be too expensive, too weak in compression and too hard to manufacture to justify its better stiffness and tensile performance.

Carbon is probably used in a limited amount by the few manufacturers that use prepregs in blades, like Vestas or Gamesa, but is not widely employed in infused structures (Hayman et al., 2008). Therefore, the issues concerning new longer blades have not been solved.

2.5 Hybrids

As wind turbine dedicated carbon fabrics presented large and up to now almost unsolvable problems, it might be interesting to combine glass and carbon fibers creating a hybrid composite. The purpose is to obtain a hybrid in which carbon fibers provide strong, stiff and low density reinforcement, while glass fibers make the structure cheap and help the flow of resin through the carbon layers.
Hybrid composites can be interply or intraply. Interply laminates are made of different fiber plies bonded together; in intraply laminates, each layer is made of two fiber materials. Interply laminates are more easily fabricated and have been developed more than intraply hybrids; this project deals with interply hybrids.

Research on hybrid materials started in the '70s and was mainly focused on improving impact and strain to failure properties of pure CFRP through glass injection (Summerscales and Short, 1978).
Large amount of research has dealt with the existence of a hybrid effect, intended as deviation from the results predicted by the rule of mixture (ROM) for stiffness and fatigue properties or from the fiber first failure model for UTS and UCS. The deviations from the values predicted by these two models are called hybrid effect and are expected to occur due to glass carbon interactions. The hybrid effects can be either positive or negative.

2.5.1 Stiffness

Stiffness generally obeys the rule of mixture. In this study the rule of mixture means the linear equation relating the mechanical properties of the hybrid to the corresponding properties of the constituent pure-composite materials; the composition parameters used for the weighing are the relative fiber fractions ξ of carbon and glass. An example is useful to clarify the ROM for stiffness. Assuming a UD hybrid material with ξ_{carbon} equal to 30 % and ξ_{glass} equal to 70 %, Young's modulus E equal to 100 GPa for carbon and 40 GPa for glass, the predicted stiffness of the hybrid results to be:

$$E_{hybrid} = \xi_{carbon} \cdot E_{carbon} + \xi_{glass} \cdot E_{glass} = \\ 0.3 \cdot 100\ GPa + 0.7 \cdot 40\ GPa = 58\ GPa$$

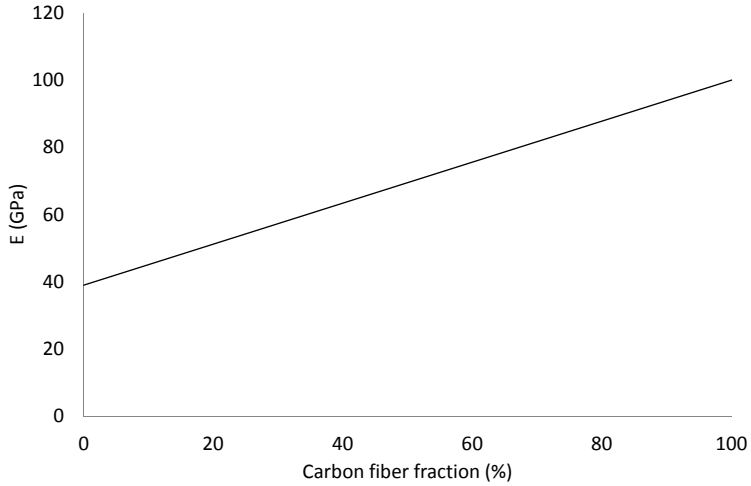

Figure 2.1: Indicative behavior of stiffness in UD hybrids

Whenever the laminate shows Young's modulus higher than 58 GPa there is a positive hybrid effect; negative below 58 GPa.

As for this hybrid effect, literature provides alternating promising and disappointing results. In 1978, Summerscales and Short (1978) did a complete review on the state of development of carbon-glass materials; from the studies they analyzed, a positive hybrid effect was generally found for stiffness, although large uncertainty was present. The expectations were actually downsized by other studies (Marom et al., 1978), (Sonparote and Lakkad, 1982) and at the end of 1980s general agreement was present on the absence of any evident hybrid effect for the Young's modulus of the hybrid composites (Kretsis, 1987), (Oldersma, 1991).

In conclusion, the longitudinal Young's modulus is expected to follow the linear behavior visible in Figure 2.1.

2.5.2 Static tension

While stiffness shows a linear trend, ultimate tensile strength is nonlinear and results to be one of the weak points of hybrids comprising materials with different stiffness; in fact, the ROM cannot be applied as the strength of hybrids is determined by ultimate strains and not by fiber fractions ξ. Carbon fibers are stiffer than glass ones and when the material is elongated they withstand the main load; however, when the material reaches the failure strain limit of carbon, the low elongation fibers fail and load is entirely transferred to high elongation fibers. At carbon failure, two different cases

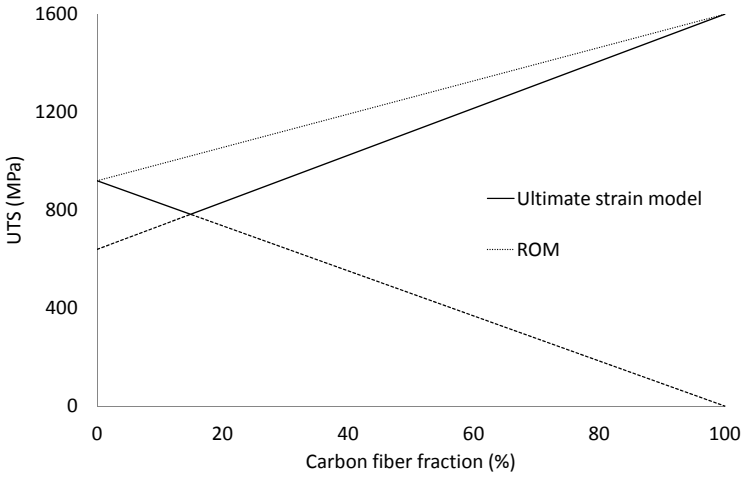

Figure 2.2: Indicative behavior of UTS in UD hybrids

may happen:

- the fraction of glass is too low to withstand the entire load; hence, the coupon fails;
- the fraction of glass is high enough to withstand the load; hence, the coupon does not entirely fail.

Assuming a linear $\sigma - \epsilon$ trend, the hybrid material is expected to follow the black continuous line in Figure 2.2. Before the knee point the percentage of glass is high enough to survive after carbon failure and the ultimate tensile strength (UTS) is represented by the equation:

$$UTS_{hybrid} = \xi_{glass} \cdot UTS_{glass}$$

After the knee point the hybrid sees the contribution of both carbon and glass and fails whenever carbon fails:

$$UTS_{hybrid} = \xi_{carbon} \cdot UTS_{carbon} + \xi_{glass} \cdot UT\epsilon_{carbon} \cdot E_{glass}$$

However, experiments often showed the presence of a positive hybrid effect: the static tensile tests returned UTS values higher than the ones predicted by this simple model. In practice, the ultimate strain model behaved more as a lower bound than as a model. Apparently strain properties of the low elongation fibers were improved by the presence of high elongation fibers and this was particularly notable in hybrids where the two components were uniformly distributed (Summerscales and Short, 1978).

This increase of ultimate strains of carbon fibers was first explained as a consequence of residual internal stresses due to the different expansion coefficients of glass and carbon; in particular, carbon has a lower thermal expansion coefficient than glass and after curing at moderate temperatures carbon fibers could result to be in compression by 10 % of the ultimate tensile strain (Bunsell and Harris, 1974). Later, the most likely explanation was that the weakest low elongation fibers that break first form cracks that are bridged by the surrounding high elongation fibers. Hence, in practice the hybrid effect would be the realization of the full potential strength of carbon rather than strain enhancement (Fukuda and Chou, 1982), (Kretsis, 1987). This explanation could also explain the particularly positive results obtained with well dispersed fibers (Shan and Liao, 2002). Anyway, similar positive results have recently been detected also with woven fabrics (Pandya et al., 2011).

Tests were conducted also in the fiber transverse direction and the same behavior was found. Carbon and glass had comparable transverse strength but a small positive hybrid effect was detected (Kretsis, 1987).

2.5.3 Static compression

While tensile strength in hybrids was widely investigated, a smaller amount of studies returned reliable results for compressive properties. In theory, the failure strain model was valid also for compressive strains and the majority of the researches in 1970s and 1980s confirmed it; however, a very large scatter was always present in the data coming from different researches and different layups. Apparently, the ultimate strain model was again only a lower bound and a stronger hybrid effect was present for compressive strength compared to tensile strength. However, it was not possible to draw any clear conclusion (Kretsis, 1987). A recent study confirmed these expectations (Pandya et al., 2011), but there is still room for uncertainty due to carbon unexpected behavior in compression.

2.5.4 Fatigue

One of the goals of glass carbon hybrids is to improve fatigue resistance of pure glass. From the beginning, it was clear how carbon could increase the lifetime of a structure, but a precise evaluation of the replacement was missing. Research started in the 1970s on aerospace fabrics; the fatigue behavior of the hybrid was found to be linear and the slope of the fatigue curves could be well predicted by the ROM (Summerscales and Short, 1978). In 1989 important tests were conducted (Dickson et al., 1989) with different

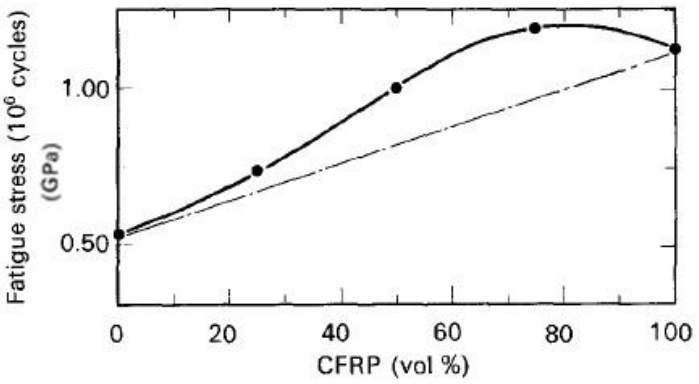

Figure 2.3: Theoretical and experimental behavior of UD G/C hybrids in tensile fatigue tests (Dickson et al., 1989)

layups and different carbon contents. Tensile tests on prepreg fabrics were conducted on various unidirectional hybrids and on a more complex layout, namely $[(\pm 45,0_2)_2]_S$. A strong positive hybrid effect was found, which can be seen in Figure 2.3 where the dashed line coming from the rule of mixtures is always below the experimental one. The introduction of carbon fibers between glass layers improved considerably fatigue strength; in the tests the slope of the S – log N curves for hybrids resulted to be even smaller than the pure CFRP one so that the data for plain carbon and for the 25 % glass – 75 % carbon overlapped significantly after 10^6 cycles. The only explanation to this hybrid effect was again the action of glass as crack arrester or damage inhibitor on micro and macro scales.
A positive hybrid effect was also detected in more recent studies on fatigue of carbon glass materials (Shan and Liao, 2002). The researchers built a simple model for fatigue comparable to the ultimate strain model that worked as lower bound for static properties. In the model, the relative damages of each component were calculated and carbon was found to fail first in almost all the load cases.

In 1990s research on wind turbine dedicated materials had a boost but little research was dedicated to fatigue of hybrid materials. Bach (1992) imposed a stop to the hybrids conducting tests for ECN that produced disappointing results. In particular, Bach could not find any positive hybrid effect and all the hybrid specimens experienced early failure, particularly for $R = -1$ tests. Bach conducted also the first variable amplitude tests for hybrid materials again reporting unsatisfying results.

The 2002 MSU report (Mandell et al., 2002) showed the first fatigue results from MSU about wind turbine blade hybrid materials with good expectations

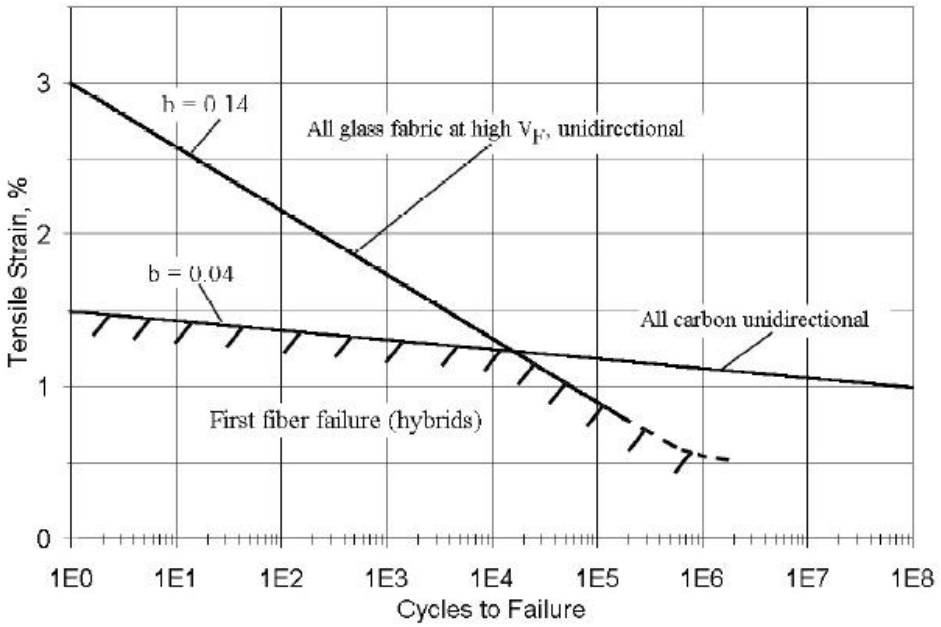

Figure 2.4: ϵ – N predicted line of hybrid UD materials (Mandell et al., 2002)

for the layup with carbon in the 0° layers and glass in the $\pm 45^\circ$ ones. This design was quite simple and the experimental results, although quite few, were satisfactory; carbon fibers withstood the main loads while glass layers made the structure slightly cheaper and improved shear and compression properties compared to a pure carbon design.
The same report also dealt with a pure UD hybrid material, with glass and carbon coexisting in the warp direction, but no large research was dedicated to this layup. This was because if a partial UD glass replacement was performed, glass and carbon fibers would be intimately mixed in the longitudinal direction and experience the same strains despite of the different moduli. This entailed that for high strains carbon would fail at a low number of cycles, causing the failure of the specimen, while the opposite would happen for low strains, with glass failing at a high number of cycles. The consequence was that, given the pure carbon and pure glass S-N lines, the hybrid material might follow the two bottom curves shown in Figure 2.4, or go slightly above them but only with a partial failure of one of the two components. This behavior was detected comparing the hybrid material CG and the equivalent pure glass D155 (Mandell and Samborsky, 2010). Figure 2.5 shows the experimental data.

In conclusion, although the stress curve of the hybrid was higher than the glass one thanks to the higher stiffness modulus, the researchers from MSU classified this layup as inefficient and non-promising and apparently did not

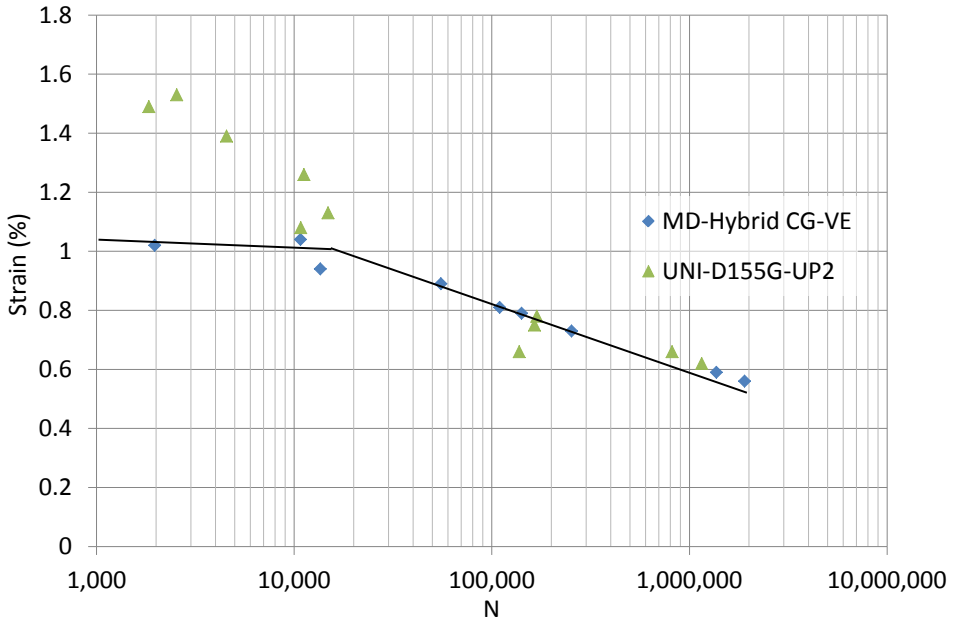

Figure 2.5: ϵ – N experimental data of hybrid vs pure glass UD materials (Mandell and Samborsky, 2010)

further investigate over it.

MSU researchers continued working on fatigue of carbon glass hybrid materials, but only with pure carbon in the warp direction and biaxial glass, confirming their primary results (Mandell et al., 2003). In 2006 new results were presented: from a stress point of view these hybrid laminates were better than glass ones, but ply drop and delamination resistance was considerably lowered; however, $\pm 45^\circ$ layers seemed to be very beneficial keeping carbon fibers straight (Samborsky et al., 2006).
Research advanced also on prepreg laminates, which showed the best performance (Ashwill and Paquette, 2008). Recently, MSU developed one particular hybrid material combining all the information from the previous experiments: the P2B prepreg hybrid laminate, with 8 layers of carbon UD and two external glass biax plies in an epoxy matrix (Mandell and Samborsky, 2010). The results from this material were very positive with good tensile and compressive static strength and much higher stiffness modulus than the glass equivalent. In Figure 2.6 a σ – N comparison is shown at R $= -1$; the red curve is the P2B material while QQ1 is a comparable pure glass layup.

P2B was intensively tested and many data are available in the MSU/SNL public database.
While prepregs were successfully characterized, all infused laminates studied in MSU suffered from poor infusibility or fiber waviness that resulted in

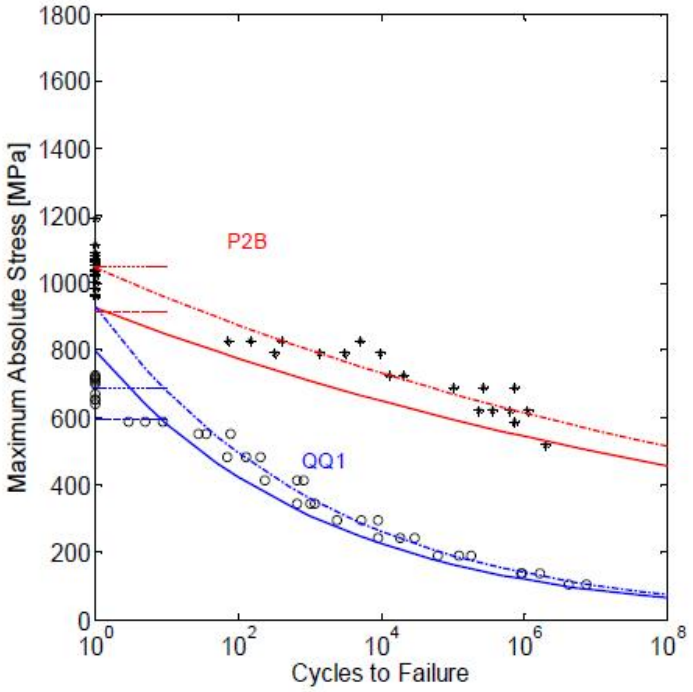

Figure 2.6: σ – N curves for materials QQ1 and P2B (Mandell and Samborsky, 2010)

disappointing results. The only exception was the laminate SN5-022X made of the triaxial hybrid fabric MMWK. MMWK was made of 75 % carbon UD and 25 % biaxial glass, the biaxial layers were external and gave stability for material handling, glass was squeezed by stitches while carbon was kept well straight. Laminate SN5-022X showed excellent static compressive strains down to -1.32 % and high fatigue resistance (Griffin and Ashwill, 2009).

To sum up, research has been quite limited on hybrid laminates for wind turbine rotor blades and has been conducted basically only in MSU. MSU researchers focused on prepregs and developed only one particular infused material, the triax SN5-022X. They also soon abandoned the idea of coexisting UD layers of glass and carbon and preferred to investigate carbon UD and glass biaxial. This in turn resulted in better mechanical performance but also in higher costs of the composites. In practice, MSU hybrids were much closer to pure carbon than to glass composites: the laminates P2B and SN5-022X had a carbon percentage equal to 85 % and 75 % respectively.

Chapter 3

Wind turbine blade design

This chapter shows the preliminary study on structural blade design. The focus is given on the materials and on the design of the spar caps, the long and thick flanges of the beam made of UD material that run along the span from the root to the tip.

3.1 Overview of blade structure

Wind turbine blades are long and slender structures basically composed by a load-carrying beam and a shell. The primary purpose of the shell, which is geometrically defined by airfoils, is to give an aerodynamic shape to the blade creating the lift force that make the wind turbine blade rotating and thus extracting energy from the wind. The aerodynamic forces are transmitted to the wind turbine hub through the load-carrying beam, which represents the structural core of the blade.

While studying blade design, some aerodynamic terms are often used:

- the airfoils define the shapes of the cross sectional areas of the blade and are defined by suction and pressure sides;
- the chord line represents the shortest path between nose and tail of each airfoil; the thickness of an airfoil is generally given as percentage of the chord;
- the flatwise direction denotes the lines that are perpendicular to the chord line, edgewise the parallel ones; the flapwise direction denotes the lines that are perpendicular to the rotor plane, lead-lag the in-plane lines;

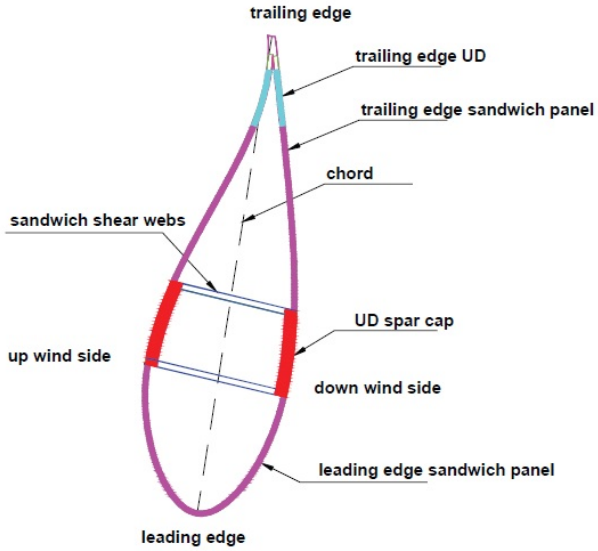

Figure 3.1: Typical blade section

- the span is the length measured from the beginning of the blade to the tip;
- the radius is the span plus the hub radius.

The main loads on a blade are wind loads, which induce both flapwise and lead-lag bending, and gravity, which induces primarily lead-lag bending when the blade is horizontal and axial tension or compression when the blade is vertical. Torsional deformations due to the asymmetry of the blade sections also need to be taken into account, as do loadings associated with accelerations.
The loads change with time because of rotation effects, inherent wind turbulence and disturbance of the air flow by the tower. Therefore, static and fatigue loads must be both carefully considered.

In a blade, each element faces different loads; hence, proper laminates need to be used in the different parts of the structure. The load-carrying beam is generally built with two spar caps and one or more stiffeners. The spar caps are designed to carry the main flatwise and axial loads and for this reason are thick laminates dominated by unidirectional fibers. The stiffeners transfer the load by shear to the spar caps and are made of a sandwich structure with the skin dominated by biaxial fibers and the core made of foam or balsa wood cubes. The shell of the blade is also usually made of sandwich panels, but its skin is often made of triaxial fabrics. The skin panels are designed to avoid buckling during compression states. Finally, long blades generally

need a reinforcement of UD fibers at the leading and at the trailing edges to withstand the edgewise loads (Tong, 2010).

3.2 Trend

While for inland turbines the maximum allowable blade length is often limited by transportation costs (Griffin, 2001), for offshore wind energy the trend is to build longer and longer blades; the main cost for an offshore turbine is indeed the foundation structure. However, larger rotors lead to higher rated power and yearly energy production but also place hard challenges for the designers. In fact, given the two blades a and b of length L_a and L_b respectively and the scaling factor α defined as:

$$\alpha = \frac{L_a}{L_b}$$

The simple up-scaling leads to (Griffith and Ashwill, 2011):

$$P_a = \alpha^2 \cdot P_b$$
$$m_a = \alpha^3 \cdot m_b$$
$$F_{aero,a} = \alpha^2 \cdot F_{aero,b}$$
$$M_{aero,a} = \alpha^3 \cdot M_{aero,b}$$
$$F_{grav,a} = \alpha^3 \cdot F_{grav,b}$$
$$M_{grav,a} = \alpha^4 \cdot M_{grav,b}$$

Where P stands for output power of the turbine, m blade mass, F_{aero} aerodynamic loads of both lift and drag, F_{grav} gravity loads and M respective bending moments.

From this basic approach it clearly appears that the advantages, namely the higher energy production, come with disadvantages that grow exponentially faster, namely the loads and the bending moments.
Manufacturers have already been able to keep the exponent α below the predicted one. For example, research has led to mass exponents ranging between 1.9 and 2.7 depending on the producers, on the manufacturing method and on the wind turbine IEC class (Griffin, 2001), (Lekou, 2010). As an example, the public data about commercial blades of the manufacturer leader LM WindPower [1] are plotted in Figure 3.2: the scaling exponent results to be even lower than 1.9. However, from the curve it can be also deduced that the improvements were considerable in the range of 30 to 50

[1] www.lmwindpower.com, accessed 16/11/2011

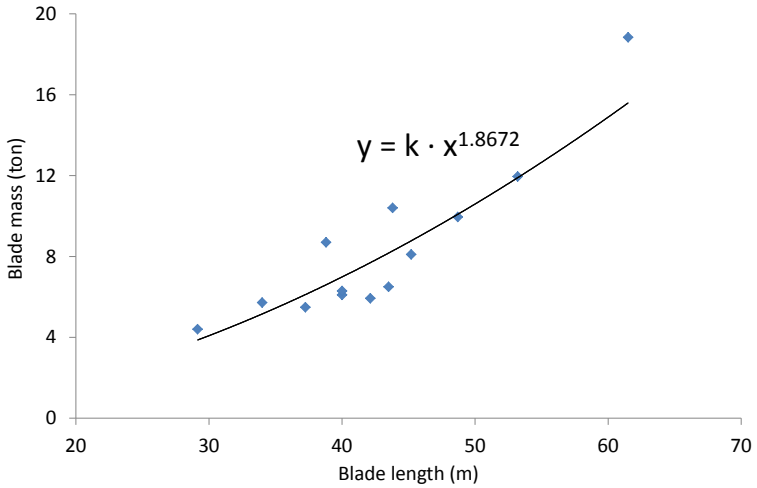

Figure 3.2: Length vs mass curve of LM WindPower commercial blades

meters, while the blade LM61.5P2, where 61.5 indicates the length in meters, is already much above the trendline.
Two scaling studies were performed on a pure glass design by SNL (Griffith and Ashwill, 2011) and by ECN and WMC (Peeringa et al., 2011). In both studies, the designers did not focus on blade mass reduction, but, in order to obtain reasonable values of bending stiffness and strains, the final scaling exponent resulted to be higher than 3. A longer blade implied the need for a third stiffener and mass resulted to grow even faster than expected.

Another strong issue in long blades is tip deflection, which is often the design driver of spar caps made of GFRP. Long and slender structures like wind turbine blades bend consistently when loaded; however, tower clearance is a strong issue for these structures because in case of excessive bending due to wind loading the blade tip could hit the tower. In order to alleviate this problem, four main solutions, shown in Figure 3.3, are often adopted to increase tower clearance:

- rotor cone angle: the three blades are not perfectly in the plane of the rotor but are few degrees tilted out of plane;
- shaft angle: the main shaft is not horizontal but few degrees tilted; this makes the upper blade to move downwind but the lower blade to move upwind;
- blade pre-bend: the blades are not built straight but bent, particularly towards the tip;
- overhang: the main shaft is built longer to move the whole rotor away from the tower.

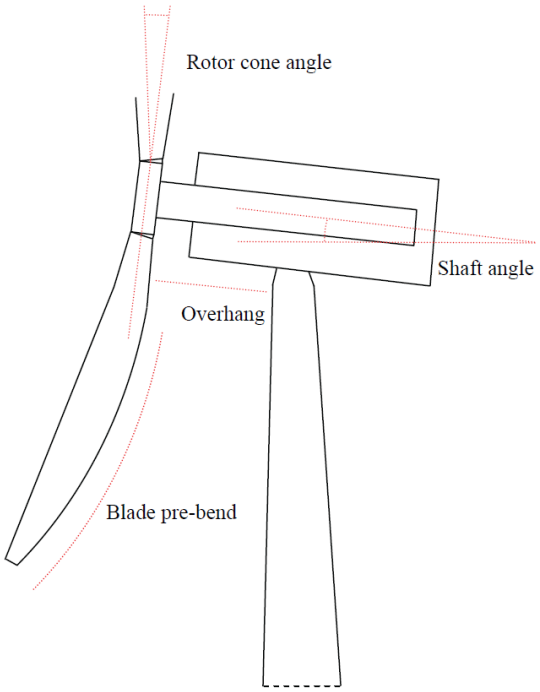

Figure 3.3: Measures to increase the maximum allowable tip deflection

Despite these measures, the thickness of the spar caps is still often determined by the maximum allowable tip deflection and not by maximum strength or fatigue resistance.

So, apparently for longer blades innovations are needed both from a design point of view and from lighter and stiffer materials; this could also help the aerodynamic design of blades that is often constrained by structural limits (Griffin, 2001).

3.3 CFRP use in blades

Although large differences exist among the manufacturers, apparently carbon fibers are still not widely used in industry (Tong, 2010). Most of the manufacturers indeed prefer to produce cheaper VARTM blades made of GFRP than facing higher materials and manufacturing costs due to CFRP. The most famous exceptions to this trend are Vestas and Gamesa that have historically used carbon prepreg fabrics and produce high quality carbon blades (Hayman et al., 2008).

In Europe, public researches on innovative materials were conducted thanks

to funding from the European Commission (Joosse et al., 2002). Despite the considerable higher cost of carbon fabrics, the design simulations returned blades made of pure carbon 60 % lighter and 14 % cheaper than the reference models made of glass. Particularly positive predictions were obtained for fatigue loads dominated turbines; on the other hand, compression weakness of carbon resulted in less positive expectations for turbines dominated by extreme loads.

Innovative concepts for wind turbine blades have been also studied and developed by SNL researchers in the project Blade System Design Studies (BSDS) (Griffin, 2002), (TPI Composites Inc., 2004), (Ashwill and Laird, 2007), (Ashwill and Paquette, 2008), (Griffin and Ashwill, 2009).
In the first phase of BSDS alternative composite materials, manufacturing processes and structural designs were investigated for multi-MW wind turbine rotor blades. In the second phase experimental tests on coupons and sub-components were conducted. The glass carbon hybrid material SN5-122X was selected as the most promising infused laminate made of carbon and was applied in three downscaled prototypes that were built in the U.S. by SNL researchers. The notable characteristics of these prototypes are here summarized. Figure 3.4 shows the blades.

- CX-100: carbon spar cap with constant thickness, glass skins and shear web, balsa core;
- TX-100: constant thickness glass spar cap, carbon fibers in the skin at 20 degrees off of the pitch axis to have passive aerodynamic load reduction, glass shear web, balsa core;
- BSDS: larger root diameter, flatback airfoils (airfoils truncated before the natural trailing edge), constant thickness carbon spar cap, glass skins and web.

One important design solution of these hybrid prototypes was the constant thickness spar cap. MSU conducted several studies on the effect of ply drop for carbon laminates and a strong drop in the performance was detected, both with prepreg and VARTM fabrics. Ply drops are necessary along the span direction of a blade to reduce the thickness of the structural elements; however, carbon ply drops are often sources of cracks (Samborsky et al., 2006).
For prepregs a solution was found with pinked edges in presence of ply drops; in practice, the edges were not cut straight but with a saw tooth profile (Samborsky et al., 2006). However, infusion fabrics showed very small benefits from these pinked edges and the ply drop effects could not be reduced; hence, it was decided to eliminate them completely with constant

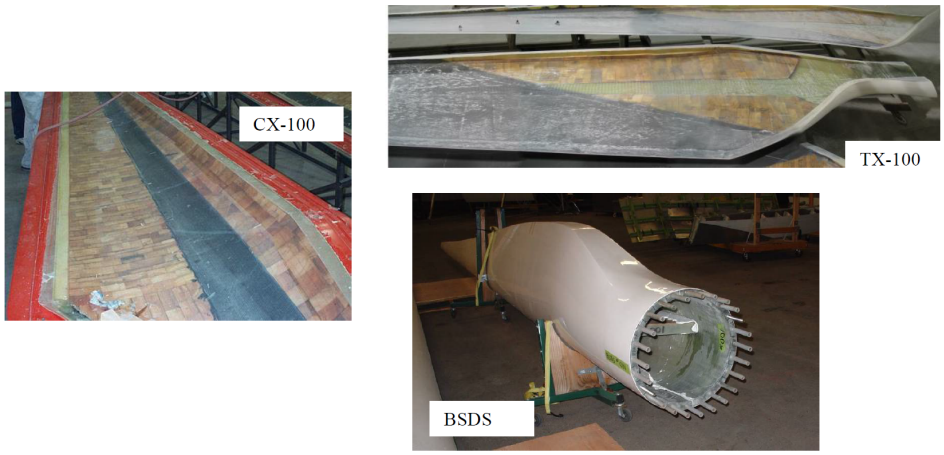

Figure 3.4: Prototypes CX-100, TX-100 and BSDS (Ashwill and Laird, 2007)

thickness spar caps (Ashwill and Laird, 2007). Obviously, this led to lower structural efficiency and higher costs.

The blades were tested statically and in fatigue in the National Wind Technology Center in Boulder, Colorado, and in a test field in Bushland, Texas, showing high performance. Apparently, the addition of a carbon spar cap, although with a constant thickness, was successful in lowering the weight and strengthening a blade. The CX design resulted to be 10 % lighter and had 70 % of tip clearance reduction compared to the equivalent pure glass design. The use of carbon in the skins with a reduced glass spar was also beneficial. Finally, the BSDS blade which had a carbon spar cap and thick flatback airfoils, resulting to be more slender and 25 % lighter than CX-100, had the best results; therefore, a combination of efficient design and carbon was very interesting (Ashwill and Laird, 2007).

	CX-100	TX-100	BSDS
Weight (kg)	174	164	131
% of design load at failure (%)	115	197	310
Max carbon strain at failure (%)	±0.31	±0.59	±0.81
Max tip displacement (m)	1.05	1.80	2.09

Table 3.1: Summary of the results of the SNL prototypes (Ashwill and Laird, 2007)

3.4 Spar caps

From literature, it can be assumed that the spar caps are generally made of a mixture of UD fibers and biaxial or triaxial fabrics (Griffin 2001), (Nijssen et al., 2007), (Peeringa et al., 2011). During WindPACT a large spar cap was designed to improve edgewise bending; the layup was made with alternating layers of UD fabrics and triaxial fabrics, resulting in 70 % UD and 30 % $\pm 45°$ (Griffin, 2001). The laminate properties were the values shown in Table 3.2.

E_x (GPa)	E_y (GPa)	G_{xy} (GPa)	ν_{xy}	UTϵ (%)	UCϵ (%)
27.1	8.35	4.70	0.37	2.20	1.05

Table 3.2: Properties of the laminate used in the spar caps during WindPACT (Griffin, 2001)

In that study, 70/30 was the adopted proportion; for structural consideration a higher percentage of UD material could have been beneficial, but a high percentage of biaxial layers was in practice useful as crack arrester.
Spar caps were made with constant thickness and width spanning from 15 % to 50 % of the maximum chord location. A parametric study was performed to analyze the effect of a tapering thickness of the spar caps to have the highest thickness in the deepest point of the airfoil section; however, the results suggested the constant thickness design. Another study analyzed the possible benefits from a decreasing width of the spar caps; this solution resulted to be beneficial for weight and costs, but detrimental for edgewise stiffness.

Carbon can be used either extensively or selectively in blade design. However, the higher cost of carbon suggests a limited employment of carbon only in crucial elements of the blade.
A study was performed by LM WindPower Holland during the project Dutch Offshore Wind Energy Converter (DOWEC) comparing a full glass blade with a full carbon blade and a blade with only the spar caps made of carbon (Kooij, 2003). Results were good as expected for the two innovative designs but costs were too high to be covered by the improved performance. Although both carbon blade models returned disappointing results, the partial carbon blade was better than the full carbon one.
In conclusion, all-carbon blades appear unlikely to be the most cost effective approach for MW-scale turbines (Griffin and Ashwill, 2009).
Carbon is then particularly interesting as selective reinforcement and stiffener in the unidirectional spar caps improving the flatwise bending stiffness. The load carrying spars can be made with different compositions:

- full carbon;
- hybrid with carbon UD and glass biaxial;
- hybrid with carbon UD and glass both UD and biaxial;
- variable composition along the spanwise direction, e.g. starting with a higher glass concentration at the root and moving towards the tip with a higher carbon concentration.

Each design shows advantages and disadvantages. The maximum materials cost and the best performance are likely to occur in the first design. A performance drop would probably happen in the second approach and even further in the third design. Nevertheless, the higher fraction of glass is expected to decrease the costs and to facilitate the infusion process.
In the BSDS program the second approach was adopted with the triaxial hybrid fabric MMWK.

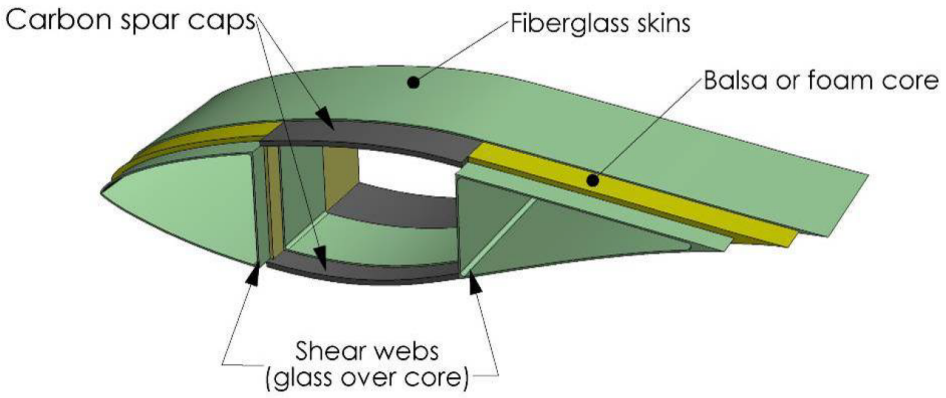

Figure 3.5: Cross sectional area adopted in BSDS (Griffin and Ashwill, 2009)

The fourth design was also analyzed because sounded particularly interesting. Blade mass is not a typical design driver itself as transportation trucks and erection cranes are dominated by blade length and hub height respectively (Griffin, 2002); the gravity induced loads have much greater importance. These loads mainly act at the root and depend on blade mass and center of mass location; this suggests that a light tip has much greater importance than a light root. Furthermore, at the tip the thickness of the airfoils is small and the spar caps are closer to the neutral bending axis than at the root; therefore, strains in the materials are low and stiffer laminates may be more useful.
In conclusion, mass reduction thanks to carbon employment may hence show the best benefits with carbon in the outer blade span. Nevertheless, during

BSDS the designers abandoned the fourth concept because a glass to carbon transition towards the tip was almost impossible to realize without a strong drop in the performance of the blade. As it has been explained, carbon extremely suffers ply drops and defects and moving from glass to carbon without large areas of coexisting UD layers was basically impossible.

Part II

Experiments

Chapter 4

Specimen preparation

This chapter describes the manufacturing process adopted to manufacture the specimens to be tested. First, the materials used are shown in Section 4.1. Then, the infusion process is described in Section 4.2 followed in Section 4.3 by the characteristics of the plates that were manufactured. Finally, the sample platforms chosen for testing are presented in Section 4.4.

4.1 Materials used

The experimental phase of this study was conducted with wind turbine dedicated materials. Table 4.1 shows the fabrics used during the manufacturing process.
All the laminates had an epoxy matrix produced by Hexion. Table 4.2 shows the two components of epoxy: the resin and the hardener; the proportion was 100:30 respectively. The final density of epoxy is 1.15 kg/dm^3.

Fabric	Article	Producer	Areal weight (g/m^2)	Density (kg/dm^3)
Glass UD	S15EU910-00950	SAERTEX	963	2.6
Glass biax	S32EX021-00820	SAERTEX	831	2.6
Carbon UD	UDO-CS-600	SGL	600	1.8

Table 4.1: Fabrics used

Component	Article	Fraction
Resin	RIM 135	77 %
Hardener	RIMH 1366	23 %

Table 4.2: Epoxy used

4.2 Laminate fabrication process

All the materials tested in this study were manufactured through vacuum assisted resin transferred molding (VARTM). This process used two rigid half molds made of steel; the mold was a square of approximately 48 cm by side and each plate was 25 mm thick.
The first step of the infusion process was to apply a releasing agent to the two plates, namely the dedicated product Honey Wax. Then, the different fibers were cut from the rolls of fabric in squares of 32 cm x 32 cm and placed with the specified order and fiber orientation on the bottom mold; the 0 ° oriented fibers were aligned with the resin flow. Tacky tape was used to minimize any undesired movement of the mats during the flow of resin and a rubber gasket was placed around the fibers to seal the mold. After that, spacer rings were placed to impose the desired thickness of the laminate and the mold was closed.

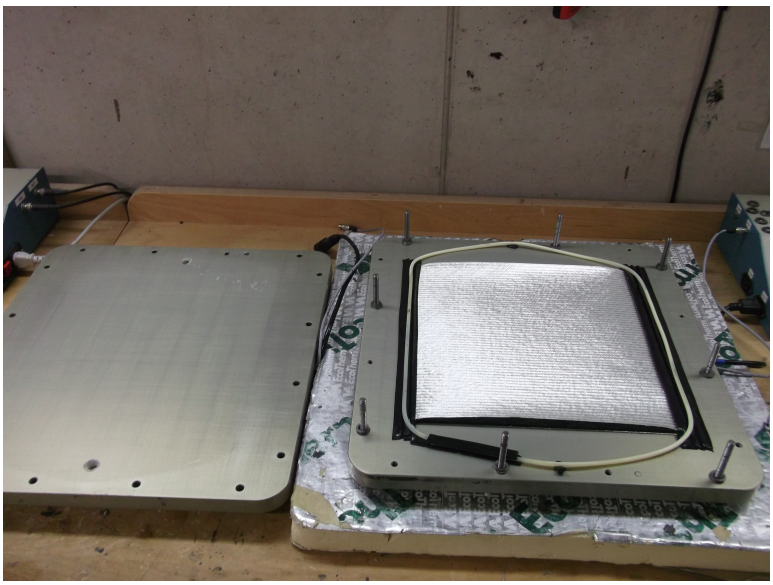

Figure 4.1: Mold ready to be closed. The fibers are placed, the rubber gasket seals the mold for vacuum and the spacer rings determine the final thickness of the laminate (WMC)

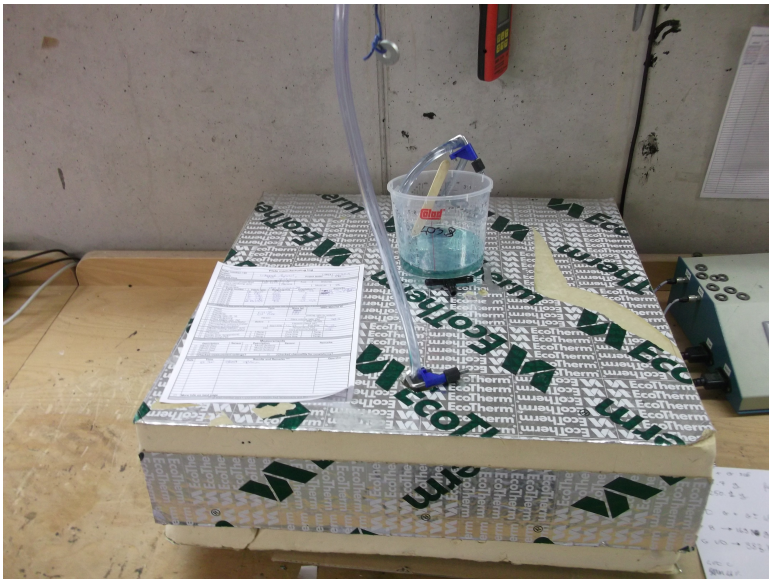

Figure 4.2: Infusion process. The inlet is connected to the resin pot, the outlet to the vacuum pump. The mold is inside an insulation box (WMC)

The upper half of the mold had one inlet and one outlet for the resin flow on either side of the fabric. First, resin and hardener were mixed with a weight ratio of 100:30; then, the mixture was degassed for 10-15 minutes at low absolute pressure, namely 10-20 mbar. After that, vacuum was applied to the mold by closing the inlet and applying the vacuum pump to the outlet. Once vacuum was obtained, the pot of resin was connected to the inlet and the resin was allowed to flow through the fibers inside the mold.

On the external sides of the mold a heating system was installed to heat the mold; this was necessary for the preheating during the infusion and for the curing. A temperature control system was used to control the temperature cycles and the ramp times.
In order to decrease resin viscosity, the mold was kept at constant temperature equal to 30 °C; this preheating was particularly necessary when the UD layers were purely made of carbon. Once the infusion was completed, the vacuum was taken off and a curing cycle was started at atmospheric pressure. The curing cycle consisted of 4 hours at 65 °C and 8 hours at 75 °C and is shown in Figure 4.3.

After that the curing cycle was completed, the plate could be tabbed and cut into several specimens. The tabbing material was 1 mm thick FR-4, which is a printed circuit board standard laminate composed of woven fiberglass cloth with an epoxy resin; the ±45 ° fibers are useful to well distribute the load during clamping. For one hybrid, aluminum tabs were used; this was

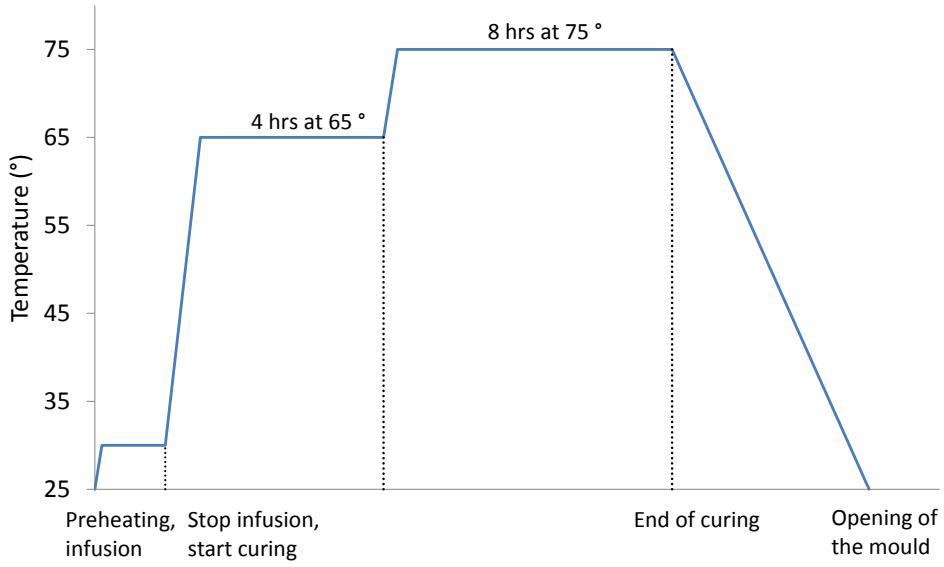

Figure 4.3: Temperature trend during infusion and curing cycle

necessary in fatigue tests to have better heat dissipation and better wear resistance.
Three small samples of approximately 6.25 cm^2 were always cut off from each plate to measure the fiber volume fraction. The procedure followed the standard ASTM D2584-08. The samples were put in an oven for few hours at high temperatures, 450 °C for carbon or hybrid samples and 565 °C for glass ones, to burn the resin. The weight difference determined the fiber volume fraction.

For all mechanical tests, two strain gauges were always glued on the gauge area of each specimen, one per side. The majority of them were axial strain gauges, so that only the stiffness and the maximum strains to failure could be detected; however, few cross gauges were also used to measure longitudinal and lateral strains and to calculate the Poisson's ratio.

4.3 Plates manufactured

Several plates were manufactured during this study. They were classified into pure glass laminates, hybrid laminates and carbon laminates. The next paragraphs describe them.

4.3.1 Common layup

A common layup was used for all the three classes: two skin layers of biaxial glass and four unidirectional layers in the core of the laminate.

$$[\pm 45, 0_2]_S$$

This layup was chosen for three main reasons. First of all, unidirectional materials are representative for the structural elements of a blade, namely the spar caps, where the most benefit from carbon is expected; therefore, UD dominated laminates were to be studied. However, WMC ran few experiments on pure carbon during Upwind that highlighted strong problems in characterizing pure UD carbon in fatigue. Basically, it was not possible to obtain valid failure modes because of failure under the tabs, and the experiments always returned very small stress and strain values. For this reason, external layers of biaxial glass were added; these layers allowed a better load distribution within the carbon layers, resulting in higher laminate strengths.
Secondly, this study included an evaluation of the different materials on a blade scale; the three materials needed to be substituted in the spar caps of a reference blade; as discussed in Paragraph 3.4, these structures are generally made not purely UD but with a percentage of off-axis fibers; the choice of this layup could make a comparison more accurate and closer to reality than pure UD laminates.
Finally, this study started with experiments on hybrids and the MSU/SNL database already had available data on this precise layup made of glass, namely material QQ1 (Mandell and Samborsky, 2010); this allowed for a first rough evaluation of the hybrid already after few weeks of testing.

4.3.2 Differences between the three laminates

The difference between the three classes of materials was in the composition of the unidirectional layers.
One layup had no carbon at all and was used as reference. Then two hybrids were created; the first group had alternating UD layers of carbon and glass and in this project was identified as “hybrid”; the second group of plates was also a hybrid but while the biaxial layers were still made of glass, the UD layers were pure carbon, hence it is here called “carbon” laminates. In the hybrid, the order of the UD layers was chosen to have alternate layers of carbon and glass. Table 4.3 shows the average relative percentages of the different components.

Class	Glass	Hybrid	Carbon
Layup	$[\pm 45_G, 0_{2G}]_S$	$[\pm 45_G, 0_C, 0_G]_S$	$[\pm 45_G, 0_{2C}]_S$
Density (kg/dm^3)	1.88	1.77	1.62
Volume of UD (%)	69.9	68.8	67.6
Weight of UD (%)	69.9	65.3	59.1
Volume of biax (%)	30.1	31.2	32.4
Weight of biax (%)	30.1	34.7	40.9
Volume of carbon (%)	0	32.6	67.6
Weight of carbon (%)	0	25.1	59.1

Table 4.3: Composition properties of the materials tested

4.3.3 Manufacturing process

For each material several plates were manufactured; however, not all of them could be used for testing. Due to infusion problems, some panels were produced with large void content, air bubbles and dry fibers; these problems arose in particular during the infusion of the carbon fabric. The few experimental results obtained from the samples that were cut from these plates were neglected. However, the failed infusion processes were useful to tune the manufacturing process parameters.
The characteristics of the good quality plates are listed in Table 4.4; the plates are classified per class and date of manufacturing. The names respect the WMC database classification.

Table 4.4 shows that the three classes of laminates had comparable thickness and values of fiber volume fraction ψ. At the beginning of the project it was indeed decided to manufacture all the plates with similar thickness to obtain a consistent comparison of the materials. However, the infusion process of the carbon layup highlighted strong problems: resin was not flowing properly and the quality of the resulting plates was affected by voids and dry fibers. This problem was already widely highlighted in literature, for example see (Mandell et al., 2002) or (Joosse et al., 2001a), and was confirmed in this study. The solution that was found was to either manufacture shorter carbon plates, namely 200 mm long and 320 mm wide, or to infuse panels with a thickness of approximately 4.50 mm and then, once all the fibers were wet, to lower the upper half mold by 0.2/0.3 mm.
From one side, these expedients only hid the infusibility problems and created doubts on the manufacturability of CFRP structures; on the other side, these properties belong to the manufacturing process and this project did not intend to analyze those aspects that are far from being dependent only on

Class	Plate	ψ (%)	Thickness (mm)
Glass	ST	49.1	4.29
	SZ	50.7	4.10
	TK	48.7	4.12
	TW	47.7	4.22
	Average	49.1	4.18
Hybrid	SH	50.2	4.01
	SK	48.7	4.05
	SP	48.9	4.04
	SW	49.7	3.98
	Average	49.4	4.02
Carbon	TI	48.6	4.02
	TJ	46.8	4.20
	TM	45.5	4.18
	TN	47.3	4.24
	TX	47.1	4.29
	UE	45.6	4.30
	UI	48.0	4.24
	Average	47.0	4.21

Table 4.4: ψ and average thickness of the plates manufactured

fiber volume fraction values. For example, at equal thickness resin flow is harder in carbon fabrics than in glass ones; however, carbon structures result to be thinner than glass ones with smaller volumes to be wet by resin. Moreover, during the infusion of large and thick structures many measures are generally taken to improve infusibility, like the use of peel plies as resin runners.

An interesting observation is that while the carbon laminates showed poor infusibility, the hybrid plates could be manufactured as the glass ones: probably, resin could flow through the glass fabrics and impregnate also the carbon layers more rapidly than in pure carbon laminates. As a consequence, during the manufacturing process it was not necessary to reduce the size of the fabrics to achieve a good flow of resin and all the plates could be produced 320 mm wide and 320 mm long like the pure glass ones.

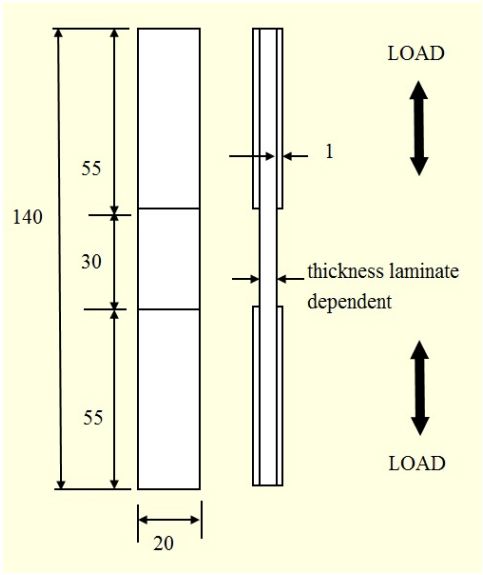

Figure 4.4: R09 dimensions in mm and load direction

4.4 Specimen geometries

Once the plates were manufactured and tabbed, the samples could be cut. The geometry of the specimen can strongly affect the experimental results and it is important to decide which one to use for the tests.
First, it was decided to use always the same geometry for all the three classes of materials tested. Then, geometry R09, which was developed internally by WMC researchers, was selected because it offers good performance in tension and compression both during static and fatigue tests. The geometrical characteristics of R09 samples are shown in Figure 4.4. All the static and fatigue tests were conducted on R09 coupons. R09 specimens were used also for the tests in transverse direction in respect to fibers orientation.

The only exceptions to geometry R09 were the specimens that had geometry I03 for static compression and 5 specimens per each class, so 15 in total, with platform I13 for shear tests.
Few tests were conducted following the standard ASTM D6641 that describes the procedure to characterize a material in axial compression. Specific specimens were cut with geometry I03, see Figure 4.5. These specimens were to be clamped inside a special fixture, see Figure 5.2a, and needed to be narrower and shorter than geometry R09; moreover, they did not used tabs. The fixture clamped the specimen on each side and the gauge length resulted to be only 12 mm to avoid buckling.
Finally, 15 specimens were used for shear tests to determine G_{12}, see Figure 4.6. The procedure followed the standard ASTM D7078. The specimens

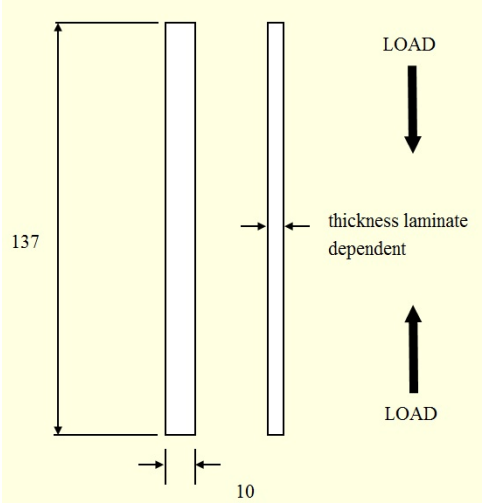

Figure 4.5: I03 dimensions in mm and load direction

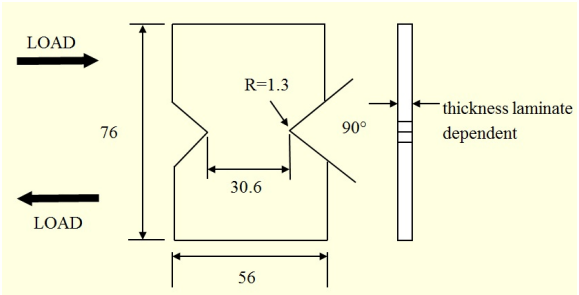

Figure 4.6: I13 dimensions in mm and load direction

were water jet cut and had V notches on the two sides; they were also tested in a special fixture shown in Figure 5.2b.

Before all the tests, each specimen was measured in several points to record thickness, width, gauge length and total length; from these values, the section and the gauge area could be determined as width times thickness and width times gauge length respectively.

Chapter 5

Testing

The testing procedure followed the WMC guidelines, the same that have been used for OptiDAT and Upwind and that are applied for industrial research. For static tests, these practical guidelines can be read in the standards from ASTM or GL; a wide theoretical background for fatigue tests can be found in Nijssen doctoral thesis (Nijssen, 2006).

During each test, different measurements were recorded. The force was measured through a load cell so that also the stress was known, namely the ratio of force to area expressed in MPa; moreover, the internal displacement of the machine and the strains were measured; finally, two temperature sensors were monitoring ambient and sample surface temperatures.

5.1 Testing equipment

The testing process lasted for approximately four months. For this reason, it was necessary to distribute the experiments on different machines based on their availability. Three servo-hydraulic test frames were used.

- MTS 100 kN
- Schenck 100 kN (3)
- ZB 250 kN

The first two machines used a 100 kN load cell, while the ZB 250 kN used a 250 kN cell. The ZB 250 kN was mainly used for carbon specimens when the required load to failure exceeded 100 kN.
An important parameter for each machine was the grip pressure; this value

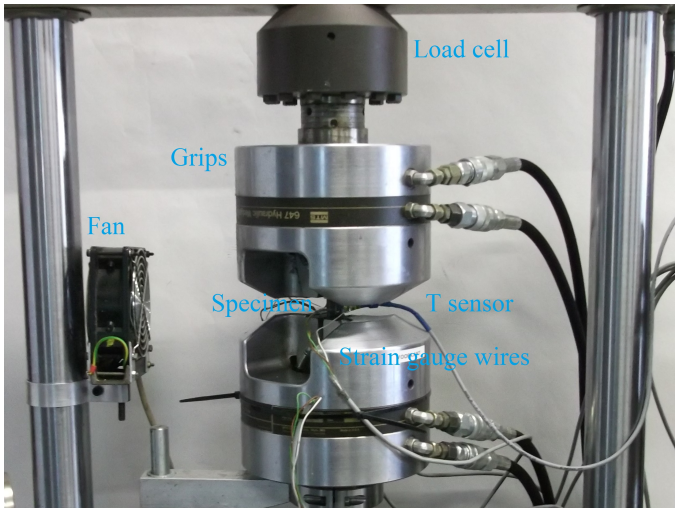

Figure 5.1: MTS 100 kN (WMC)

was set to avoid slipping but also excessive stress concentration; in practice, OptiDAT was used as reference.
Each machine was equipped with a control system, the data acquisition system and a fan to air cool the specimen during fatigue tests.

The compression dedicated tests used the special fixture described in the standard ASTM D6641, see Figure 5.2a: the samples were clamped in it and force was introduced by combined loading, shear from the sides and axial compression from top and bottom; the clamping pressure imposed the ratio between these two loads; the samples had a very small gauge length and did not suffer from buckling.
Finally, static shear tests were performed to determine the shear stiffness of the various materials thanks to the dedicated fixture described in the standard ASTM D7078 and shown in Figure 5.2b.

5.2 Static tests

Once the specimens were prepared and measured, the testing process began with static tests to characterize the material both in tension and compression. Static tests were displacement controlled tests where the displacement was imposed to the grips. The displacement rate was kept equal to 1 mm/min. During the static tests, maximum force and maximum displacement were measured; moreover, the strain gauges recorded longitudinal and lateral strains. From these values, the Young's modulus and the Poisson's ratio

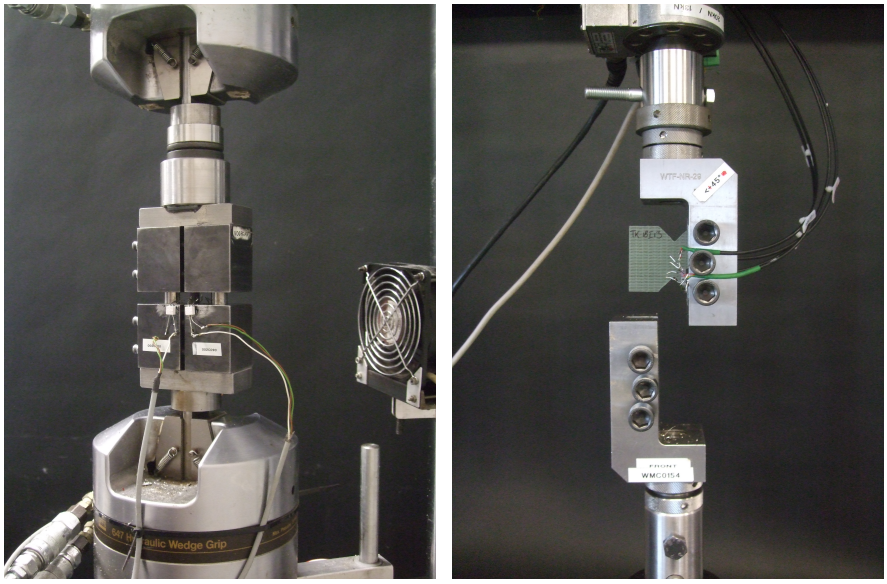

(a) ASTM D6641 compression setup (b) ASTM D7078 shear setup

Figure 5.2: Compression and shear test setups (WMC)

were calculated.

The majority of the tests were conducted on specimens with platform R09; in addition to these, compressive and shear dedicated tests were run with the special setups.

Static tests were crucial to set the first indicative values for the following fatigue tests.

5.3 Fatigue tests

Fatigue tests were load controlled tests. Fatigue resistance was tested simulating a fatigue load, which was represented by a sinusoid. The sinusoid was characterized by the maximum load and by the R-value, which is the ratio between minimum and maximum load.

$$R = \frac{F_{min}}{F_{max}} \tag{5.1}$$

The frequency of testing was determined by the temperature of the sample. The cyclic loading of a coupon leads to heating of the sample because of mechanical energy dissipation and heating from grip friction. High frequency

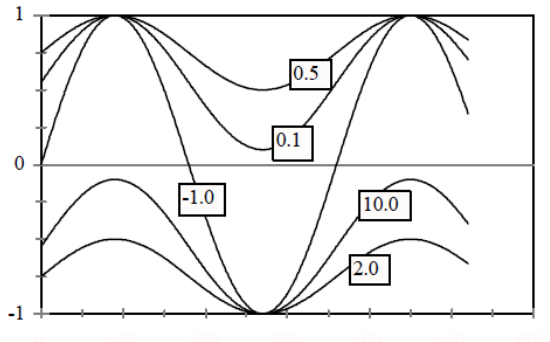

Figure 5.3: Different loading curves at different R-values

means shorter testing times but also higher temperatures. To avoid temperature effect upon the results, heat needs to be dissipated adequately by external cooling. A temperature sensor was always applied on the surface of the specimen, which was cooled by one or more fans; during tests on carbon an air conditioner was also often used. Only surface temperatures lower than 4 °C above ambient were allowed. The allowable frequencies resulted to be between 0.5 Hz for high loads in carbon samples up to 5 Hz for low loads in glass samples.

Fatigue tests started with a slow cycle to measure the strains in order to determine stiffness and Poisson's ratio; this slow cycle was performed up to + 3000 $\mu\epsilon$ in tension before R = 0.1 tests, down to −3000 $\mu\epsilon$ in compression before R = 10 tests and in both ranges before R = −1 tests. After the slow cycle, the cyclic load was applied and the cycle counter was started.

5.3.1 S–N curves

The results of the fatigue tests are shown on a double logarithmic S–N diagram, where S stands for maximum absolute stress σ (or strain ϵ) and N for the number of cycles to failure.
Fatigue tests were load controlled and hence stress representation was more immediate. Strain representation could also be done with initial strains, obtained as stress divided by Young's modulus, measured during the initial slow cycle. Due to stiffness degradation, stress representation appeared to be more correct (Nijssen, 2006); however, strain representation could provide useful indications.
Although N was the dependent variable, the number of cycles was represented on the x-axis. Nevertheless, the ordinary least squares regression algorithm used S as independent variable.

In this study, the S–N curves were formulated in a log–log form, also called

power law:

$$\log N = -m \cdot \log \frac{S}{b} \tag{5.2}$$

Where:
N is the number of cycles to failure
S is the maximum absolute stress (or max strain ϵ)
m is the slope
b is the intercept of the y-axis at N=1

Following the guidelines of Nijssen (2006), static tests were not included in fatigue calculations.

5.3.2 Constant life diagram

In addition to the S–N curves, a useful tool was used to show the fatigue behavior of a certain material: the constant life diagram (CLD). In this graph, the mean stress is on the x-axis, while the amplitude stress is on the y-axis; this means that the UTS and UCS points lay on the x-axis (zero stress amplitude), while the R = −1 points belong to the y-axis (zero mean stress). It is then possible to represent fatigue strength for different R-values and for constant N. The constant life lines connect points based on different R-value loads but with the same number of cycles to failure.
The constant life diagram can also be thought as a 3D diagram with the z-axis corresponding to the number of cycles. A schematic illustration is shown in Figure 5.4.

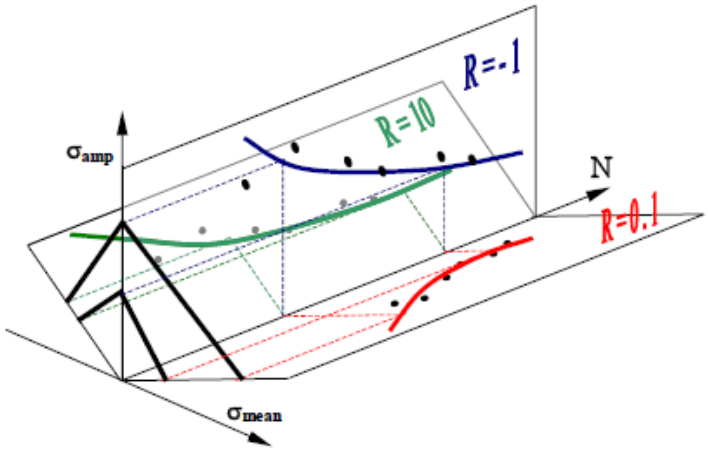

Figure 5.4: Illustrative 3D CLD diagram for three R-values (Nijssen, 2006)

In literature different CLD diagrams have been described (Nijssen, 2006).

The simplest one is the linear Goodman diagram where only the R = −1 and the static values are plotted on the y-axis and on the x-axis respectively; these points are then connected by straight lines.
This simple diagram can then be changed in different ways; for example, the GL standards prescribe to use a particular shifted linear Goodman diagram, described in Paragraph 9.4.1.
In Chapter 6, the multiple R-value CLD diagrams were used: the values were plotted for R equal to 0.1, −1 and 10 at N equal to 10^3, 10^4, 10^5 and 10^6. The points between the R-value lines were connected by straight lines.

Chapter 6

Experimental results

The summary of all the test results is here presented.
For the static results, four values are reported: the average $\bar{x}$, the estimation of the standard deviation based on a sample s, the coefficient of variation θ, which is the ratio of s to $\bar{x}$, and the number of valid tests #.
For the fatigue results, the slope of the S–N curve, the intercept b and the R squared value R^2 are shown for both stress and strain values; the parameter R^2 gives an indication of the variability of the data and of the "quality" of the regression: the closer R^2 to 1, better the fitting.
All the tests were conducted on R09 specimens, except where diversely specified.

The complete database of all the test results is available in the technical report from the Knowledge Centre WMC (Bortolotti, 2012).

6.1 Static tension and compression

6.1.1 Ultimate tensile strength

The ultimate strength values were measured both in UD fiber direction and in transverse direction. Table 6.1 reports the results of the tests performed in UD direction, while the results from transverse test can be consulted in Table 6.2.

UTS at 0°	$\overline{UTS}$ (MPa)	s (MPa)	θ (%)	#
Glass	764.97	17.98	2.35	6
Hybrid	885.70	30.51	3.44	7
Carbon	1176.55	23.84	2.03	6

Table 6.1: UTS results in UD fiber direction

UTS at 90°	$\overline{UTS}$ (MPa)	s (MPa)	θ (%)	#
Glass	136.86	6.95	5.08	3
Hybrid	108.00	5.67	5.25	3
Carbon	70.59	0.87	1.23	3

Table 6.2: UTS results in transverse direction

6.1.2 Ultimate compressive strength

The compression tests were run on both I03 and R09 specimens; the results are shown in Tables 6.3 and 6.4 respectively. The I03 samples returned higher values than tests on R09 samples primarily thanks to the shorter gauge section. R09 tests were though a useful indication for the following fatigue tests.

Several I03 tests were performed but invalid values were often found. This was because of failure under the grips and bottom or top crushing; it is notable that for the hybrid samples the invalid tests returned considerably better results than the valid ones, namely an average UCS value equal to -551.32 MPa, which means an improvement of 8 %. This was caused by non-homogeneous materials with gauge sections considerably stronger than gripping sections; it was then decided to include in the post-processing the invalid results for the hybrid layup.
Another important aspect is the high s and θ values detected in the I03

UCS at $0°, I03$	$\overline{UCS}$ (MPa)	s (MPa)	θ (%)	#
Glass	-666.76	34.31	5.15	6
Hybrid	-528.48	28.04	5.31	9
Carbon	-693.87	67.61	9.74	7

Table 6.3: UCS results in UD fiber direction on I03 samples

UCS at 0°, *R*09	$\overline{UCS}$ (MPa)	s (MPa)	θ (%)	#
Glass	−489.95	30.66	6.26	6
Hybrid	−488.68	25.17	5.15	7
Carbon	−594.69	22.87	3.85	8

Table 6.4: UCS results in UD fiber direction on R09 samples

UCS at 90°	$\overline{UCS}$ (MPa)	s (MPa)	θ (%)	#
Glass	−215.96	3.25	1.50	3
Hybrid	−189.19	1.22	0.64	3
Carbon	−163.56	2.85	1.74	3

Table 6.5: UCS results in transverse direction

tests on carbon samples, see Table 6.3: the large scatter had significant consequences in the characteristic values assumed during the blade design process, see Paragraph 9.2.

Tests were also run in transverse direction on R09 specimens. The results can be consulted in Table 6.5.

6.1.3 Ultimate tensile strain

Strains were measured with strain gauges placed in the middle of the gauge area of each sample, one per side. The majority of the strain gauges were single axial, so that only the longitudinal strains could be recorded; however, some cross gauges were also used to measure both longitudinal and transverse elongations.

During the static tests, maximum strains were recorded at failure. The results obtained during the tests performed in UD direction are shown in

UTϵ at 0°	$\overline{UT\epsilon}$ (%)	s (%)	θ (%)	#
Glass	2.89	0.08	2.77	4
Hybrid	1.57	0.06	3.82	6
Carbon	1.45	0.05	3.45	6

Table 6.6: UTϵ results in UD fiber direction

UCϵ at 0 °, I03	$\overline{UC\epsilon}$ (%)	s (%)	θ (%)	#
Glass	−2.29	0.09	3.93	6
Hybrid	−1.12	0.10	8.93	9
Carbon	−1.02	0.13	12.75	7

Table 6.7: UCϵ results in UD fiber direction on I03 samples

UCϵ at 0 °, R09	$\overline{UC\epsilon}$ (%)	s (%)	θ (%)	#
Glass	−1.46	0.14	9.59	6
Hybrid	−1.04	0.05	4.81	7
Carbon	−0.94	0.11	11.70	6

Table 6.8: UCϵ results in UD fiber direction on R09 samples

Table 6.6.

During transverse direction tests, strains to failure were also measured, but the maximum values were almost always inconsistent. The strain gauges were often running out of maximum measuring range or breaking before failure. As an indication, the maximum tensile strains were higher than 3 % for pure glass and higher than 2 % for hybrid and carbon laminates; the $\sigma_{22} - \epsilon_{22}$ curves were strongly non-linear for all the three laminates.

6.1.4 Ultimate compressive strain

Strains were measured also during compressive tests, see Tables 6.7 and 6.8 for results from I03 and R09 tests respectively. Again, larger scatter was found during tests on carbon samples compared to tests on glass samples; the hybrid coupons also showed significant dispersion in the data during I03 tests combined with several invalid tests.
In transverse direction the maximum strains were again inconsistent due to strong bending before failure.

6.1.5 Ultimate shear stress

Shear tests were performed following the standard ASTM D7078. Table 6.9 reports the experimental data of the ultimate shear stress USS; USS is the maximum of τ, the shear stress defined as ratio of transverse load to gauge area.

USS	$\overline{USS}$ (MPa)	s (MPa)	θ (%)	#
Glass	141.05	5.77	4.09	5
Hybrid	149.77	2.12	1.42	5
Carbon	137.48	4.55	3.31	5

Table 6.9: USS results

USϵ	$\overline{US\epsilon}$ (%)	s (%)	θ (%)	#
Glass	3.53	0.28	7.93	5
Hybrid	3.95	0.23	5.82	5
Carbon	3.07	0.16	5.21	5

Table 6.10: USϵ results

During the shear tests, two cross strain gauges were used on each sample; the elongation was measured at 45 ° and at 135 ° relatively to UD fiber direction on both sides. The $\tau - \epsilon$ curves resulted to be strongly nonlinear except for small strains, namely in the range 0 to $\pm$ 5000 $\mu\epsilon$.
Following the standard, the shear strains were calculated for front and back gauge areas as the sum of the absolute values of the strains at 45 ° and at 135 °; the maximum strains were recorded at maximum load. Table 6.10 shows the results.

6.2 Stiffness moduli and Poisson's ratio

The stiffness parameters that were calculated were longitudinal stiffness E_1, transverse stiffness E_2 and shear stiffness G_{12}. The longitudinal stiffness E_1 is the slope of the σ_{11}–ϵ_{11} curve, the transverse stiffness E_2 is the slope of the σ_{22}–ϵ_{22} curve and finally the shear stiffness G_{12} is the slope of the τ_{12}–ϵ_{12} curve. In Tables 6.11, 6.12 and 6.13 the respective results are shown.
These values were generally calculated in a strain range of 500 to 2500 $\mu\epsilon$ (0.05 % to 0.25 %), where stiffness was assumed to be linear. These strains were measured at the beginning of each static test or during an initial slow cycle performed before fatigue tests; small variations in the calculation range were sometimes necessary because of diverging signals between front and back strain gauges.

E_1	$\overline{E_1}$ (GPa)	s (GPa)	θ (%)	#
Glass	30.95	0.75	2.42	56
Hybrid	52.84	1.75	3.31	49
Carbon	73.58	2.53	3.44	80

Table 6.11: E_1 results

E_2	$\overline{E_2}$ (GPa)	s (GPa)	θ (%)	#
Glass	14.27	0.24	1.68	6
Hybrid	12.65	0.29	2.29	6
Carbon	9.70	0.27	2.78	6

Table 6.12: E_2 results

G_{12}	$\overline{G_{12}}$ (GPa)	s (GPa)	θ (%)	#
Glass	6.29	0.10	1.59	5
Hybrid	6.51	0.18	2.76	5
Carbon	6.37	0.22	3.45	5

Table 6.13: G_{12} results

ν_{12}	$\overline{\nu_{12}}$	s	θ (%)	#
Glass	0.374	0.018	4.81	11
Hybrid	0.430	0.016	3.72	6
Carbon	0.515	0.026	5.05	8

Table 6.14: ν_{12} results

The Poisson's ratio is the ratio of lateral strains to longitudinal strains. ν_{12} is the ratio of strains in direction 2, transverse to the fiber orientation, to strains in direction 1, the fiber direction. Like the Young's modulus, the Poisson's ratio was generally calculated between 500 and 2500 $\mu\epsilon$. Table 6.14 lists the results.

6.3 Fatigue

Fatigue tests were conducted at three R-values: 0.1, −1 and 10. For each value, different load levels were applied trying to obtain a well-defined curve approximately between 1000 and 1 million cycles. Outside this range two different problems generally arise: for N smaller than 1000 cycles the scatter is often very large and the points lie on a plateau, while for N bigger than 10^6 the testing time becomes excessively long. In this project, few tests had indeed to be considered run outs, which means tests were stopped before failure. Run out tests were considered in the regression and are shown in the S-N diagrams with an arrow pointing to higher N values.
Results are here presented with the slope m and the intercept b of the double logarithmic regression line from Equation 5.2; also, the R squared value (R^2) is indicated to show how well the line fitted the points. The regression line used N as dependent and σ or ϵ as independent variable.

6.3.1 Tension – tension R = 0.1

The results of the regression from R = 0.1 tests are reported in Table 6.15.

The tension – tension tests returned the most consistent results and showed the smallest scatter. From a stress point of view, the carbon laminate showed the best results. The hybrid samples also behaved well, while glass ones suffered the tensile fatigue loading. Figure 6.1 shows the three stress regression lines.

Looking at the strains, the hybrid samples returned the best behavior at high loads despite the stiff carbon fibers, but had a ϵ – N curve slightly steeper than the carbon one; therefore, at low loads the carbon laminate had the longest fatigue life. For small numbers of cycles, the strains of the three materials were almost all coincident; however, the S–N lines diverged and at high N the glass coupons had a significantly lower performance. Figure 6.2 shows the ϵ – N diagram.

R = 0.1	Stress regression			Strain regression			
	m	b (MPa)	R^2	m	b (%)	R^2	#
Glass	10.00	894.21	0.97	9.72	2.974	0.98	12
Hybrid	15.15	1293.15	0.73	14.99	2.419	0.75	11
Carbon	35.13	1120.91	0.85	28.50	1.622	0.71	6

Table 6.15: R = 0.1 results

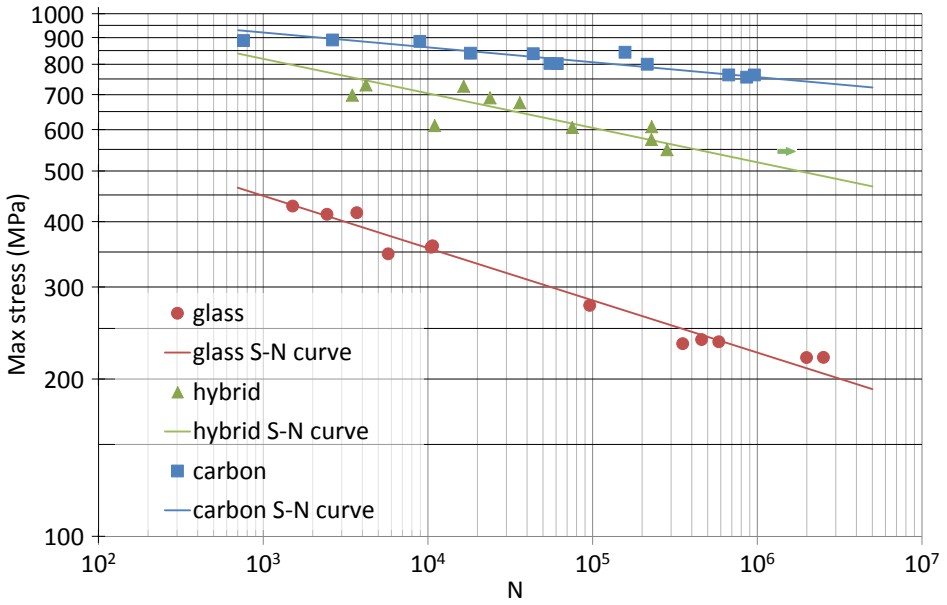

Figure 6.1: Stress diagram at $R = 0.1$

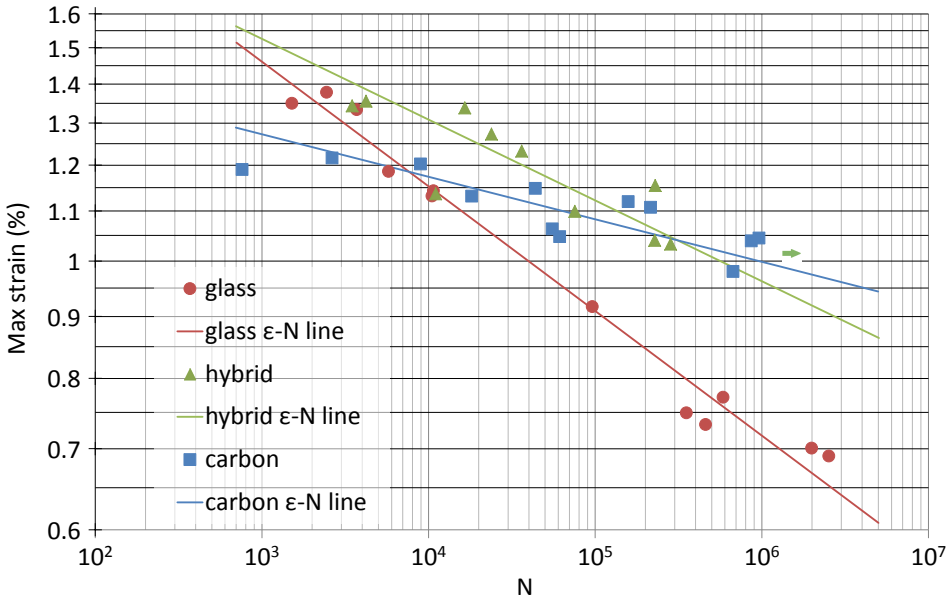

Figure 6.2: Strain diagram at $R = 0.1$

6.3.2 Tension – compression R = −1

As literature widely states, see for example (Nijssen, 2006), the R = −1 loading is the most critical case and leads to the lowest lines in the S–N diagrams.
In the tests performed during this project, the hybrid and carbon laminates behaved better than the pure glass layup from a stress point of view, see the lines in Figure 6.3, while worse from a strain point of view, see Figure 6.4. However, the fatigue slope value of the hybrid panel was much better than the pure glass one, see Table 6.16, and at high N the $\epsilon - N$ lines crossed.

Unfortunately, while the R = 0.1 tests ran quite smoothly, the tension – compression tests presented two serious problems. First, the characterization of both hybrid materials at R = −1 showed large scatter in the test results, particularly at high loads. Secondly, the carbon laminate could not be well tested in tension – compression due to failure of the tabs or failure under the tabs, in particular for high number of cycles tests. In practice, all these tests could be thought as run outs because they had to be stopped before failure of the gauge section. Therefore, it was decided to consider them in the regression. The regression line that was obtained was suspected to be too steep but it allowed a conservative blade design.
The preliminary failures of the carbon coupons could be reduced with aluminum tabs but could not be eliminated, as failure kept occurring in the bonding between tabs and laminate. The two solutions that could have been effective were thickness reduction of the carbon samples, in order to lower the loads required, or the use of a specimen geometry with larger grip sections; nevertheless, both solutions would have invalidated the comparison between the three materials and no thinner, longer or dog-bone shape specimens were manufactured.

In conclusion, the R = −1 S–N curve of the carbon layup is based on many invalid tests and is expected to be too steep. All the invalid/run out tests were included in the regression and are reported in the S–N diagrams shown in Figures 6.3 and 6.4 with empty squares.

R = −1	Stress regression			Strain regression			
	m	b (MPa)	R^2	m	b (%)	R^2	#
Glass	10.90	641.67	0.93	11.04	2.077	0.92	15
Hybrid	36.51	490.37	0.56	42.98	0.892	0.54	14
Carbon	16.18	839.94	0.62	14.99	1.210	0.63	20

Table 6.16: R = −1 results

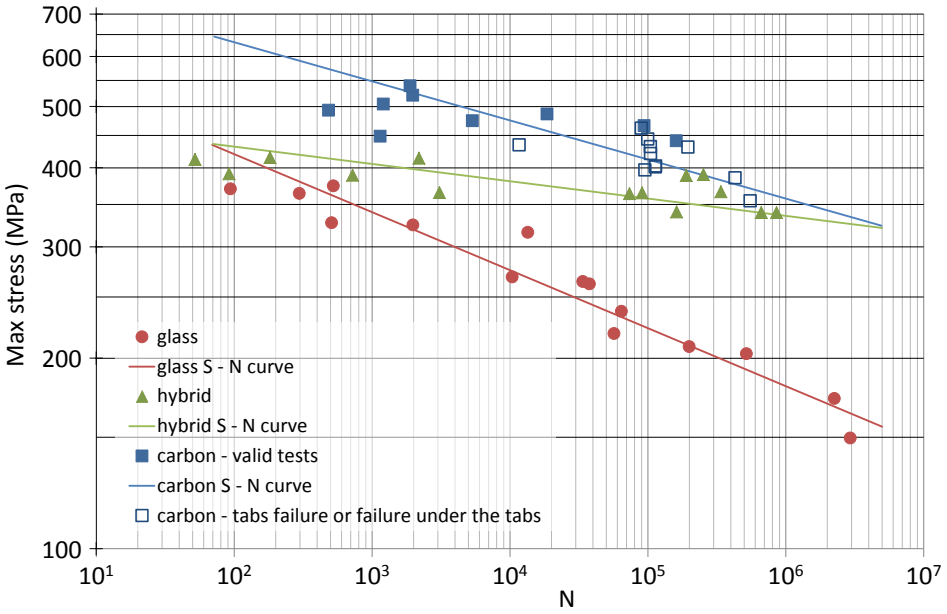

Figure 6.3: Stress diagram at $R = -1$

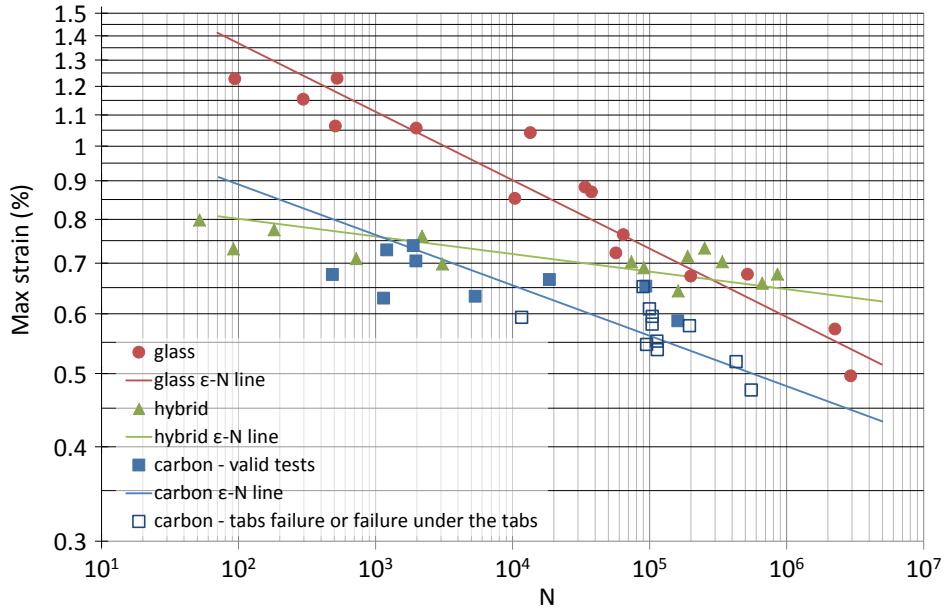

Figure 6.4: Strain diagram at $R = -1$

Based on these data, apparently the carbon laminate had better stress fatigue resistance compared to the hybrid laminate, but it allowed smaller strains. Glass showed the shortest fatigue lifetime with the lowest m slope values, but also the smallest scatter.

6.3.3 Compression – compression R = 10

As expected from literature, the compression – compression tests on the glass and hybrid laminates returned the flattest curves, which means highest m slope values. The regression parameters can be consulted in Table 6.17, while the lines are plotted in Figures 6.5 and 6.6.

Unfortunately, it was not possible to characterize the carbon laminate under pure compressive cyclic loading. Due to the very high fatigue resistance, at R = 10 the samples could reach failure only at stresses just below the UCS level, and small deviations in this value were causing large differences in N. This in turn caused a very large scatter because the uncertainty on UCS affected the uncertainty on fatigue lifetime. A regression S–N line could be obviously calculated but was practically meaningless: the R^2 value was approximately 0.3.

From a stress point of view, the experimental results show that the carbon laminate had anyway the best behavior, while the hybrid laminate returned promising values only at high numbers of cycles. Finally, the glass laminate proved to be compression fatigue resistant with a rather flat S–N line.

From a strain point of view, pure glass samples clearly had the best performance. The hybrid laminate showed significant lower allowable strains but a very flat S–N line. Finally, the carbon data lie on a wide plateau.

R = 10	Stress regression			Strain regression			
	m	b (MPa)	R^2	m	b (%)	R^2	#
Glass	20.11	701.29	0.68	20.26	2.210	0.69	9
Hybrid	85.51	482.70	0.82	84.23	0.930	0.78	9
Carbon	–	–	–	–	–	–	14

Table 6.17: R = 10 results

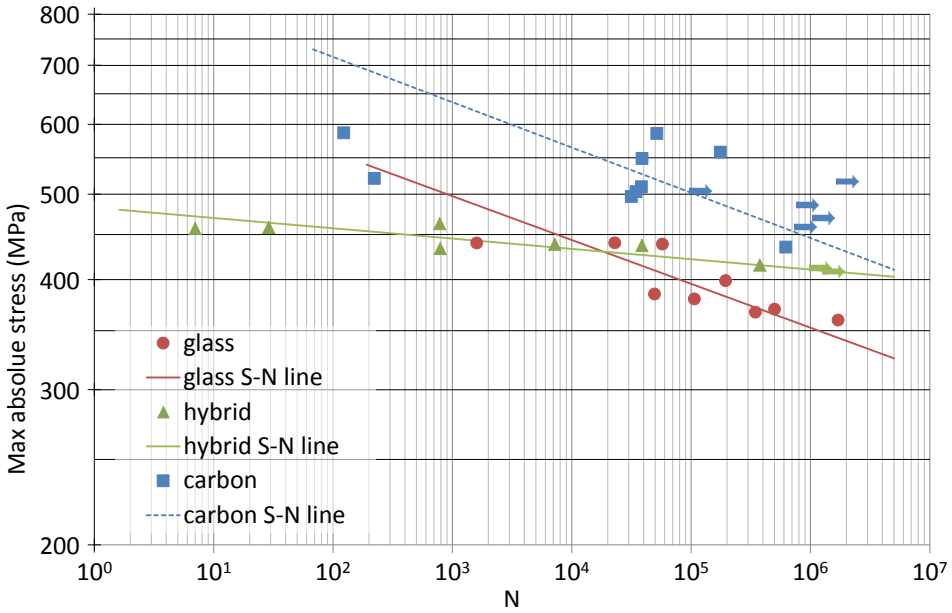

Figure 6.5: Stress diagram at $R = 10$

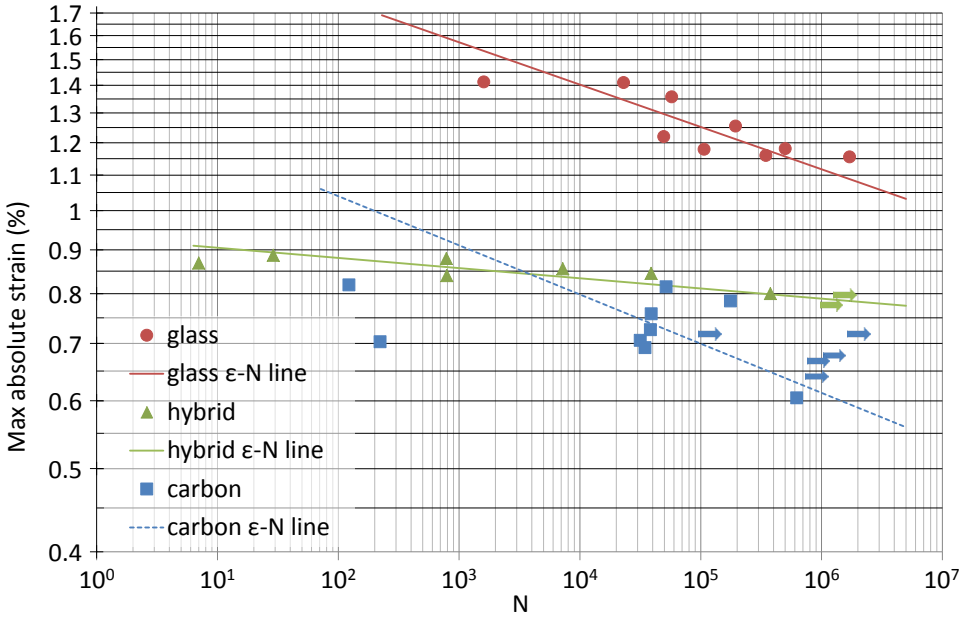

Figure 6.6: Strain diagram at $R = 10$

6.3.4 Constant life diagrams

The constant life diagrams were described in Section 5.3.2. In this project, it was decided to plot multiple R-value CLD with straight lines connecting from left to right: UCS, R=10 S–N line, R=−1 S–N line, R=0.1 S–N line and UTS. The UCS value was taken from tests on I03 samples. For the carbon laminate, it was decided to connect the UCS point to the R = −1 point with a straight line as in a linear Goodman diagram.
For clearness, three diagrams are plotted, one per laminate, see Figures 6.7, 6.8 and 6.9. In each graph, 4 lifetimes are shown: 10^3, 10^4, 10^5 and 10^6.
For negative mean stresses, it is easily visible that the three materials returned a comparable behavior at high loads; however, the different slope values made the glass laminate properties inferior at high cycles.
In tension, the performance of the hybrid and carbon panels was much better than the pure glass one for all the lifetimes; in particular, the carbon laminate produced very high lines.

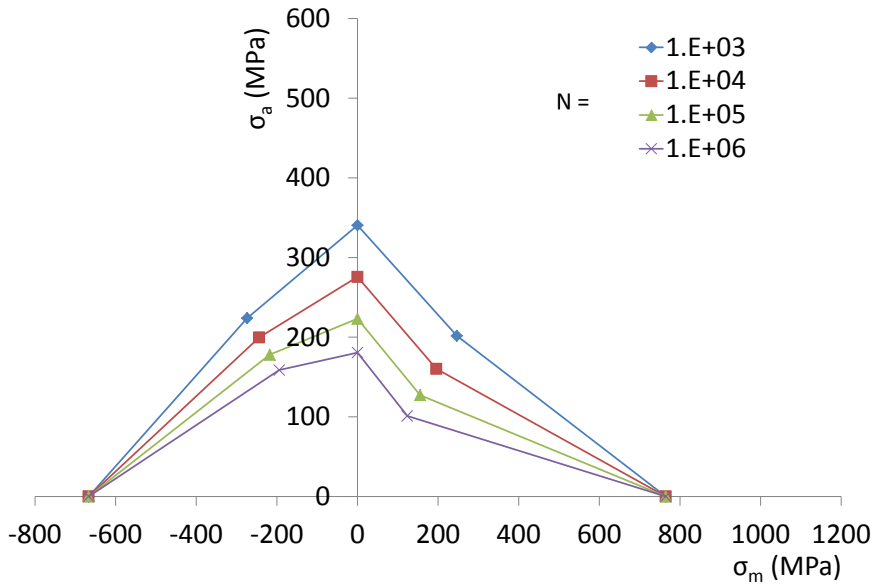

Figure 6.7: CLD diagram of the glass laminate

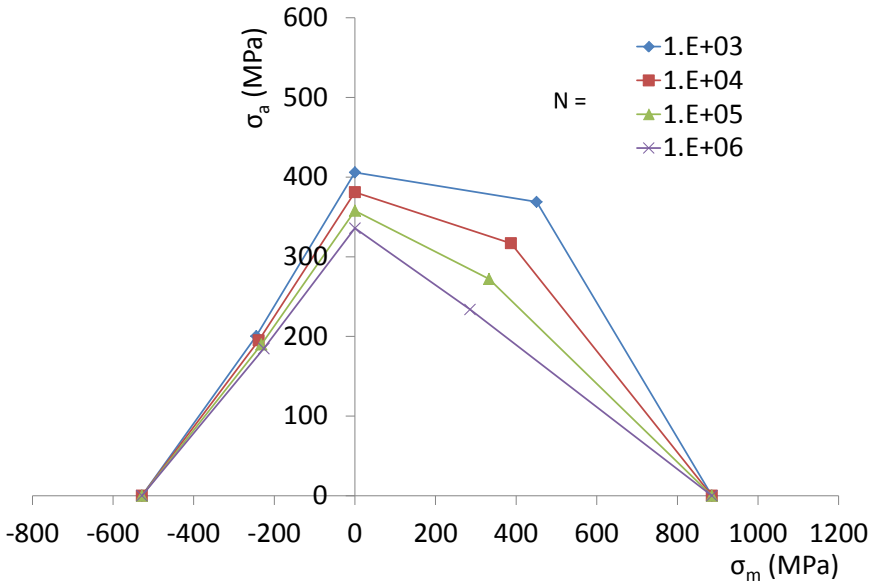

Figure 6.8: CLD diagram of the hybrid laminate

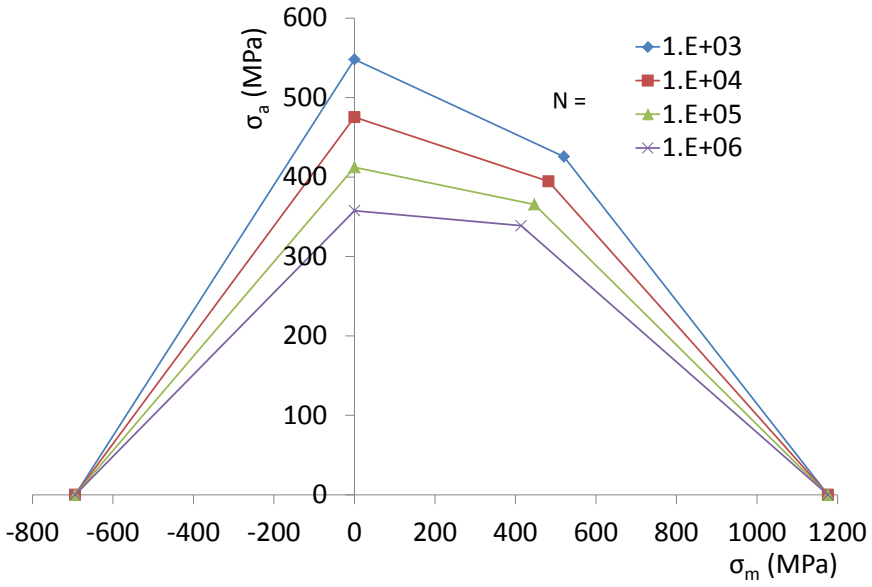

Figure 6.9: CLD diagram of the carbon laminate

Chapter 7

Analysis of the experimental results

The results obtained during the experimental phase of this project were presented in the previous chapter. Here, they are analyzed and discussed.

First, Section 7.1 deals with the static results and looks for an explanation to the positive hybrid effect that was detected. Later, Section 7.2 deals with the results about Young's modulus in longitudinal and transverse direction, shear stiffness and Poisson's ratio. Finally, Section 7.3 reports the analysis of the fatigue data and includes a comparison with the data present in the MSU/SNL database.

7.1 Static tension and compression

7.1.1 Tensile tests results

The tensile test results provided quite clear indications and as expected the carbon layup produced the best performance. The carbon samples were so strong that some tests had to be invalidated due to slipping of the tabs; it was found that aluminum tabs and a high grip pressure could help to reach failure in the gauge area.
Although the ultimate strains of the glass laminate were the highest, glass coupons returned the lowest values for UTS.
Finally, the static tensile results also showed a good behavior of the UD hybrid laminate: UTS did not follow the rule of mixture, but the UTS value of the hybrid material resulted to be higher than the glass layup one. This can be attributed to the sufficient fraction of carbon fibers present in the

hybrid layup, to the much higher tensile performance of the carbon fibers compared to the glass ones and to a positive hybrid effect. The ultimate strains of the hybrid coupons were indeed limited by carbon failure, but a gap was detected between the ultimate tensile strain UTϵ of the carbon and the hybrid laminates: the hybrid layup did not fail at a strain of 1.45 % as the carbon layup, but reached 1.57 %, that is an increment of 8.3 %.

Experimental UTϵ carbon laminate (%)	1.45
Expected UTϵ hybrid laminate (%)	1.45
Experimental UTϵ hybrid laminate (%)	1.57
Variation	**+8.3 %**

Table 7.1: Tensile hybrid effect due to glass carbon coexistence

It was not possible to provide a clear explanation to this effect and the hypotheses presented in Paragraph 2.5.2 were not convincing. On one side, the difference in thermal expansion coefficients (Bunsell and Harris, 1974) was not expected to influence the results because the curing temperature of the plates imposed during this project was relatively low; on the other side, the idea of high elongation fibers bridging low elongation ones (Kretsis, 1987) also appeared to be not applicable, particularly because this project studied interply laminates with discrete layers.
The most likely explanation to this hybrid effect was then that the presence of glass allowed a better infusion and the creation of higher quality laminates; this theory was supported by the better infusibility of the hybrid laminates compared to the carbon ones.
A further reason could have also been a poor adhesion between carbon and glass layers; this would have caused a lower sensitivity of the hybrid laminate to stress concentrations.

During the static tensile tests of the hybrid layup an interesting phenomenon sometimes also appeared. As static tests were displacement controlled, the coupons failed whenever the ultimate strain of carbon fibers was reached; however, at that strain glass fibers did not fail so that the fracture was only partial and the coupons were still able to withstand some load after failure. The residual force detected was well approximated by:

$$F = (\xi_{UD,glass} \cdot E_{UD,glass} \cdot UT\epsilon_{hybrid} + \xi_{biax} \cdot E_{biax} \cdot UT\epsilon_{hybrid}) \cdot Area$$

This behavior is shown in Figure 7.1 where several force – time curves from the hybrid coupons are reported together with a dashed line representing the force value assumed from the equation above. From the graph, it is visible that the force did not fall to zero after failure as it happened for all the glass and carbon specimens tested in static tension.

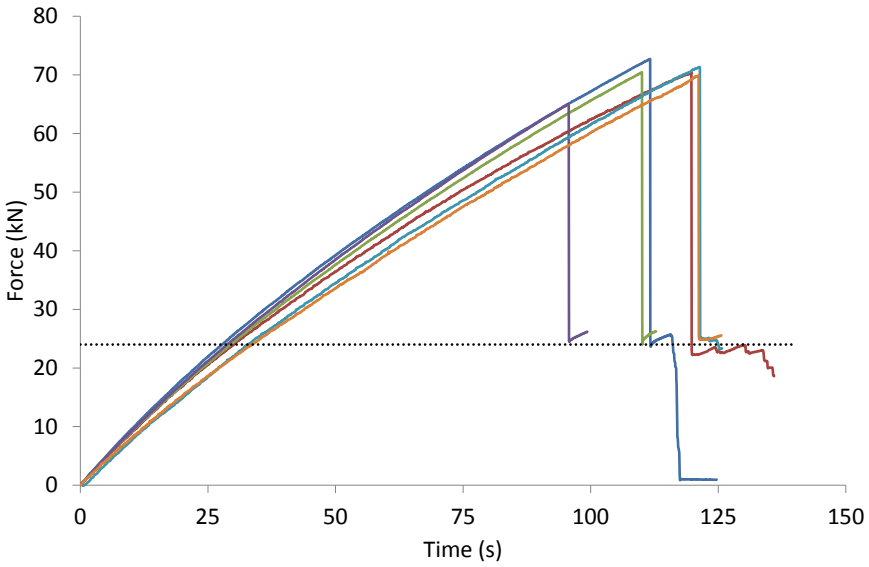

Figure 7.1: Partial failure of the hybrid coupons

7.1.2 Compressive tests results

The analysis of the static compressive results leads to more controversial considerations. The results of the static compressive tests can be consulted in Tables 6.3 and 6.4.
The carbon coupons returned again the best stress results, but the measurements were characterized by a high level of scatter. Glass samples had very good results from tests on the dedicated compression geometry I03, but mediocre ones from tests on the generic geometry R09. Finally, although the hybrid laminate showed compressive stress properties comparable to the glass laminate in tests on R09 samples, the tests with I03 samples produced values considerable lower than glass ones.
On a strain basis, the glass specimens produced the best results, followed by the hybrid and finally by the carbon coupons. Although not excellent, the hybrid and the carbon laminates returned quite good maximum strains to failure, above the 0.6 - 0.8 % level that was often detected by MSU research on infused laminates. As for the hybrid layup properties, a positive hybrid effect was again found for UCϵ, visible in the numbers reported in Table 7.2.

In this scenario, the carbon layup produced the best compressive properties. The biaxial layers of glass improved the compressive properties of pure UD carbon and their use appeared to be positive, at least for carbon experimental characterization. Unfortunately, although the average UCS was the highest, the large scatter that affected the results had negative consequences on the

	I03 tests	R09 tests
Experimental UCϵ carbon laminate (%)	−1.02	−0.94
Expected UTϵ hybrid laminate (%)	−1.02	−0.94
Experimental UTϵ hybrid laminate (%)	−1.12	−1.04
Variation	**+9.8 %**	**+10.6 %**

Table 7.2: Compressive hybrid effect due to glass carbon coexistence

characteristic values that could be assumed for the carbon laminate during the wind turbine blade design phase, described in Section 9.2.

On the other hand, despite the positive hybrid effect, the hybrid laminate did not sound promising for compressive properties. The compressive strength was limited by the maximum strain to failure of carbon fibers, and the small difference between the UCS of pure UD carbon and glass components made the overall performance of the hybrid laminate the lowest of the three, with a UCS from I03 tests equal to −528.48 MPa; this value resulted to be lower by 20.7 % compared to the glass laminate UCS and by 23.8 % compared to the carbon laminate UCS.

The partial failure phenomenon as described in the previous paragraph could theoretically also occur in hybrid samples, but in practice could not be detected because of catastrophic failures of carbon in the coupons.

To summarize, the external biaxial layers were found to be beneficial to characterize carbon in compression. The tests showed that the carbon layup had the best performance and although large scatter was present in the measurements, consistent values could be measured. The glass laminate also returned very good static compression results, while the hybrid coupons suffered from early failure and a comparison of data from I03 tests highlighted the weakness of the hybrid layup under compressive load states.

7.2 Stiffness moduli and Poisson's ratio

The most notable aspect regarding stiffness results was the higher longitudinal stiffness of the hybrid materials compared to the pure glass layup. This was as expected and was one of the main reasons to add carbon fibers between glass layers.

Nevertheless, the stiffness of all the three laminates studied in this project suffered from the significant presence of biaxial fibers. Stiffness could be well described by the ROM linear prediction and the Young's moduli of the three laminates were indeed lower than the ones from pure UD components. The

	Glass	Hybrid	Carbon
E_1 calculated (GPa)	30.79	51.43	73.58
E_1 measured (GPa)	30.95	52.84	73.46
Variation	**+0.5 %**	**+2.7 %**	**−0.2 %**

Table 7.3: Stiffness comparison

values for the single components, namely glass biax, glass UD and carbon UD, could be assumed from OptiDAT [1] and the calculated values were very close to the measured ones. Table 7.3 shows the minimal differences between the predicted and the measured values; in the hybrid laminate a small positive effect was present, but it was probably mainly caused by the slightly higher $\overline{\psi}$ of the hybrid laminate compared to the UD carbon values.

While longitudinal stiffness was significantly lowered by biaxial layers, the opposite happened for transverse and shear stiffness. As for transverse stiffness E_2, the glass laminate showed the best results thanks to the 8 % of 90 ° reinforcement fibers of the UD fabric; in the carbon fabric the fibers were 100 % UD oriented so that E_2 resulted to be lower; the hybrid laminate showed an intermediate value.

As for shear stiffness G_{xy}, very similar values between the three materials were found; shear was indeed dominated by the two biaxial skin layers that were common in all the three laminates.

Finally, the Poisson's ratio highlighted a significantly different behavior between carbon and glass FRP. When the carbon coupons were loaded longitudinally, they showed a strong contraction or expansion, for tension and compression respectively; for pure glass samples, this ratio was considerably lower, while for the hybrid laminate a trade-off was present. This behavior occurred because of the different ratios of transverse to longitudinal stiffness between the three layups.

7.3 Fatigue

Fatigue tests were conducted at three R-values. The behavior of the three materials for tension – tension, tension – compression and compression – compression loads was significantly different; the CLD diagrams of Figures 6.7, 6.8 and 6.9 show that clearly. From a general point of view, the carbon laminate behaved very well for tensile conditions or at high numbers of cycles,

[1] Glass biax: Panels KE-LH, E_1=11.60 GPa; Glass UD: Panels AO-BL-BS-BT-BU E_1=39.06 GPa; Carbon UD: Panel IH, E_1=103.29 GPa

while pure glass behaved well in compression but relatively poorly in tension. The hybrid laminate had properties closer to carbon than to glass in tension or at high cycles, while behaving poorly under high compressive loads.

7.3.1 Stress analysis

A stress analysis of the fatigue data highlighted that the carbon layup had the best results for all the loading cases, but showed very large scatter in presence of compressive loads. While for tension – tension cyclic loads the material response could be well described, the data at R equal to -1 and 10 showed large dispersion, see Figures 6.3 and 6.5. From the test results, no reliable estimate of the S–N curve could be made; however, the data could be used to make a conservative estimate.
For the tension – compression fatigue behavior, it was decided to assume a conservative regression line including all the invalid tests. As it is shown in Section 10.3, the carbon laminate returned anyway the best blade performance despite of the relatively small m slope value, and the conclusions about the blade design were not changed by the inclusion of the invalid test results.
For the compression – compression loads, it was not possible to obtain any consistent S–N line. The failure depended on the gap between the unknown UCS level of the coupon and the applied load; the very high fatigue resistance of the carbon laminate in compression made drawing a meaningful curve not possible. Nevertheless, as explained in Section 9.4.1, the slope and intercept values at $R = 10$ were not necessary for the blade design study.
Further research would be anyway necessary to better describe the carbon compressive behavior.

On the opposite, the glass laminate returned the worst fatigue resistance, particularly under tensile conditions, but with small scatter and well defined lifetimes. Moreover, while the gap between the glass and the carbon S–N lines in tension – tension tests was very wide, see Figure 6.1, in compression smaller differences were present, particularly at high loads, see Figure 6.5.

As for the hybrid laminate, the behavior was quite positive and was usually more similar to the carbon laminate one than to the glass laminate one. Furthermore, the experiments returned low scatter data and the fatigue lifetime could be sufficiently well predicted.
The absolute tension – tension stress values were lower than the carbon laminate ones, but returned a similar slope, see Table 6.15 and Figure 6.1. At $R = -1$, the gap between the stress curves was smaller and the slope of the hybrid laminate was even better than the carbon laminate one, see Table 6.16 and Figure 6.3. This could have happened both due to carbon testing

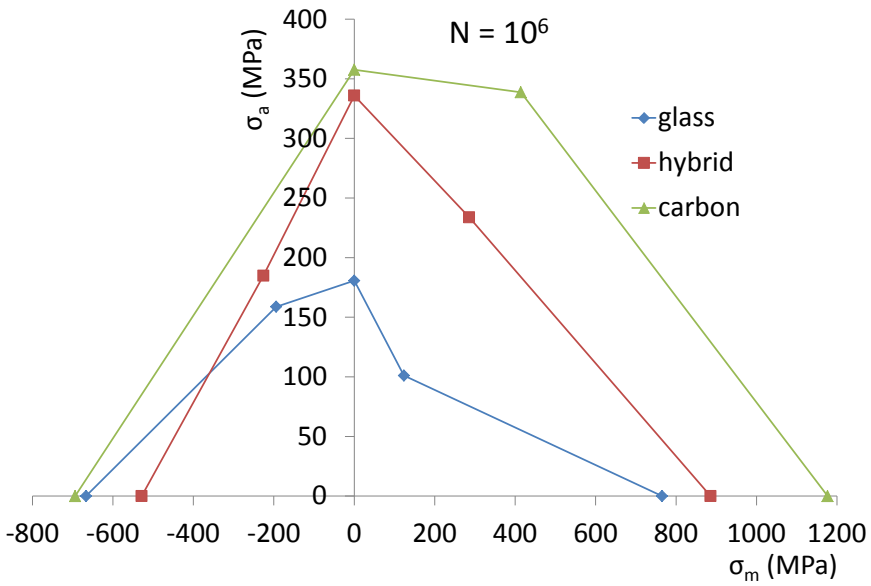

Figure 7.2: Comparison of fatigue lifetimes at N = 10^6

problems or thanks to a better quality of the hybrid laminate. Moreover, compared to the glass layup, the R = 0.1 and −1 stress S–N lines were much higher. Finally, at R = 10, although the fatigue behavior at high loads was poorer than glass, thanks to a much higher slope m the S–N line of the hybrid laminate crossed the glass laminate one between N equal to 10^4 and 10^5, see Figure 6.5. Hence, above approximately 10^5 cycles the hybrid layup behaved better than pure glass for all the three loading cases.

Figure 7.2 shows the CLD diagram with the comparison of the three materials at 10^6 cycles. The general higher performance of the hybrid and carbon laminates compared to the glass layup is clearly visible, particularly for positive mean stresses.

7.3.2 Strain analysis

Looking at the strains, the conclusions were different. Under compression – compression loads, the strains of the glass coupons were the highest of the three laminates, see Figure 6.6. However, this was not true for pure tensile conditions and for fully reversed loading, see Figures 6.2 and 6.4, where above a certain N the higher steepness of the glass laminate ϵ – N lines made the glass laminate lines crossing the hybrid laminate one. At R = −1, the line coming from the glass laminate data intercepted the hybrid laminate one at $3 \cdot 10^5$ cycles. At R = 0.1, the hybrid laminate line was always higher than the glass laminate one while the carbon laminate line crossed at N lower

than 10^4. Therefore, above these relatively small N values, the glass layup allowed lower strains than the other two laminates.

The analysis of the ϵ – N curves also showed how apparently the hybrid laminate fatigue line was not limited by the strain curve of carbon layers at low cycles and by the one of glass layers at high N, as predicted by MSU researchers and shown in Figure 2.4 (Mandell et al., 2002). The results that were obtained in this project showed that at least for tensile – tensile conditions the hybrid layup enhanced the maximum strains of pure glass, see Figure 6.2.
This phenomenon could have had different explanations. One hypothesis was the different stiffness degradation between glass and carbon fibers. However, UD FRP are not expected to experience significant stiffness degradation, namely no more than 1-2 % (Eliopoulos and Philippidis, 2011). Then, the second possibility was that the carbon layers withstood the large majority of the load and glass experienced only partial failure; this means that although pure glass samples were not able to survive these high strains for such large N values, the presence of carbon fibers could reduce damage progression. It is nevertheless to be noted that carbon layers would have not been able to withstand the whole force without any help from glass; glass layers were indeed withstanding a percentage of the load.
Stiffness degradation tests are being currently performed in WMC with traditional strain gauges and with innovative optical techniques; therefore, new experimental data will be available in the future and are likely to contribute to explain this positive hybrid behavior.

In conclusion, the carbon laminate produced the best results, particularly under tension – tension fatigue, but showed very large scatter under compressive loading. The hybrid laminate also behaved well in tension, returning a ϵ – N curve higher than the glass laminate curve; this was likely to occur thanks to some kind of damage inhibition at micro or macro scale. Under compression – compression cyclic states, the three materials behaved in a comparable way at high loads but showed different slopes of the S–N lines, with the hybrid and carbon panels being flatter than glass. Finally, the $R = -1$ fatigue tests returned carbon and hybrid laminates superior performance, particularly at high cycles.

7.3.3 Comparison with MSU materials

To conclude the analysis of the fatigue data, a short comparison with the material tested in MSU was performed.

One of most important material at the beginning of this project was the glass laminate QQ1 from MSU/SNL database (Mandell and Samborsky, 2010).

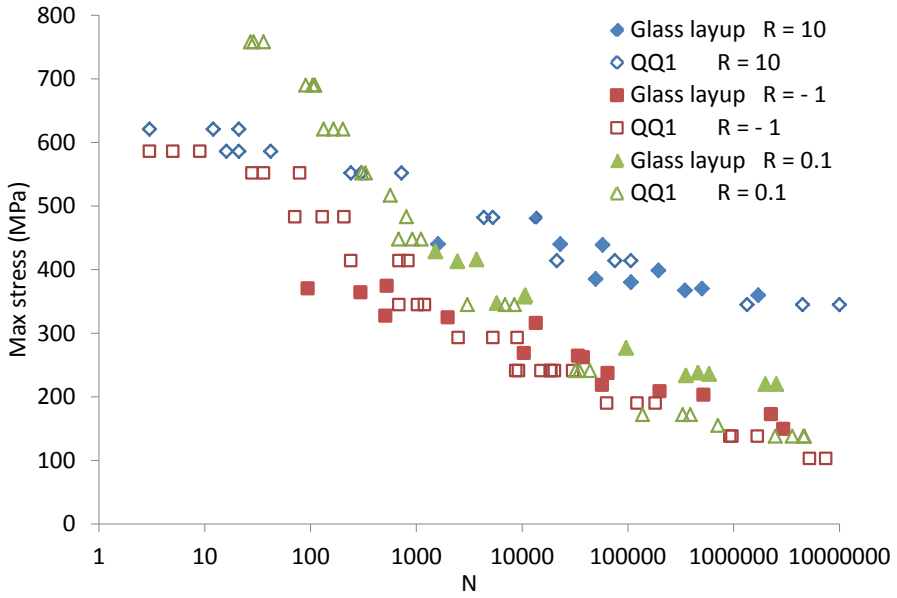

Figure 7.3: Comparison between the glass laminate and the glass material QQ1 from MSU/SNL database (Mandell and Samborsky, 2010)

Having the same layup as the laminates tested in this study, it was a useful reference to evaluate the performance of the three materials.
In respect to the glass composite of this project, QQ1 behaved in a comparable way for R = 10, but showed a lower performance during tensile fatigue tests; hence, at R= -1 and R = 0.1 the glass laminate curves were better, see the diagram in Figure 7.3. The slope m for R = 0.1 of material QQ1 was equal to 6.34 while in this project was found to be 10.00. This could have been caused by different fibers, a different architecture of the fabrics or by the different geometry of the samples.

Although no useful materials could be found to compare the hybrid laminates, an indicative comparison could be established between the carbon laminate and the triax material SN5-022X (Griffin and Ashwill, 2009). Both materials had comparable ξ of UD carbon and biaxial glass, 68/32 and 75/25 respectively, and an epoxy matrix.
The static properties of SN5-022X resulted to be significantly better than the carbon laminate, particularly in compression; for example, the UCϵ of SN5-022X was -1.32 %, while the carbon failed at -0.94 % in the tests performed during this project. Moreover, the SN5-022X showed a slightly higher stiffness thanks to the higher fraction of carbon fibers.
On the other side, the fatigue properties of the carbon laminate proved to be comparable to those of the SN5-022X material. The graph in Figure 7.4

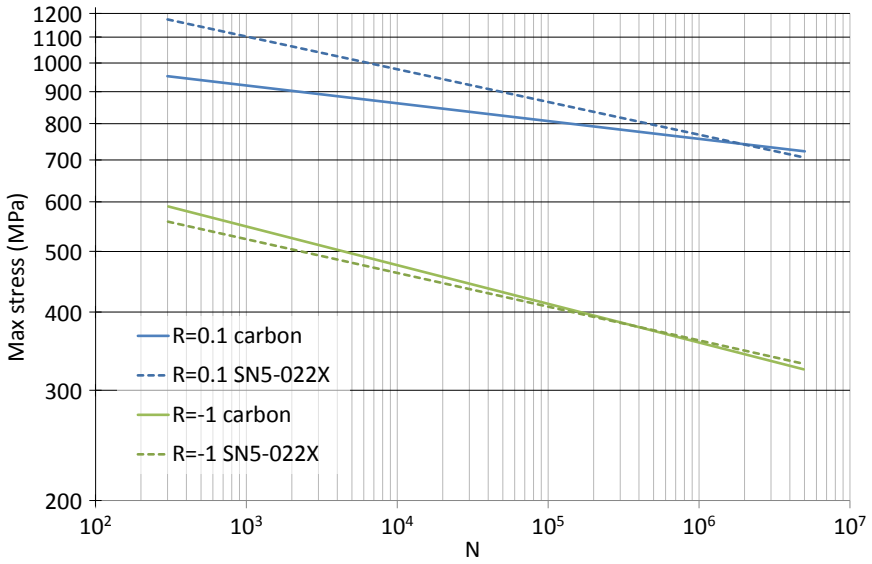

Figure 7.4: Comparison of fatigue behavior between the carbon and the SN5-022X laminates

shows how the two S–N lines at R = −1 had a similar slope m, despite the conservative assumptions taken during the regression calculation, see Section 6.3. At R = 0.1, the carbon laminate showed an S–N line flatter but lower than the SN5-022X one.
In conclusion, the carbon laminate studied in this project produced lower performance in static tests but a comparable behavior under fatigue loading.

Part III

Blade modeling

Chapter 8

Upwind turbine and blade models

In this project several blade models were designed to evaluate the potential of hybrid composites compared to pure carbon and glass laminates by comparison on cost and weight on a blade scale. Using the wind turbine design dedicated software package Focus 6, the three layups could be substituted in the spar caps and in the trailing edge reinforcement of the 5 MW blade model developed during Upwind.
This chapter presents the description of the turbine and blade models.

8.1 Turbine model

During different research programs some computational turbine models were developed as a reference. During Upwind a 5 MW turbine was intensively studied (Jonkman et al., 2007). The characteristics are listed in Table 8.1.

8.2 Blade model

The turbine model was provided with a blade model based on the baseline of the 61.5 meter long commercial blade LM61.5. LM WindPower provided the bending stiffness distribution to the Upwind participants, while keeping the structural layup confidential. Using the Focus 6 software package, WMC scientists developed a blade structure to achieve the same deflections (Nijssen et al., 2007) and performed an upscaling study together with ECN (Peeringa et al., 2011). This 5 MW computational blade model is publicly available in

Rating	5 MW
Rotor orientation, configuration	Upwind, 3 blades
IEC class	II B
Control	Variable speed, collective pitch
Drive train	High-speed, Multiple-stage gearbox
Rotor diameter (m)	129
Hub diameter (m)	4
Cut in wind speed (m/s)	4
Cut out wind speed (m/s)	25
Rotor speed (rpm)	12.1
Cone angle (°)	−2.5
Rotor tilt (°)	5

Table 8.1: Upwind turbine model properties

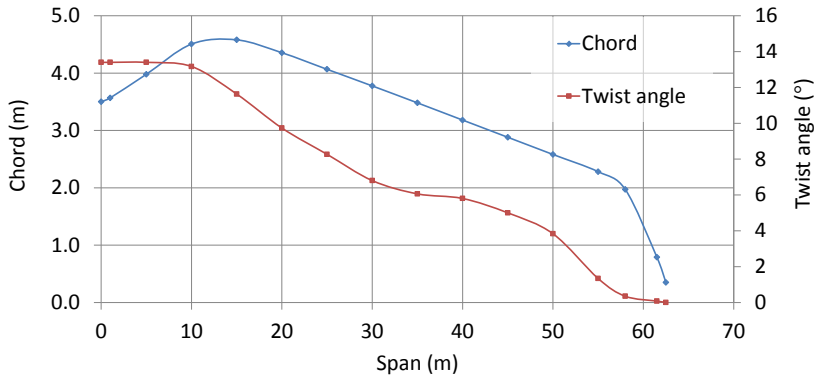

Figure 8.1: Chord and twist distribution of the Upwind 5 MW blade

the software package Focus 6 and was used in this project to evaluate the different materials.

8.2.1 Blade geometry

The blade has a mass of 21478 kg and a span of 62.5 meters; the core structure is made of two spar caps and two stiffeners. The section varies along the span from the circular root to thinner airfoils towards the tip. The maximum chord location is at a span of 12 meters. The chord and twist distributions of the blade are reported in the diagram of Figure 8.1 while the several airfoils used along the span are shown in Figure 8.2.

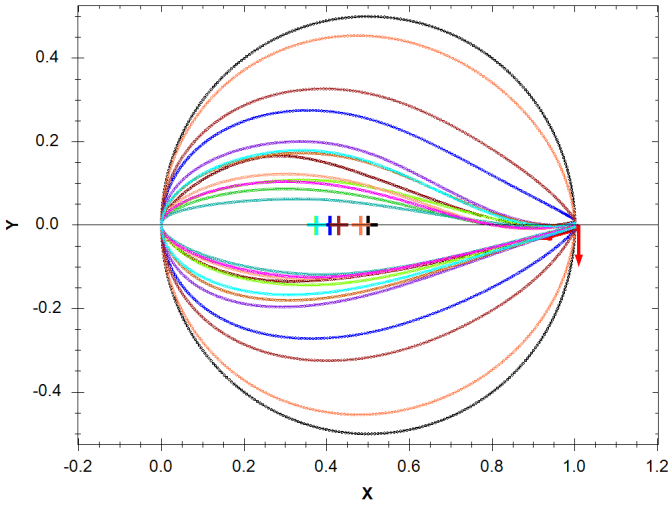

Figure 8.2: Airfoils of the Upwind 5 MW blade (FOCUS6)

The blade has two spar caps with variable thickness but constant width equal to 75 cm; they run from a span of 1.5 m to a span of 58 m. The load carrying beam is completed by two stiffeners at the edges of the spar caps. The blade has four elements mainly made of unidirectional material: the two spar caps and two reinforcements at the trailing edge near the root, one on the pressure side and one on the suction side. The thickness profile of these four elements is shown in Figure 8.3: the spar caps have a large variation of thickness along the span with few layers of fabric starting at the root, maximum thickness at a span of 12 meters (rotor radius equal to 14 m), almost constant profile until a span of 50 m and then rapid reduction up to a span of 58 m, where the spar caps end. The reinforcement at the trailing edge runs from a span of 1.5 m to a span of 25 m, it has a maximum thickness of 25 mm and is 60 cm wide.

The UD material is not pure but is a mixture of approximately 90 % UD fibers and 10 % biaxial fibers. The mechanical characteristics are listed in Table 8.2. Compared to the values of Table 3.2, it is clear how the properties assumed during Upwind are different; the spar caps mixture is much closer to a pure UD material than a MD material: E_x higher but G_{xy} lower; this results in a

E_x (GPa)	E_y (GPa)	G_{xy} (GPa)	ν_{xy}	UTS (MPa)	UCS (MPa)
38.90	9.00	3.60	0.249	706	498

Table 8.2: Mechanical properties of the spar caps and trailing edge reinforcement mixture of the Upwind 5 MW blade

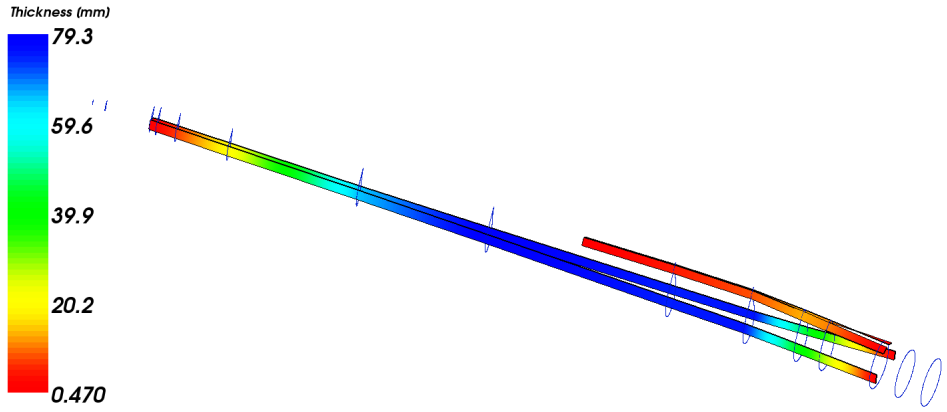

Figure 8.3: Spar caps and trailing edge reinforcement of the Upwind 5 MW blade (FOCUS6)

stiffer blade in flatwise direction. The strength values are the characteristic values as prescribed by the international standards of Germanischer Lloyd.

The rest of the blade is composed by different elements:

- the shell is composed by a sandwich structure made of two skins of triaxial glass and foam cubes in the core;
- the two stiffeners are made in a similar way, but the skin is made of pure biaxial glass;
- the tip of the blade is made of skin layers of triaxial laminate;
- the root is modeled as a rigid body made of steel for the hub connection and a thick layer of triaxial for the transition towards the structure made of inner box and external shell.

The mass distribution of the blade is shown in Figure 8.4.

8.2.2 Load cases

The mechanical behavior of the blade was studied simulating some standard loads and analyzing the response of the blade. The Upwind 5 MW blade was designed to undergo 20 years of lifetime under the loads prescribed by the GL standards. The standards schedule a long list of occurring loads divided in two large categories: extreme and fatigue. The first class encloses the load cases to verify the ultimate strength of the structure, while the second group includes all the loads to assess fatigue resistance.

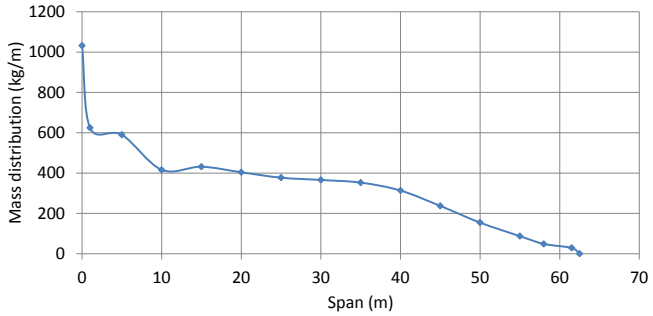

Figure 8.4: Mass distribution of the Upwind 5 MW blade

A turbine of class II B is assumed to experience a Weibull wind speed distribution with shape parameter equal to 2 and wind shear exponent equal to 0.2.

Class	II B
Characteristic site type	Coastal
Average wind speed at hub height (m/s)	8.5
50 years wind speed (m/s)	42.5
Turbulence intensity at 15 m/s	0.14

Table 8.3: Class II B characteristics (IEC 61400-1)

All the load cases were modeled during Upwind. The manual of Phatas from ECN provides a full classification of all the load cases (Lindenburg, 2005).

8.2.3 Bending stiffness

One crucial parameter during blade design is the maximum tip deflection in x-direction towards the tower. The simulations of the 5 MW blade returned the critical extreme load cases 1641, 1651, 3260 and 4260.

The load cases 1641 and 1651 represent the 50-year extreme operating gust, namely the wind gust that has a return time of 50 years, occurring while the turbine is operating at rated power; the two load cases differ for the average wind speed. During 1641 and 1651 the turbine has a yaw error. The yaw is the angle between the horizontal axis of the rotor and the direction of the wind; a yaw error means that the blade is not facing the wind perpendicularly. The load case 3260 simulates the occurrence of a 1-year extreme operating gust interfering with the start procedure. In 4260 the gust interferes with a stop procedure.

The maximum tip deflections towards the tower are listed in Table 8.4.

Load case	Tip deflection (m)
1641	10.35
1651	9.87
3260	9.84
4260	9.35

Table 8.4: Maximum tip deflections during extreme loads of the Upwind 5 MW blade

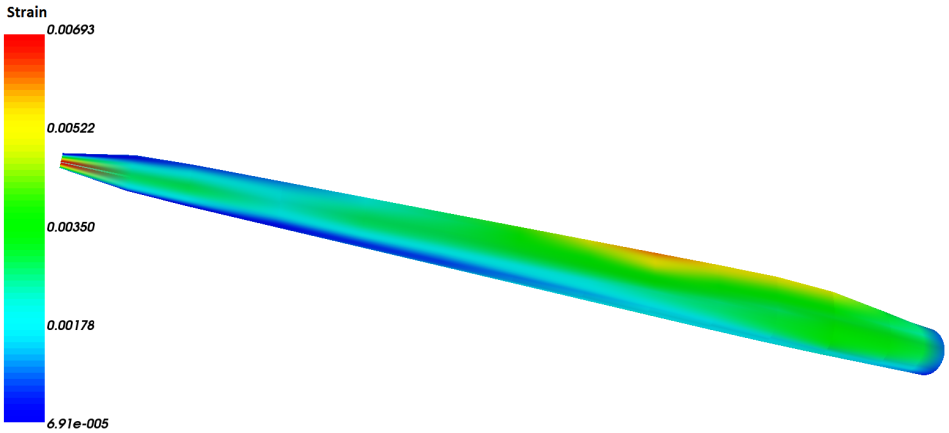

Figure 8.5: Strain field along the 5 MW Upwind blade (FOCUS6)

So, the blade had a maximum allowable tip deflection of 10.35 meters. This value had to be respected when changes were applied to the blade design.

8.2.4 Strength

Considering the extreme load cases, also a structural strength analysis was performed to calculate the maximum strains occurring in different sections of the blade and in different points for each section. This gave the possibility to have a clear visualization of the strain fields along the whole blade and to achieve an efficient design. Each load case gave a different strain distribution, but a representation with the absolute maximum strains could also be plotted, see Figure 8.5.
The maximum strains occurred at the tip and along the trailing edge near the maximum chord location; the trailing edge strains caused the need for a UD reinforcement. At the tip, the strains were artificially high due to unrealistic modeling of the tip structure.

8.2.5 Fatigue

Another strong driver to design the blade was fatigue resistance; the blade needed to fulfill its target lifetime of 20 years and the structure was designed for this. In the blade, each material was characterized by a fatigue slope parameter m and a simplified constant life diagram (CLD) defined in the GL standards, see Paragraph 9.4.1.
The CLD diagrams allow calculating the equivalent load, which is the load at a given R-value that gives the same relative damage as the load considered at another R-value. This is necessary to simulate the damage induced on a structure by real loads that vary with time.
Thanks to the m slope parameter, to the strains coming from the structural analysis and to the occurrence of the different load cases, the relative damage D for each point of the structure could be obtained. D was assumed to accumulate linearly according to the Miner's rule.

$$D = \sum \frac{n_i}{N_i}$$

Where n is the effective number of cycles of the equivalent load obtained from the load cases and the CLD diagram, and N is the number of cycles to failure of the equivalent load obtained from the S-N curves and the CLD diagram.

In a material, D needs to be smaller than 1 to achieve its target lifetime. In Focus 6, the visualization uses the fatigue stress factor (FSF); FSF uses the same concept of D but is the ratio of stress to failure to actual stress. Hence, the whole blade was designed to have all the points with FSF higher than 1.

$$FSF = \sum \frac{S_i}{s_i}$$

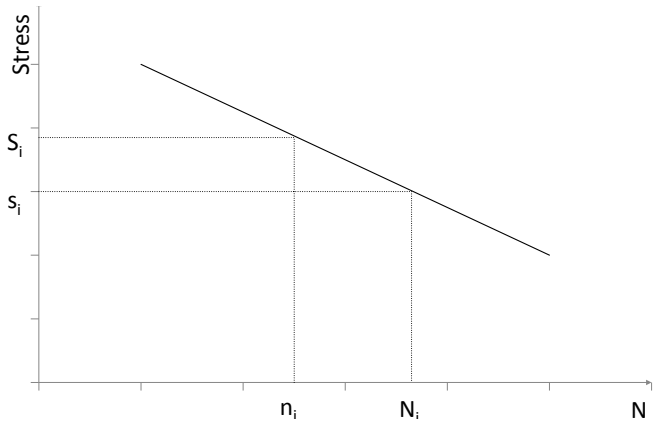

Figure 8.6: Relative damage D and fatigue safety factor FSF

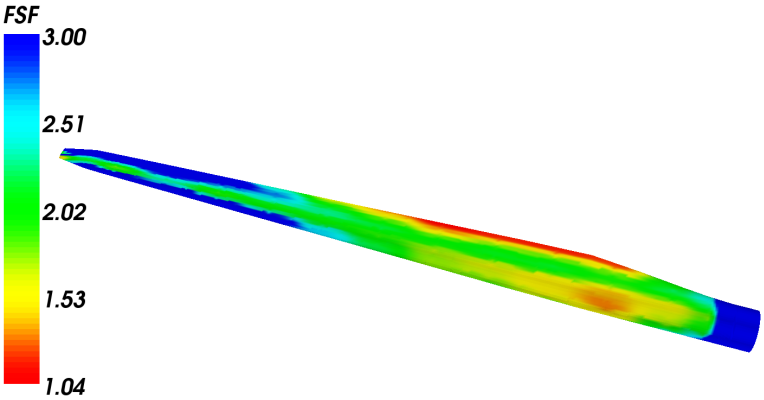

Figure 8.7: Fatigue safety factor field along the 5 MW Upwind blade (FOCUS6)

Therefore, the goal of the new design process was to reach a minimum FSF higher than 1.
During Upwind, the blade was optimized for fatigue and Figure 8.7 shows the FSF trend. The weakest areas were close to the root and corresponded to leading and trailing edges, with the latter having the FSF values very close to unity.

8.2.6 Buckling

An additional analysis that was made was resistance to buckling. Different elements are subjected to compression loads in a wind turbine blade and this leads to buckling phenomena. The parts of the structure that are mostly subjected to buckling are the sandwich panels of the shell, which are often wide and thin panels without structural supports.
In blades made of glass, the spar caps are very thick elements that do not present problems for buckling. This might not be true for carbon spars that, thanks to the higher stiffness modulus, can be made very thin.

Focus 6 provides a specific calculation step to verify structure resistance to buckling. The 5 MW reference blade model developed during Upwind and used in this project had not been fully optimized for buckling but fulfilled the analysis. The most critical panels were at a span of 17 m and at 57 m both on the suction side towards the trailing edge; those panels were particularly wide and thus sensitive to buckling. The spar caps did not show any problem.

Chapter 9

Blade design

This chapter explains the procedure that was adopted to design the new blade models. Particularly, Section 9.1 explains the design guidelines, while Sections 9.2 and 9.3 the characteristic values and the safety factors prescribed by the GL standards for the mechanical properties of the laminates. Then, Section 9.4 explains the fatigue analysis that Focus 6 performs. Finally, Section 9.5 lists the materials costs that were assumed during the simulations.

9.1 Design procedure

The design process followed the same procedure for all the four designs created during this project; the flowchart in Figure 9.1 illustrates it. As the original layup, the blade was first optimized for bending stiffness, then for buckling resistance and finally for fatigue resistance.
As first step, an iterative process looked for the best thickness distribution of the spar caps that could ensure tip deflection equal to 10.35 m in flapwise direction for the most critical load case, minimizing at the same time the mass of the UD material. For all the blade models, the most critical loadcase was always the same as the baseline model: 1641, namely the 50-year wind gust during operating conditions of the turbine.
Attention was also paid to bending stiffness in lead-lag direction but no critical situations were ever denoted.
The iterative process was set to return a thickness distribution of the spar caps for ten equidistant blade stations; between them a linear interpolation was used. After the automatic optimization, a further tuning was performed to smooth the thickness profile to avoid unrealistic quick transitions of thickness in the spar caps.

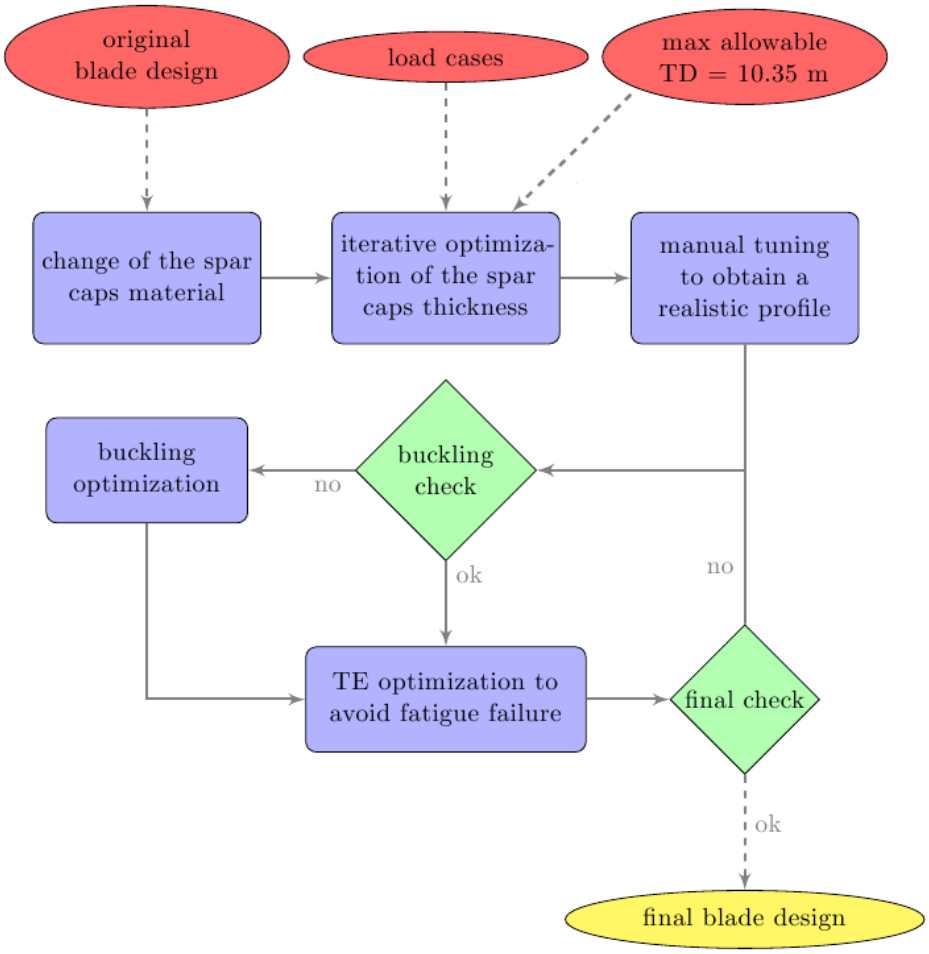

Figure 9.1: Blade design process

When a realistic profile with minimum mass for the maximum allowable tip deflection was obtained, two analyses were performed: buckling and fatigue resistance. Buckling was checked for all the sandwich panels and for the two spar caps. A manual tuning ensured that the blade was safe against buckling.
Finally, a fatigue analysis was run to achieve the 20-year lifetime; the design value of the fatigue stress factor FSF, defined in Section 8.2.2, was assumed to be equal to 1. In all the designs, the most stressed locations were the trailing edge UD reinforcement and the sandwich panels near the root; particularly, the thickness of the reinforcement was always design limited by fatigue resistance.

Some constraints were used during the design process. Firstly, the general

geometry of the blade elements was not modified and only thickness variations were applied to the spar caps, to the trailing edge reinforcement and to the foam in the sandwich panels. The only two exceptions were the spar cap width reductions that were implemented in the carbon blade design, see Section 10.3, and in the variable carbon content blade, see Section 10.4. In addition to these geometry constraints, it was also decided to keep always symmetric elements between suction and pressure side of the blade. Finally, the loads were assumed to be equal to the Upwind baseline and no new aeroelastic simulations were performed. This rather strong simplification was made because the global bending stiffness and the outer geometry of the blade did not change; moreover, the turbine controller was also not modified. Hence, loads were assumed not to vary significantly from one design to the other.

9.2 Characteristic values

The first part of this project consisted of experimental testing to characterize the glass and the hybrid materials. During the blade design process, these material properties could be used to characterize the laminates used in the blade and to simulate the mechanical behavior of the whole structure.
Chapter 6 shows the mean values that were obtained from the tests. In the blade design process, density, stiffness and Poisson's ratio values could be assumed to be equal to the average values obtained during the experimental tests. Nevertheless, it was not possible to assume mean values for ultimate stress and strain because the experimental results had to be scaled down for structural safety.
The GL standards give guidelines on the values that can be assumed.
The characteristic values of materials resistance R_k are prescribed to be:

$$R_k = \bar{x} \cdot \left[1 - \theta \cdot \left(U_\alpha + \frac{U_p}{\sqrt{n}}\right)\right]$$

Where:
$\bar{x}$ is the mean of the test values
θ is the coefficient of variation, defined as the ratio of standard deviation to mean
U_i the i % fractile (percentile) of a normal distribution
n is the number of tests

The GL standards also prescribe to assume a normal distribution and the $\alpha = 5$ % fractile for a probability P = 95 %. This leads to:

$$R_k = \bar{x} \cdot \left[1 - \theta \cdot \left(1.645 + \frac{1.645}{\sqrt{n}}\right)\right]$$

The standards do not prescribe any exact procedure to determine the fatigue slope m, which can be either obtained during experimental tests approved by GL or assumed equal to 10 for glass laminates and 14 for carbon laminates; no indications are given for the hybrids. In this project, data were available for the slopes of the R = −1 S–N curves, so experimental values were adopted, see Section 9.4. The low slope value of the carbon laminate allowed a conservative design.

In conclusion, the values used for the simulations were:

	Glass	Hybrid	Carbon
Density (kg/dm^3)	1.88	1.77	1.62
E_1 (GPa)	30.95	52.84	73.58
E_2 (GPa)	14.27	12.65	9.70
G_{12} (GPa)	6.29	6.51	6.37
ν_{12}	0.374	0.430	0.515
UTS (MPa)	732.32	816.54	1121.32
UCS (MPa)	−587.28	−466.98	−540.61
UTϵ (%)	2.69	1.43	1.33
UCϵ (%)	−2.08	−0.90	−0.73
USϵ (%)	2.86	3.40	2.69
m	10.90	36.51	16.18

Table 9.1: Values assumed during blade design simulations

9.3 Safety factors

To move from the characteristic values to the design values, also the safety factors γ_{M_x} have to be included. These are obtained by multiplying the constant safety factor $\gamma_{M_0} = 1.35$ with the reduction factors C_{ix}:

$$\gamma_{M_x} = \gamma_{M_0} \cdot \prod C_{ix} = 1.35 \cdot \prod C_{ix}$$

The design values of the component resistances R_d result to be equal to:

$$R_d = \frac{R_k}{\gamma_{M_x}}$$

The reduction factors are also defined by GL. They are divided into two categories: static and fatigue; the first group includes:

- $C_{1a} = 1.25$ for influence of ageing
- $C_{2a} = 1.0$ for temperature effects
- $C_{3a} = 1.1$ for VARTM processed materials
- $C_{4a} = 1.0$ for post-cured laminates

For fatigue analysis, the reduction factors to be used are:

- $C_{1b} = N^{1/m}$, in this project it was assumed equal to 1.0
- $C_{2b} = 1.1$ for temperature effects
- $C_{3b} = 1.0$ for UD reinforcement materials
- $C_{4b} = 1.0$ for post cured laminates
- $C_{5b} = 1.0$ for dynamic simulations

These assumptions lead to the safety factors γ_{M_a} equal to 1.86 for static properties and γ_{M_b} equal to 1.49 for fatigue ones.

9.4 Fatigue analysis

9.4.1 GL indications

For fatigue analysis the GL standards for wind turbine certification prescribe to use the slope m as shown in Table 9.1 and the safety factors listed in Paragraph 9.3; these values have to be included in a shifted linear Goodman diagram, shown in Figure 9.2. This diagram is a modified linear Goodman diagram with the top moved to the right, that is to the mean of the characteristic values of UTS and UCS. Equation 9.1 represents the constant life lines shown in Figure 9.2. This formulation is used to calculate the cycles to failure N and the fatigue stress factor FSF, see Figure 8.6.

$$N = \left[\frac{R_{k,t} + |R_{k,c}| - |2 \cdot \gamma_{Ma} \cdot S_{k,M} - R_{k,t} + |R_{k,c}||}{2 \cdot (\gamma_{M,b}/C_{1b}) \cdot S_{k,A}} \right]^m \tag{9.1}$$

Where:
$S_{k,M}$ is the mean value of the characteristic stress
$S_{k,A}$ is the amplitude value of the characteristic stress
$R_{k,t}$ is the characteristic value of UTS
$R_{k,c}$ is the characteristic value of UCS

m is the slope of the S–N curve
N is the number of cycles to failure
γ_{Ma} is the partial safety factor for static properties
γ_{Mb} is the partial safety factor for fatigue properties
C_{1b} is prescribed to be equal to $N^{1/m}$

In the CLD of Figure 9.2, $R_{k,A}$ is the characteristic value of the intercept at N=1 and is prescribed to be:

$$R_{k,A} = \frac{(R_{k,t} + |R_{k,c}|)}{2} \tag{9.2}$$

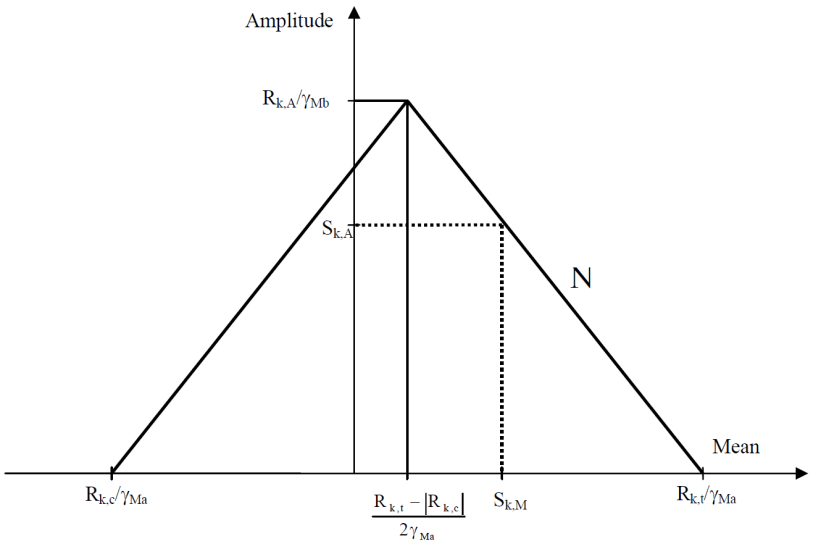

Figure 9.2: Shifted linear Goodman diagram prescribed by GL standards and used in Focus 6 (GL, 2010)

9.4.2 Multiple R-value CLD diagram

In the blade design study performed in this project, the GL standards were respected. Nevertheless, the hybrid materials were characterized experimentally at 3 R-values and not only at R = −1; it would have then been possible to use the multiple R-values CLD diagrams in Focus 6 for a more accurate life prediction. In order to do so, the equations of the four constant life lines were derived. Two of them required a numerical iterative solving process and Focus developers implemented it.

The equations of the constant life lines are here reported; Appendix B includes the calculations to achieve them.

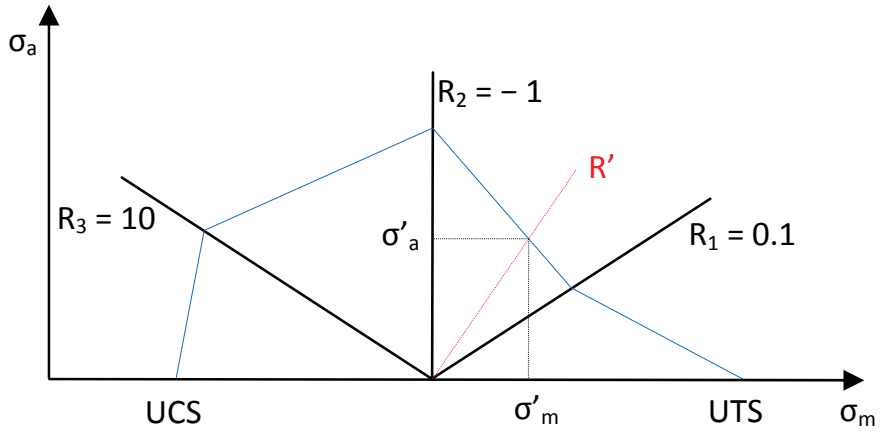

Figure 9.3: Multiple R-values CLD diagram

Given a stress level characterized by mean σ'_m and amplitude σ'_a, the R' value can be calculated easily from Equation 5.1.

$$R' = \frac{\sigma'_m - \sigma'_a}{\sigma'_m + \sigma'_a} \tag{9.3}$$

The CLD diagram is divided in four sectors delimited by the x-axis with the points UTS and UCS and by three lines, R = 0.1, −1 and 10. These lines are called in the formulas with the subscript 1, 2 and 3 respectively and are described by $m_{1,2,3}$ and by $k_{1,2,3}$, which are slope and intercept of the σ_a–N lines at R = 0.1, −1 and 10 respectively. The formulas also show the parameter r, defined as:

$$r = \frac{1+R}{1-R} = \frac{\sigma_m}{\sigma_a}$$

This results in $r_1 = 1.22$, $r_2 = 0$, $r_3 = -1.22$. The equations of the constant life lines result to be:

$$N = \left[\frac{k_1 \cdot \left(\frac{UTS}{\sigma'_a} + r_1 - r' \right)}{UTS} \right]^{m_1} \tag{9.4}$$

When R' lies between R_1 and the x-axis

$$\sigma'_a = \frac{r_1 - r_2 + \sigma'_m \cdot \left(\frac{k_1 \cdot N^{-\frac{1}{m_1}} - k_2 \cdot N^{-\frac{1}{m_2}}}{k_1 \cdot k_2 \cdot N^{-\left(\frac{1}{m_1} + \frac{1}{m_2}\right)}} \right)}{\frac{r_1}{k_2} \cdot N^{+\frac{1}{m_2}} - \frac{r_2}{k_1} \cdot N^{+\frac{1}{m_1}}} \tag{9.5}$$

When R' lies between the R_1 and R_2 lines

$$\sigma'_a = \frac{r_2 - r_3 + \sigma'_m \cdot \left(\frac{k_2 \cdot N^{-\frac{1}{m_2}} - k_3 \cdot N^{-\frac{1}{m_3}}}{k_2 \cdot k_3 \cdot N^{-\left(\frac{1}{m_2} + \frac{1}{m_3}\right)}} \right)}{\frac{r_2}{k_3} \cdot N^{+\frac{1}{m_3}} - \frac{r_3}{k_2} \cdot N^{+\frac{1}{m_2}}} \tag{9.6}$$

When R' lies between the R_2 and R_3 lines

$$N = \left[\frac{k_3 \cdot \left(\frac{|UCS|}{\sigma'_a} + r' - r_3 \right)}{|UCS|} \right]^{m_3} \tag{9.7}$$

When R' lies in the bottom left sector between R_3 and the x-axis

Equations 9.5 and 9.6, which represent the two central sectors bridging the $R = -1$ line, cannot be made explicit for N and need to be solved iteratively. To perform a consistent analysis, the safety factors γ_{Ma} and γ_{Mb} are also to be included in Focus.

Compared to the shifted linear Goodman diagram prescribed by GL standards, the experimental diagrams returned less conservative fatigue lifetimes for the hybrid and the carbon laminates, producing higher FSF values along the blade structure. This advantage occurred thanks to the high tensile performance.

9.5 Materials cost

A rough cost comparison was also useful to evaluate the different blade designs. The cost of the three laminates was predicted thanks to few assumptions.

The carbon fabric, which was purchased for this study in a limited amount, had a commercial price of 19.80 €/m^2, equal to 33 €/kg. This price was likely to be considerably higher than the one that a blade manufacturer would face. So, the reference price for glass could not be the 2-3 €/kg present

	Cost (€/kg)
Glass	6.50
Hybrid	11.10
Carbon	16.80

Table 9.2: Materials cost assumption

in literature (TPI Composites, 2004). A more accurate assumption for the price might be 6.3 €/kg, which was the price of SGL unidirectional glass for an equivalent amount of material. Assuming these two prices, the cost ratio of carbon fabric to glass fabric was approximately 5.
However, as all the laminates used the same resin with comparable fiber volume fractions, the laminate cost ratio was slightly lower. The epoxy density equals 1.15 kg/l and its cost was assumed equal to 7 €/kg (TPI Composites, 2004). This means that a pure glass laminate at 50 % ψ indicatively cost 6.5 €/kg while a pure carbon laminate cost 22.9 €/kg, that means a ratio of 3.5. As a comparison, the material costs assumed in (TPI Composites, 2004) returned a ratio of 4.2.
Considering the relative fractions of the materials reported in Table 4.3, the costs of the laminates shown in Table 9.2 were obtained.

Chapter 10

Blade models

This chapter presents the results of the computational simulations of the blade models with the glass, hybrid and carbon laminates used in the spar caps.
First, the glass laminate was substituted to create the glass baseline and the blade design was optimized for the new material properties, see Section 10.1; then, the models were changed applying the hybrid and the carbon laminates, see Sections 10.2 and 10.3 respectively. Finally, a blade design with variable content of CFRP along the span was simulated; the results are reported in Section 10.4. The chapter is closed by Section 10.5, which shows the comparison of the different blade models and a discussion of possible sources of uncertainty.

10.1 Glass blade model

The first design that was developed was still made of pure GFRP. However, the properties of the spar cap laminate were changed based on the experimental results obtained during this project. These variations caused significant changes from the original blade design.
In the design process of long blades made of glass, often the design driver of the geometry of the spar caps is bending stiffness. This was evident in the original 5 MW baseline design where the spar caps had to be designed much thicker than required for ultimate strength or fatigue resistance. As the GFRP laminate studied in this project had a higher fraction of biaxial layers, which caused a significant lower Young's modulus E_1, even thicker spar caps had to be designed to achieve the same bending stiffness. This resulted in a significant increase of blade weight compared to the original design, namely + 2.7 tons.

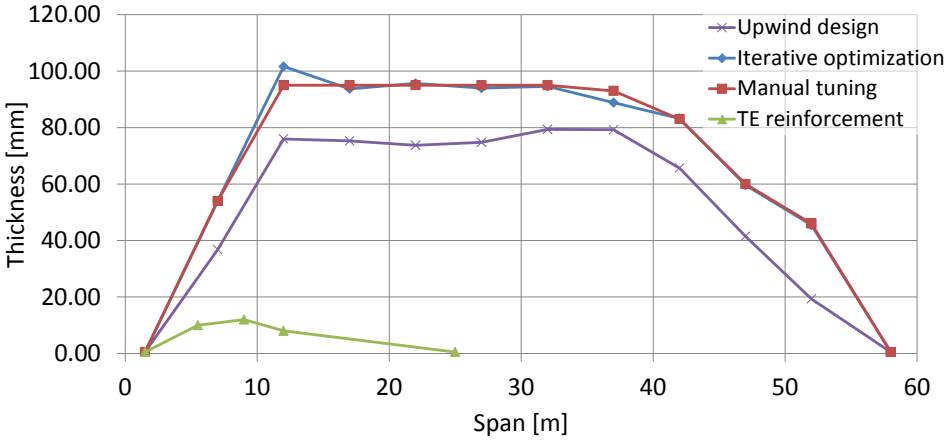

Figure 10.1: Glass UD elements thickness distributions

The thick GFRP structures returned FSF values much higher than 1 and no danger of buckling in the spar caps.
Fatigue resistance was obtained with the FSF profile shown in Figure 10.2. The spar caps had very high FSF values, particularly towards the tip, where the thin airfoils required thick structural elements to achieve the design bending stiffness.

As the global bending stiffness of the blade remained almost constant, the strains of the sandwich panels did not change significantly and buckling resistance was ensured everywhere without any tuning; only minor changes in the thickness of the foam had to be implemented at a span of 17 meters,

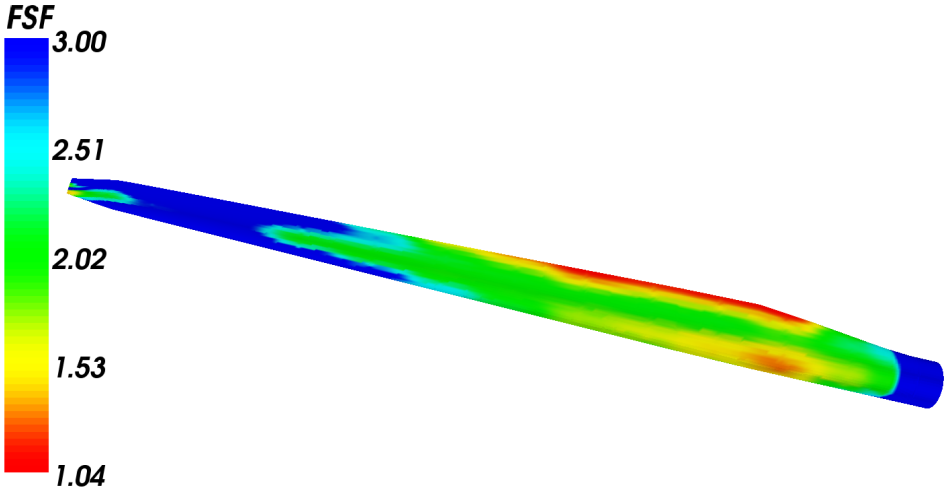

Figure 10.2: Glass blade model fatigue resistance (FOCUS6)

namely + 2 mm on the trailing edge panels.

While the spar caps were far from being fatigue optimized, the trailing edge reinforcement was highly stressed and its thickness was limited by fatigue resistance. This happened because the reinforcement was far away from the edgewise bending neutral axis and the fatigue load cases caused high strains.

Table A.1 and Figure 10.1 show the thickness profiles obtained from the iterative process, the manual tuning and the trailing edge reinforcement optimization.

This blade design resulted in the masses shown in Table 10.1. Assuming the costs of Table 9.2, the cost of the UD structures could also be estimated.

	Mass (kg)	Cost (€)
Spar caps	11 373	74 000
Trailing edge reinforcement	326	2100
Blade	24 245	

Table 10.1: Glass blade model, masses and costs of UD elements

10.2 Hybrid blade model

The glass blade required very thick spar caps to achieve the maximum allowable deflections. The hybrid material tested in this project was considerably stiffer than pure glass and therefore led to thinner structural components. However, the maximum tip deflection remained the design constraint and the lower compressive strength of the hybrid laminate, which was detected in the experimental phase and discussed in Section 7.1.2, did not cause any problem.
Buckling resistance was again satisfied without any specific tuning, except the + 2 mm of foam thickness on the trailing edge panels at 17 m.

After that the blade was proved to satisfy both the constraints of bending stiffness and buckling resistance, a study on the trailing edge reinforcement was performed.
As it was already noted in Paragraph 10.1, in long blades with large chords, the trailing edge is far away from the bending neutral axis and thus needs high allowable strains; this is a problem with stiff carbon fibers. Nevertheless, in this project the results of the simulations showed that the hybrid material could still be beneficial in reducing the mass of the trailing edge reinforcement with costs comparable to the glass design. It was therefore decided to use the hybrid laminate also at the trailing edge, saving additional 130 kg.

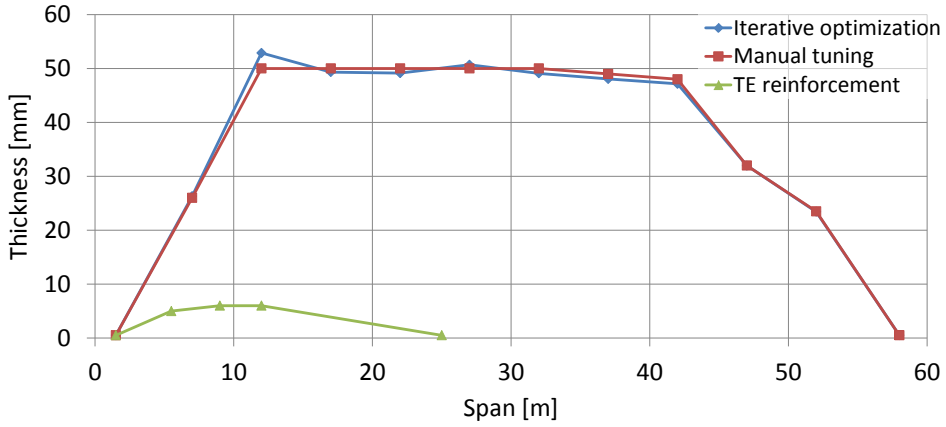

Figure 10.3: Hybrid UD elements thickness distributions

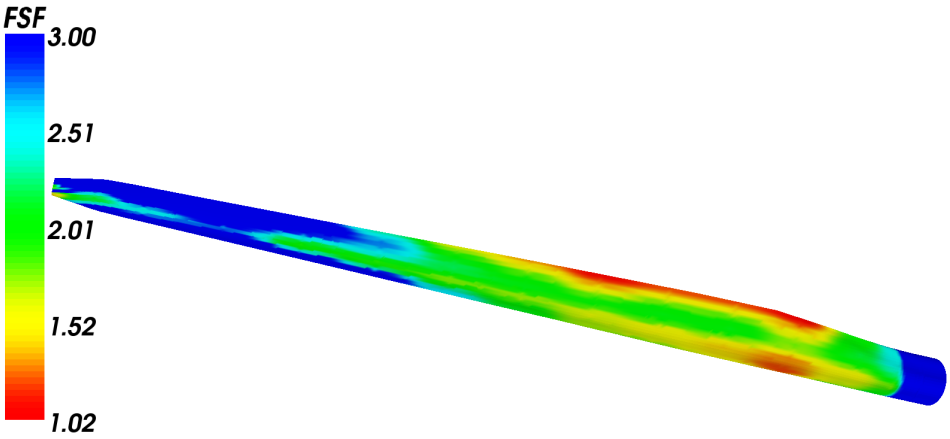

Figure 10.4: Hybrid blade model fatigue resistance (FOCUS6)

The fatigue resistance behavior is shown in Figure 10.4. The main difference compared to Figure 10.2 is the slightly lower FSF values along the span thanks to the thinner spar caps.

As a final result, the hybrid blade design resulted to be considerably lighter than the equivalent pure glass one. Particularly, the spar caps had a 50 % weight reduction, which made them cheaper than the glass blade design. Moreover, the reinforcement at the trailing edge was also made of the new material and resulted to be lower by 130 kg compared to the pure GFRP design.

	Mass (kg)	Cost (€)
Spar caps	5696	63 000
Trailing edge reinforcement	193	2100
Blade	18 467	

Table 10.2: Hybrid blade model, masses and costs of UD elements

10.3 Carbon blade model

The carbon laminate was the stiffest laminate of the three that were studied in this project. Thanks to the high Young's modulus, the spar caps could be made very thin: the iterative process of optimization returned a mass of UD material equal to only 3.6 tons. Nevertheless, this structural solution could not be directly adopted because the spar caps suffered buckling; the two most sensitive locations were on the suction side at a span of 12 m, see Figure 10.5, and on both suction and pressure side at 57 m. The design constraint indeed shifted from maximum allowable tip deflection in x-direction to buckling resistance.

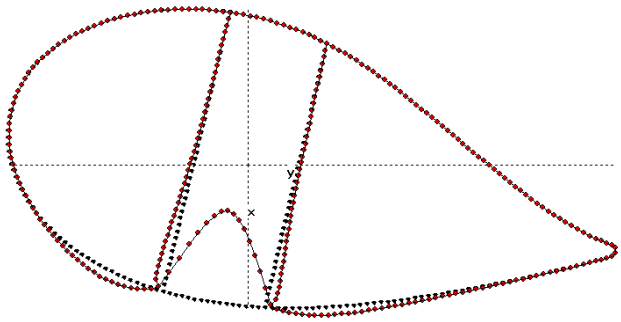

Figure 10.5: Buckling mode of the spar caps in the carbon blade design (FOCUS6)

To solve this problem, different approaches could be adopted:

- thicker spar caps;
- narrower and thicker spar caps;
- additional internal layers of foam and triax to contrast buckling.

Among these possibilities, the first one sounded to be the easiest but also the least efficient. A relatively small growth of thickness at 12 m and 57 m

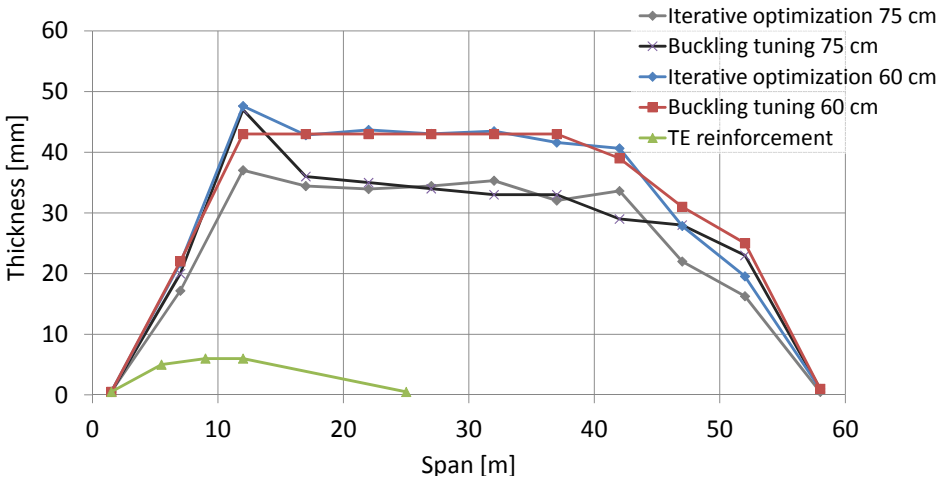

Figure 10.6: Carbon UD elements thickness distributions

could eliminate risk of buckling. The result of the first approach returned a blade of 3.9 tons with a maximum tip deflection of 9.90 m.
The second solution appeared to be much more promising instead. To achieve the same bending stiffness, narrower spar caps could be made thicker, and buckling sensitivity was assumed to be significantly reduced. The two main drawbacks of this solution were expected to be the higher edgewise oscillations and the buckling sensitivity of the sandwich panels, which resulted to be wider; however, edgewise stiffness could also be improved with a thicker reinforcement at the trailing edge while buckling could be contrasted with thicker foam cubes.
Simulations were conducted at decreasing width of the spar caps and 60 cm (the original design had 75 cm wide spars) was found to be a good trade-off between buckling resistance and edgewise stiffness. As for the sandwich panels, wider panels due to narrower spar caps did not result in significant problems; at a span of 17 m, 2 mm of foam had to be added as usual.
Finally, the last solution could have also been effective but was not investigated because of doubts about the manufacturability of such a construction.

In the carbon blade design, the trailing edge optimization was conducted in parallel with the buckling analysis. First of all, it was decided not to use carbon as reinforcement. As it was already highlighted for the hybrid design, the trailing edge reinforcement needed to survive high strains; this was not feasible with carbon layers: a carbon reinforcement could have been beneficial for a small weight reduction but was not economically justified. A hybrid reinforcement was hence found to be more weight/cost effective and was applied in the model.

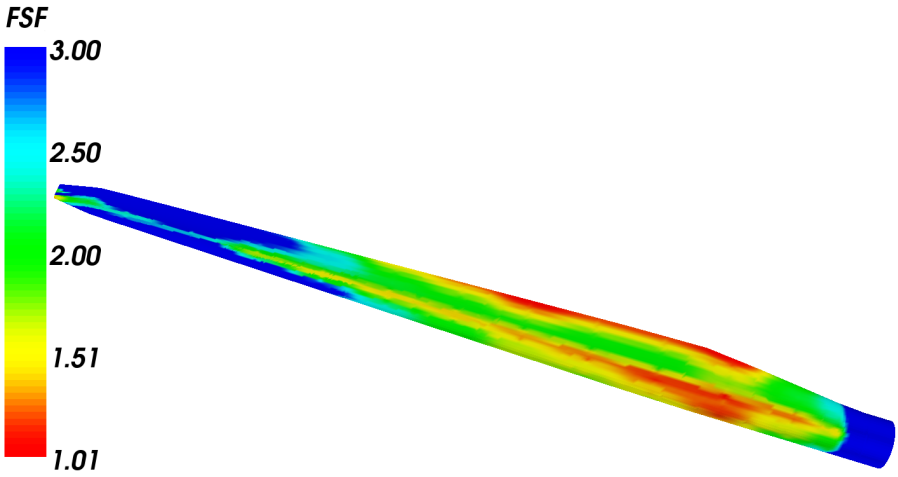

Figure 10.7: Carbon blade model fatigue resistance (FOCUS6)

Simulations were performed also at higher slope values to simulate a carbon S–N curve less conservative than the one assumed in Section 6.3, but conclusions did not change.
Different design solutions were analyzed varying the width of the spars and at the end the same reinforcement used for the hybrid blade design was adopted. Apparently, the FSF factor at the edges was only slightly affected by the spar caps width and no additional material was required.
The FSF profile shown in Figure 10.7 also shows that in the first 40 m of span the thin spar caps reached a better trade-off between flapwise bending stiffness and fatigue lifetime compared to the glass and hybrid blade designs.

In conclusion, the best blade design was the one with 60 cm wide spar caps and hybrid trailing edge reinforcement; the thickness profiles are shown in Figure 10.6, while the mass in Table 10.3.

	Mass (kg)	Cost (€)
Spar caps	3642	61 100
Trailing edge reinforcement	193	2100
Blade	16 546	

Table 10.3: Carbon blade model with 60 cm wide spars, masses and costs of UD elements

10.4 Variable carbon content blade model

The last blade design followed the idea of designing a blade with hybrid spar caps at the root, only glass ply drops along the span and pure UD carbon spar caps at the tip.
To model this blade, three different materials were substituted along the span. Near the root the hybrid laminate was used in the spars, while at the tip the carbon layup was applied. Between these two materials a mixture of the two laminates was assumed to be employed. The properties of this mixture were a linear interpolation of the hybrid and carbon materials, see Table 10.4.

To avoid buckling problems at the tip, the spar caps were made with a linearly tapered width: at the root the spars were 75 cm wide, while at the tip they were 50 cm. This helped to minimize buckling threats.

The optimization process was run to minimize the total cost of the spar caps assuming the prices listed in Table 10.4. Table A.1 shows the results of the automatic optimization and of the manual tuning; small modifications had to be added to the optimal profile to smooth it and to avoid buckling at the tip.
During the blade design, it was decided to use again a trailing edge reinforcement made of the hybrid laminate. Fatigue resistance was ensured without any further modification compared to the previous blade models.

Span section	1	2	3
from / to (m)	1.5 / 17	17 / 37	37 / 58
Density (kg/dm^3)	1.77	1.70	1.62
E_1 (GPa)	52.84	63.20	73.58
E_2 (GPa)	12.65	11.18	9.70
G_{12} (GPa)	6.51	6.44	6.37
ν_{12}	0.430	0.473	0.515
UTS (MPa)	816.54	968.93	1121.32
UCS (MPa)	−466.98	−503.80	−540.61
UTϵ (%)	1.43	1.37	1.33
UCϵ (%)	−0.90	−0.81	−0.73
USϵ (%)	3.40	3.04	2.69
m	36.51	26.97	16.18
Price (€/kg)	11.10	14.00	16.80

Table 10.4: Values assumed for the variable content blade simulations

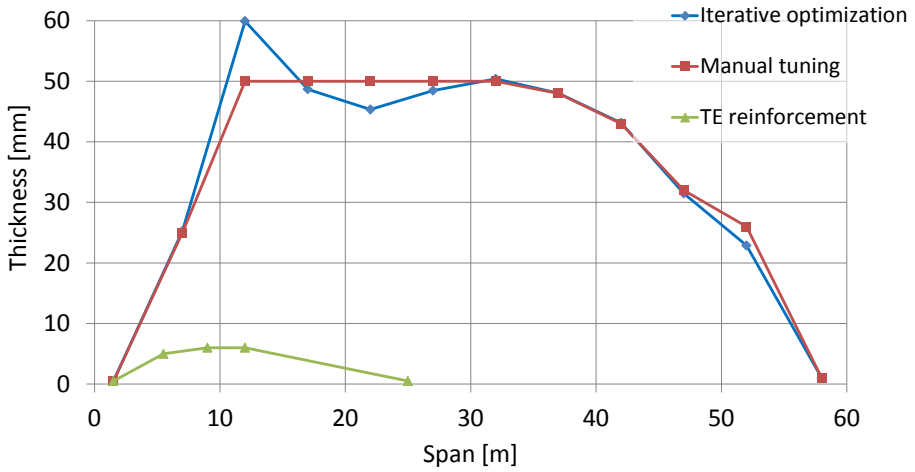

Figure 10.8: Variable carbon content blade UD elements thickness distributions

	Mass (kg)	Cost (€)
Section 1	1248	13 850
Section 2	2123	29 700
Section 3	1145	19 250
Spar caps	4516	62 800
Trailing edge reinforcement	193	2100
Blade	17 400	

Table 10.5: Variable carbon content blade model, masses and costs of UD elements

With the price of CFRP and GFRP assumed in this project, this blade design resulted to be a trade-off in weight and cost between the hybrid and the carbon blade, see Table 10.5.

10.5 Discussion

10.5.1 Comparison of the blade designs

Four blade designs were developed based on the reference 5 MW model substituting in the spar caps the materials that were characterized in this project: a baseline blade model made of pure glass, two blades with the hybrid and the carbon laminates, and finally a variable carbon content design.

The chart in Figure 10.9 shows the mass and weight results of these four designs. The model with carbon spar caps resulted to be the lightest and cheapest blade. The variable carbon content blade also behaved well, while the blade with hybrid spar caps had similar cost but considerable higher weight. Finally, the glass blade model was the heaviest and most expensive design.

In all the blade models, the thickness of the spar caps was limited by the maximum allowable tip deflection in flapwise direction towards the tower.
For the carbon design, buckling also arose as design limiting factor, but the problems were solved with narrower spar caps. For the variable carbon content blade, the spar caps were made narrower only at the tip so that they had tapering width from 75 cm to 50 cm.
Narrower spar caps might cause buckling problems in the sandwich panels; in this study this problem was not detected but this could have happened

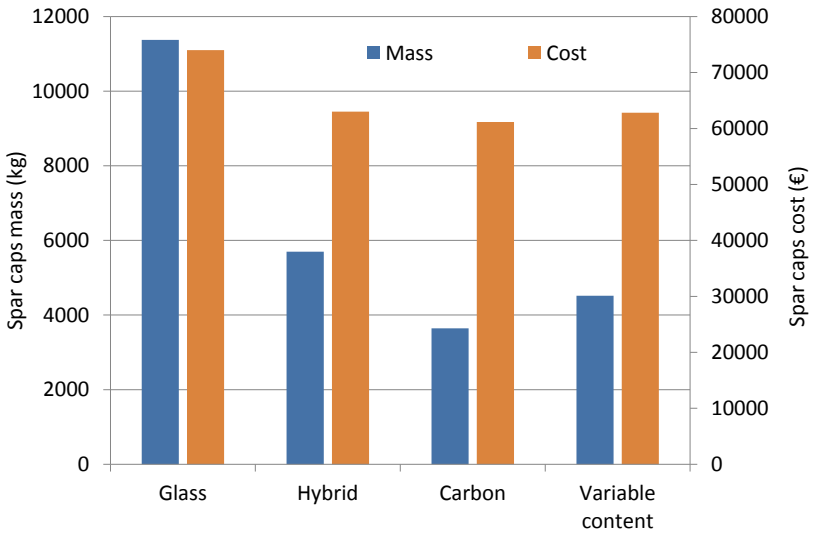

Figure 10.9: Mass and cost of the spar caps in the different blade models

because the original baseline model had not been fully optimized for buckling; excess of foam was indeed present from the beginning. However, foam is a cheap material and few millimeters were often sufficient to strongly improve buckling resistance.

One important aspect during the design process of a wind turbine rotor blade is frequency analysis. In order to avoid resonance, the natural frequencies of blades must be away at least from the 1P frequency, namely the rotational speed of the rotor ω, but also from the 3P $(3 \cdot \omega)$, and possibly from the nP frequencies. Unfortunately, a realistic analysis could not be performed in this project as the original blade model was not optimized for frequency and the turbine controller was not tuned for that particular design. However, the eigen-frequencies of the different design could be compared quantitatively. The bending stiffness of the blade did not change substantially from one design to the other; however, the mass distribution saw large changes. As expected, the partial use of carbon increased then the values of the natural frequencies of the blades both in flapwise and lead-lag direction, see lines in Figure 10.10; the torsional natural frequency also grew with carbon content. Although these considerations might become very important in a real blade design stage, it was not possible to draw any conclusion about potential issues of carbon or hybrid designs.

The main conclusion of this comparison is that hybrid and carbon blades could be significantly lighter while having comparable or even lower costs in

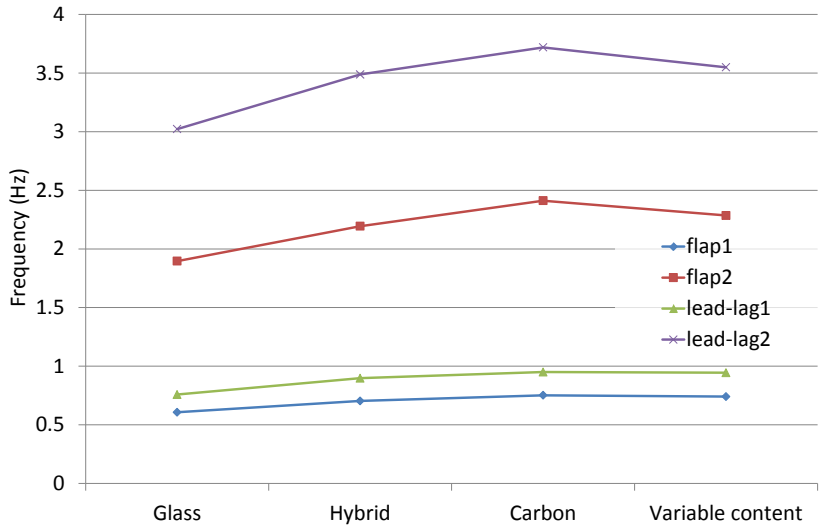

Figure 10.10: Flapwise and lead-lag eigenfrequencies for first and second modes of the blade models

respect to a full glass blade design. This is very important because a light blade may induce other considerable savings in a turbine: the main shaft and bearings, the bedplate and the tower are influenced by the rotor weight. Moreover, transportation and erection may present additional advantages.

10.5.2 Sources of uncertainty

The reliability of the blade design comparison might be affected by three main factors: the relevant percentage of biaxial fibers in the tested laminates, the blade design constraints and the costs that were assumed for the glass and carbon fabrics. However, all these things appeared not to undermine the advantages of the hybrid and carbon designs.

As for the biaxial fibers, this should not affect the comparison too much for several reasons.
Firstly, all the employed materials were indeed characterized by similar high biaxial fiber fractions. The high fractions strongly influenced the blade design because the flatwise stiffness of the blade was lowered for the same spar cap thickness, but all the designs were expected to suffer the same negative effect. Although the absolute values of mass and cost of the blade designs could have been away from the optimum, the global comparison of the materials was expected to be consistent.
Secondly, literature also supported the ratio of 70 % UD and 30 % biax fibers (Griffin, 2001).
Thirdly, some rough simulations were performed in Focus 6 to simulate stiffer materials but no significant difference in the comparison was detected. The carbon design resulted to be again much lighter than the hybrid one and especially than the glass one. With thin carbon spar caps, buckling could become an issue, but the reduction of the spar caps width was an available counter-measure. As for the hybrid layup, no particular buckling risk was denoted.

In addition to the fraction of biaxial fibers, the design constraints that were assumed markedly influenced the conclusions. The blade designs were limited by the maximum allowable tip deflection, taken equal to 10.35 m, and the optimization process led to thick spar cap profiles to achieve the target bending stiffness. If bending stiffness was not the limiting factor, the blade comparison would be different.
On one hand, fatigue resistance seemed to favor anyway the hybrid and carbon blade designs, thanks to the higher fatigue lifetime of these laminates. On the other hand, it is expected that if static strength was taken as limiting factor, the hybrid and carbon laminates would not justify their higher cost due to the relatively low compression strength. Buckling resistance could

also be more limiting for a carbon design than for a glass one.
Said that, all the blade models were strongly limited by bending stiffness and an hypothetic different constraint would have caused very large tip deflections; therefore, bending stiffness seems to be a reliable design driver for long blades.

Finally, the cost comparison could be argued to be not realistic as the dominance of glass fiber blades in the market suggests a more favorable price of GFRP compared to CFRP. A precise cost comparison was hard to establish and in this project it was based on commercial products, see Table 9.2. Moreover, the effect of fiber type on manufacturing was not considered. Therefore, the cost comparison of the different blade designs could be away from reality. However, a higher carbon fiber cost could turn out beneficial for the hybrid laminate compared to the carbon laminate. Moreover, the three hybrid blades would maintain the economic advantages brought by the significant weight reduction.

In conclusions, the blade design comparison shows the potential of hybrid laminates as an alternative to carbon or glass designs. More specific studies for a carbon partial implementation in a wind turbine rotor blade structure would be valuable.

Chapter 11

Conclusions

The concluding remarks of this thesis and the recommendations for future work are presented in this last chapter.

11.1 Conclusions

The objective of this thesis was to evaluate the potential of glass carbon hybrid composites for wind turbine rotor blade structures. This project consisted of an experimental study to investigate the mechanical properties of the hybrid materials followed by a computational study to evaluate the impact of the implementation of these innovative materials in a blade design.

In the first phase, three VARTM laminates were characterized: a baseline GFRP and two hybrids. They all were UD dominated composites with a common layup: $[\pm 45, 0_2]_S$. One of the two hybrids had alternating UD layers of carbon and glass and was called "hybrid", the other laminate had biaxial glass layers and pure UD carbon layers and was called "carbon".

The manufacturing process showed the lower infusibility of the carbon layup compared to the glass and the hybrid layups. In the hybrid laminate, it is expected that the UD glass layers succeeded in facilitating the resin flow between the two carbon layers.

The mechanical testing phase included longitudinal and transverse tensile and compressive static tests, static shear tests and fatigue tests at three R-values, namely 0.1, -1 and 10. From the static tests, the following conclusions could be drawn:

- the static performance of the carbon laminate was the highest, particu-

larly under tensile longitudinal loading;

- the hybrid layup behaved positively and a beneficial hybrid effect was detected both under tensile and compressive longitudinal loads; nevertheless, compression tests returned a UCS value markedly lower than from the glass and the carbon laminates due to carbon fibers failure;
- the glass baseline laminate returned a general lower performance, but also smaller scatter compared to the other two laminates;
- the rule of mixture could quite accurately predict the longitudinal stiffness behavior of the three laminates, with the hybrid and carbon being significantly stiffer than the glass laminate;
- less significant differences were detected for transverse and shear strength and stiffness; the glass laminate had the best transverse stiffness thanks to the transverse fibers present in the fabric, while the shear behavior was similar in all the three laminates thanks to the comparable fraction of biaxial fibers.

As for the fatigue tests, the main conclusions from this study were:

- the carbon laminate had the best results for all the load ratios; however, the tension – compression and the compression – compression results of the carbon panels showed very large scatter, frequent invalid tests and several run outs; it was then decided to assume a conservative S – N line at R $= -1$, while no linear regression could be made at R $= 10$;
- the hybrid laminate returned good regression parameters, with slope values similar or higher than the carbon layup; its main weakness was linked to high compressive loads where for small numbers of cycles the hybrid laminate produced the lowest S – N lines;
- the glass baseline had worse results for tensile loads or at high numbers of cycles, but behaved comparably to the other two laminates at high compressive loads.

The experimental phase was followed by a study of rotor blade design, which produced very good expectations about the implementation of the carbon and the hybrid laminates in a blade structure.
The three materials were substituted in the spar caps of an optimized blade model designed during Upwind and based on the commercial blade LM61.5. An additional blade model was developed with variable carbon content along the span direction. The four different blade designs were tuned for the

mechanical properties of the new materials and their mechanical behavior was simulated using the software package Focus 6. Using the parameter optimization tools available in Focus 6, the thickness of the spar caps was optimized for bending stiffness to ensure a maximum tip deflection towards the tower of 10.35 m. Subsequently, small modifications were applied to achieve fatigue and buckling resistance.

The main conclusions of the blade design study were:

- in all the blade models, the thickness of the spar cap elements was limited by flapwise stiffness; therefore, thanks to the higher Young's modulus E_1 of the hybrid laminates, the new thickness profiles could be made much thinner compared to the full glass design;
- the blade models that used the hybrid and the carbon laminates resulted to be significantly lighter and slightly cheaper than the glass model; the blade that used the carbon laminate had the best results;
- the trailing edge reinforcement was fatigue limited; this occurred because the large distance from the edgewise bending neutral axis caused large strains; the best design solution was found with a hybrid laminate reinforcement;
- buckling issues generally arose in the sandwich panels near the root and in the thin spar caps made of the carbon laminate; in the first case, a small increase in foam thickness was successful in solving the problems, while for the second issue the best solution appeared to be width reduction of the spar caps.

In conclusion, the blade design analysis returned positive expectations for the implementation of CFRP in wind turbine rotor blade structures. The simulations performed in this project returned final designs considerably lighter than the original glass blade model. Moreover, the variable carbon content blade design also proved to be promising.
The main drawback of structures made of carbon fibers appeared to be the poorer infusibility of CFRP compared to GFRP elements. However, the hybrid laminate studied during this project could help to overcome this manufacturing barrier.

11.2 Recommendations

To conclude this project, a few recommendations are provided for future works:

- the carbon laminate was quite accurately described under tensile static and fatigue loading; however, it would be useful to conduct a specific study to better understand the CFRP behavior under static and fatigue compressive loads;
- the hybrid laminate returned decent mechanical properties; however, the different stiffness of glass and carbon fibers might affect the flexural properties of the laminate; Dong et al. (2011) did not report any particular weakness and detected a positive hybrid effect, but dedicated tests on wind turbine blade materials would anyway be recommended;
- in this project, the blade design process used the experimental 5 MW Upwind blade model; it would be interesting to analyze the design results from other blade models to better evaluate the advantages and disadvantages of stiffer spar caps; it is expected that longer blades may favor stiffer and lighter materials but blades where bending stiffness is not the limiting factor may favor glass elements;
- this study was limited to hybrids consisting of pure glass and pure carbon laminae; intraply laminates made of hybrid fabrics should also be studied comparing mechanical performance and infusibility;
- finally, the most important recommendation is to perform a dedicated study on the manufacturability of GFRP, CFRP and hybrid structures; particularly, it would be interesting to look for the best trade-off between strength, stiffness, weight, cost and infusibility of a hybrid material to achieve the successful production of full-scale commercial blades.

Appendix A

Spar cap and trailing edge reinforcement thickness profiles

	Glass blade			Hybrid blade			Carbon blade					Variable content bl		
Blade stations (m)	IT (mm)	MT (mm)	TE (mm)	IT (mm)	MT (mm)	TE (mm)	IT (75cm) (mm)	MT (75cm) (mm)	IT (60cm) (mm)	MT (60cm) (mm)	TE (mm)	IT (mm)	MT (mm)	TE (mm)
1.5	0.50	0.5	0.5	0.50	0.5	0.5	0.50	0.5	0.50	0.5	0.5	0.50	0.5	0.5
5.5			10.0			5.0					5.0			5.0
7	54.04	54.0		26.29	26.0		17.17	20.0	21.71	22.0		25.26	25.0	
9		0.5	12.0			6.0					6.0			6.0
12	101.64	95.0	8.0	52.89	50.0	6.0	37.03	47.0	47.62	43.0	6.0	59.92	50.0	6.0
17	93.74	95.0		49.33	50.0		34.43	36.0	42.83	43.0		48.68	50.0	
22	95.65	95.0		49.14	50.0		33.93	35.0	43.69	43.0		45.33	50.0	
25			0.5			0.5					0.5			0.5
27	93.74	95.0		50.69	50.0		34.44	34.0	43.03	43.0		48.46	50.0	
32	94.60	95.0		49.10	50.0		35.32	33.0	43.47	43.0		50.38	50.0	
37	88.85	93.0		48.06	49.5		32.04	33.0	41.60	43.0		48.02	48.0	
42	83.82	83.0		47.15	48.0		33.62	29.0	40.65	39.0		43.12	43.0	
47	59.59	60.0		31.98	32.0		22.00	28.0	27.85	31.0		31.48	32.0	
52	45.48	46.0		23.43	23.0		16.27	23.0	19.55	25.0		22.88	26.0	
58	0.50	0.5		0.50	0.5		0.50	1.0	1.00	1.0		1.00	1.0	

Table A.1: Thickness profiles of the UD elements in the different blade designs. IT = Iterative Optimization, MT = Manual Tuning, TE = Trailing Edge Reinforcement, (75cm) = standard width spar caps, (60cm) = 60 cm wide spar caps

Appendix B

Constant lifetime line equations

Equations 9.4, 9.5, 9.6 and 9.7 represent the constant lifetime lines of the four sectors of the multiple R-value CLD diagram shown in Figure 9.3. These four equations were derived based on the formulation proposed by Philippidis and Vassilopoulos (2004). These equations are:

$$\sigma_a' = \frac{UTS}{\frac{UTS}{\sigma_{a_1}} + r' - r_1} \tag{B.1}$$

When R' lies between R_1 and the x-axis

$$\sigma_a' = \frac{\sigma_{a_1} \cdot (r_1 - r_2)}{(r_1 - r') \cdot \frac{\sigma_{a_1}}{\sigma_{a_2}} + (r' - r_2)} \tag{B.2}$$

When R' lies between the R_1 and R_2 lines

$$\sigma_a' = \frac{\sigma_{a_2} \cdot (r_2 - r_3)}{(r_2 - r') \cdot \frac{\sigma_{a_2}}{\sigma_{a_3}} + (r' - r_3)} \tag{B.3}$$

When R' lies between the R_2 and R_3 lines

$$\sigma'_a = \frac{UCS}{\frac{UCS}{\sigma_{a_3}} - r' + r_3} \tag{B.4}$$

When R' lies in the bottom left sector between R_3 and the x-axis

The notation is the same as in Section 9.4.1.

Equation B.1 can be made explicit for N by considering that σ'_1 is a function of N:

$$\log N = -m_1 \cdot \log \frac{\sigma_{a_1}}{k_1} \tag{B.5}$$

Where k_1 is proportional to the intercept b_1 of the standard S – N line presented in Equation 5.2:

$$k_1 = b_1 \cdot \frac{(1 - R_1)}{2} \tag{B.6}$$

Equation B.1 becomes:

$$\sigma'_a = \frac{UTS}{\frac{UTS}{\left(N^{-\frac{1}{m_1}} \cdot k_1\right)} + \frac{\sigma'_m}{\sigma'_a} - r_1} \tag{B.7}$$

$$N^{\frac{1}{m_1}} = \frac{k_1}{UTS} \cdot \frac{1}{\sigma'_a} \cdot \left(UTS + r_1 \cdot \sigma'_a - \sigma'_m\right) \tag{B.8}$$

$$N = \left[\frac{k_1 \cdot \left(\frac{UTS}{\sigma'_a} + r_1 - r'\right)}{UTS}\right]^{m_1} \tag{B.9}$$

The same procedure can be applied to Equation B.4, the only difference is that as b_3 is the intercept of the $|S|_{\max}$ – N curve, k_3 is:

$$k_3 = b_3 \cdot \frac{\left(1 - \frac{1}{R_3}\right)}{2} \tag{B.10}$$

In Equation B.4 the absolute value of UCS is taken, so to avoid confusion |UCS| was reported in Equation 9.7.

While Equations B.1 and B.4 can easily be made explicit for N, this cannot be done for Equations B.2 and 9.6, which require a numerical solving process. In

Equations B.2 and 9.6, all the σ_a terms were replaced by the N formulations. Equation B.2 becomes:

$$\sigma'_a \cdot r_1 \cdot \frac{\sigma_{a_1}}{\sigma_{a_2}} - \sigma'_m \cdot \frac{\sigma_{a_1}}{\sigma_{a_2}} + \sigma'_m - r_2 \cdot \sigma'_a = \sigma_{a_1} (r_1 - r_2) \tag{B.11}$$

$$\sigma'_a = \frac{r_1 - r_2 + \sigma'_m \cdot \left(\frac{1}{\sigma_{a_2}} - \frac{1}{\sigma_{a_1}}\right)}{\frac{r_1}{\sigma_{a_2}} - \frac{r_2}{\sigma_{a_1}}} \tag{B.12}$$

Substituting Equation B.5 into Equation B.12, Equation 9.5 is obtained:

$$\sigma'_a = \frac{r_1 - r_2 + \sigma'_m \cdot \left(\frac{k_1 \cdot N^{-\frac{1}{m_1}} - k_2 \cdot N^{-\frac{1}{m_2}}}{k_1 \cdot k_2 \cdot N^{-\left(\frac{1}{m_1} + \frac{1}{m_2}\right)}}\right)}{\frac{r_1}{k_2} \cdot N^{+\frac{1}{m_2}} - \frac{r_2}{k_1} \cdot N^{+\frac{1}{m_1}}} \tag{B.13}$$

Exactly the same process can be performed from Equation B.3 to obtain Equation 9.6.

Bibliography

[1] Burton, T., Sharpe, D., Jenkins, N., Bossanyi, E., *Wind Energy Handbook*. John Wiley & Sons, 2001.

[2] Dowling, N.E., *Mechanical Behaviour of Materials*. Second Edition, Prentice Hall, 1998.

[3] Manwell, J.F., McGowan, J.G., Rogers, A.L., *Wind Energy Explained*. John Wiley & Sons, 2002.

[4] Tong, W., *Wind Power Generation and Wind Turbine Design*. WIT Press, 2010.

[5] Ashwill, T.D., *Materials and Innovations for Large Blade Structures: Research Opportunities in Wind Energy Technology*. 50th AIAA Structures, Structural Dynamics & Materials Conference, Palm Springs, May 2009.

[6] Ashwill, T.D., Laird, D., *Concepts to Facilitate Very Large Blades*. 45th AIAA Aerospace Sciences Meeting and Exhibit, Reno, Nevada, January 2007.

[7] Ashwill, T.D., Paquette, J.A., *Composite Materials for Innovative Wind Turbine Blades*. Wind Energy Technology Department, Sandia National Laboratories, Albuquerque, New Mexico, 2008.

[8] Avery, D.P., Samborsky D.D., Mandell, J.F., Cairns, D.S., *Compression Strength of Carbon Fibre Laminates Containing Flaws with Fibre Waviness*. Proceedings ASME Wind Energy Symposium, ASME/AIAA, pp. 54-63, 2004.

[9] Bach, P.W., *Fatigue Properties of Glass and Glass/Carbon Polyester Composites for Wind Turbines*. Energy Centre of The Netherlands ECN, Petten, The Netherlands, November 1992.

[10] Bortolotti, P., *Carbon Glass Hybrid Materials for Wind Turbine Rotor Blades - Project Overview and Datasheets*. WMC Report WMC-2012-026a-j, Wieringerwerf, The Netherlands, April 2012.

[11] Brøndsted, P., Lilholt, H., Lystrup, A., *Composite Materials for Wind Power Turbine Blades*. Risø National Laboratory, Roskilde, Denmark, 2005.

[12] Brood, R., Numan, R., de Winkel, G., *Focus 6 Workshop – Advanced Features for Structural Blade Design*. Report WMC-2010-43, August 2011.

[13] Bunsell, A.R., Harris, B., *Hybrid Carbon and Glass Fibre Composites*. Composites, pp. 157-163, July 1974.

[14] van Delft, D.R.V., Joosse, P.A., Rink, H.D., *Fatigue Behaviour of Fibreglass Wind Turbine Blade Material at the Very High Cycle Range*. Proceedings EWEA Conference and Exhibition, pp. 379-384, 1994.

[15] Dickson, R.F., Fernando, G., Adam, T., Reiter, H., Harris, B., *Fatigue Behaviour of Hybrid Composites – Part 2 Carbon-Glass Hybrids*. Journal of Materials Science, Volume 24, pp. 227-233, 1989.

[16] Dong, C., Ranaweera-Jayawardena, H.A., Davies, I.J., *Flexural Properties of Hybrid Composites Reinforced by S-2 Glass and T700S Carbon Fibres*. Composites: Part B, Volume 43, pp. 573-581, 2012.

[17] Eliopoulos, E.N., Philippidis, T.P., *A Progressive Damage Simulation Algorithm for GFRP Composites under Cyclic Loading. Part I: Material Constitutive Model*. Composites Science and Technology, Volume 71, pp. 742-749, 2011.

[18] Fukuda, H., Chou, T.W., *Monte Carlo Simulation of the Strength of Hybrid Composites*. Composite Materials, Volume 16, pp. 371-382, September 1982.

[19] Griffin, D.A., *WindPACT Turbine Design Scaling Studies Technical Area 1 – Composite Blades for 80 to 120 Meter Rotor*. NREL report no.: SR-500-29492, 2001.

[20] Griffin, D.A., *Blade System Design Studies Volume I: Composite Technologies for Large Wind Turbine Blades*. Report SAND2002-1879, Sandia National Laboratories, Albuquerque, New Mexico, July 2002.

[21] Griffin, D.A., Ashwill, T.D., *Blade System Design Studies Part II: Final Project Report*. Sandia National Laboratories, Albuquerque, New Mexico, May 2009.

[22] Griffith, D.T., Ashwill, T.D., *The Sandia 100-meter All-glass Baseline Wind Turbine Blade: SNL100-00*. Sandia National Laboratories, Report SAND2011-3779, June 2011.

[23] Jonkman, J., Johansen, P., Lindenburg, C., Chaviaropoulos, P., v/d Hooft, E., Witcher, D., Hendriks, B., van Langen, P., *Upwind Reference Wind Turbine v. 8*. xls file, Upwind, 2007.

[24] Joosse, P.A., van Delft, D.R.V., *Fatigue Behaviour of Fibre Glass Wind Turbine Blade Material*. Proceedings European Community Wind Energy Conference, Lübeck-Travemünde, Germany, pp. 133-136, March 1993.

[25] Joosse, P.A., van Delft, D.R.V., Kensche, Chr., Soendergaard, D., van den Berg, R.M., Kooij, J.F., *Fatigue Properties of Low-Cost Carbon Fibre Material*. Proceedings of the European Wind Energy Conference Copenhagen, Denmark, July 2001a.

[26] Joosse, P.A., van Delft, D.R.V., van Wingerde, A.M., Kensche, Chr., Soendergaard, D., Korsgaard, J., Kooij, J.F., van den Berg, R.M., Hagg, F., Kortbeek, P.J., *Towards Cost Effective Large Blade Components with Carbon Fibres*. Proceedings of the European Wind Energy Conference Copenhagen, Denmark, July 2001b.

[27] Joosse, P.A., van Delft, D.R.V., Kensche, Chr., Soendergaard, D., van den Berg, R.M., Hagg, F., *Cost Effective Large Blade Components by Using Carbon Fibres*. Proceedings of the ASME Wind Energy Symposium, Reno, Nevada, January 2002.

[28] Kensche, C.W., *Fatigue of Composites for Wind Turbines*. Proceedings of the Third International Conference on Fatigue of Composites, Kyoto, Japan, 2004.

[29] Kooij, J.F., *One Dimensional Variations: Blades*. DOWEC project, LM Glasfiber Holland BV, September 2003.

[30] Kretsis, G., *A Review of the Tensile, Compressive, Flexural and Shear Properties of Hybrid Reinforced Plastics*. Composites, Volume 10, Issue 1, pp.13-23, January 1987.

[31] Kretsis, G., Matthews, F.L., Morton, J., Davies, G.A.O., *Tensile Behaviour of Multi-Directional Glass/Carbon Hybrid Laminates*. Imperial College of Science and Technology, London, U.K., 1989.

[32] Lekou, D.J., *Scaling Limits & Costs Regarding WT Blades*. Upwind Report, September 2010.

[33] Lindenburg, C., *Aeroelastic Modelling of the LMH64-5 Blade*. DOWEC project, December 2002.

[34] Lindenburg, C., *PHATAS Release "APR-2005n" User's Manual*. ECN, April 2005.

[35] Mandell, J.F., Reed, R.M., Samborsky, D.D., *Fatigue of Fiberglass Wind Turbine Blade Materials*. Report SAND92-7005, Sandia National Laboratories, Albuquerque, New Mexico, 1992.

[36] Mandell, J.F., Samborsky, D.D., Cairns, D.S., *Fatigue of Composite Materials and Substructures for Wind Turbine Blades*. Report SAND02-0771, Sandia National Laboratories, Albuquerque, New Mexico, March 2002.

[37] Mandell, J.F. Samborsky, D.D., Wang, L., *Effects of Fibre Waviness on Composites for Wind Turbine Blades*. Proceedings of the 48th International SAMPE Symposium, Long Beach, California, pp. 2653-2678, May 2003.

[38] Mandell, J.F. Samborsky, D.D., *DOE / MSU Composite Material Fatigue Database*. Sandia National Laboratories, Version 19.0, Updated at 31st March, 2010.

[39] Mandell, J.F., Samborsky, D.D., Agastra, P., Sears, A.T., Wilson, T.J., *Analysis of SNL/MSU/DOE Fatigue Database Trends for Wind Turbine Blade Materials*. Report SAND2010-7052, Sandia National Laboratories, Albuquerque, New Mexico, 2010.

[40] Marom, G., Fischer, S., Tuler, F.R., Wagner, H.D., *Hybrid Effects in Composites: Conditions for Positive or Negative Effects versus Rule of Mixtures Behaviour*. Journal of Materials Science, Volume 13, pp. 1419-1426, 1978.

[41] Nijssen, R.P.L., *Fatigue Life Prediction and Strength Degradation of Wind Turbine Rotor Blade Composites*. PhD thesis, TU Delft, The Netherlands, 2006.

[42] Nijssen, R.P.L., de Winkel, G.D., Peeringa, J.M., *WMC5MW laminate lay-out of reference blade for WP 3*. Confidential Upwind report, May 2007.

[43] Oldersma, A., *A Literature Survey on the Fatigue Behaviour of Hybrid Composites*. National Aerospace Laboratory NLR, Amsterdam, The Netherlands, 1991.

[44] Pandya, K.S., Veerraju, Ch., Naik, N.K., *Hybrid Composites Made of Carbon and Glass Woven Fabrics Under Quasi-Static Loading*. Materials and Design, Volume 32, pp. 4094-4099, 2011.

[45] Paquette, J., van Dam, J., Hughes, S., *Structural Testing of 9 m Carbon Fiber Wind Turbine Research Blades*. Proceedings of the 45th AIAA Aerospace Sciences Meeting and Exhibit, Reno, Nevada, 2007.

[46] Peeringa, J., Brood, R., Ceyhan, O., Engels, W., de Winkel, G., *Upwind 20 MW Wind Turbine Pre-Design – Blade Design and Control*. ECN, December 2011.

[47] Philippidis, T.P., Vassilopoulos, A.P., *Life Prediction Methodology for GFRP Laminates Under Spectrum Loading*. Composites: Part A, Volume 35, pp. 657-666, 2004.

[48] Reis, P.N.B., Ferreira, J.A.M., Costa, J.D.M., Richardson, M.O.W., *Fatigue Life Evaluation for Carbon/Epoxy Laminate Composites Under Constant and Variable Block Loading*. Composites Science and Technology, Volume 69, pp. 154-160, 2009.

[49] Samborsky, D.D., Wilson, T.J., Agastra, P., Mandell, J.F., *Delamination at Thick Ply Drops in Carbon and Glass Fiber Laminates Under Fatigue Loading*. Proceedings of the Wind Energy Symposium, Reno, Nevada, January 2006.

[50] Shan, Y., Liao, K., *Environmental Fatigue Behaviour and Life Prediction of Unidirectional Glass-Carbon/Epoxy Hybrid Composites*. International Journal of Fatigue, Volume 24, pp. 847-859, 2002.

[51] Sonparote, P. W., Lakkad, S. C., *Mechanical Properties of Carbon/Glass Fibre Reinforced Hybrids*. Fibre Science and Technology, Volume 16, Issue 4, pp. 309-312, June 1982.

[52] Summerscales, J., Short, D., *Carbon Fibre and Glass Fibre Hybrid Reinforced Plastics*. Composites, Volume 10, Issue 3, pp. 157-166, July 1978.

[53] TPI Composites Inc., *Innovative Design Approaches for Large Wind Turbine Blades – Final Report*. Report SAND2004-0074, May 2004.

[54] Wagner, H.D., Marom, G., *Delamination Failure in Hybrid Composites: the Effect of the Stacking Sequence*. Proceedings of the 38th Annual Conference, Reinforce Plastics/Composites Institute, The Society of the Plastics Industry, February 1983.

Standards

[55] ASTM D2524-08, *Standard Ignition Method for Ignition Loss of Cured Reinforced Resins*. American Society for Testing and Materials, 2008.

[56] ASTM D7078, *Standard Test Method for Shear Properties of Composite Materials by V-Notched Rail Shear Method*. American Society for Testing and Materials, 2005.

[57] ASTM D6641, *Standard Test Method for Compressive Properties of Polymer Matrix Composite Materials Using a Combined Loading Compression (CLC) Test Fixture*. American Society for Testing and Materials, 2009.

[58] Germanischer Lloyd, *Guidelines for the Certification of Wind Turbines 2010*. GL report, Hamburg, Germany, July 2010.

[59] IEC 61400-1, *Wind turbines – Part 1 – Design Requirements*. International Electrotechnical Commission, May 2004.